Computer-assisted electrophysiological intervention treating complex ventricular arrhythmias

Philip Hoyland

Computer assisted electrophysiological intervention treating complex ventricular arrhythmias

Thesis
presented for the degree of
Docteur en Sciences de l'Université de Lorraine
École Doctorale IAEM – Mention Automatique, Traitement du Signal et des Images

by **Philip Hoyland**

Defense on December 3rd 2021

Reviewers:

Pr. Blanca Rodriguez	Professor, Computational Medicine, University of Oxford
Pr. Rémi Dubois	Professor, IHU Liryc, Université de Bordeaux

Examiners:

Pr. Laurence Jesel-Morel (President)	PUPH, INSERM 1260, Université de Strasbourg
Dr. Freddy Odille (Supervisor)	CR-HDR, IADI INSERM 1254, Université de Lorraine
Pr. Christian de Chillou (Co-supervisor)	PUPH, IADI INSERM 1254, Université de Lorraine

Diagnosis and Interventional Adaptive Imaging Laboratory

Acknowledgements

Completing my thesis at IADI/Biosense Webster has been a fantastic journey and there are many people that I am very grateful to.

First, I would like to thank my research supervisors, Freddy Odille and Christian De Chillou, for choosing me as their PhD student. Without them I would never have ended up spending so much time exploring the fascinating world of electrophysiology.

I am grateful to Christian De Chillou who had the initial idea of me doing a PhD. Together with Jacques Felblinger, they made sure it became a reality. I am grateful to Freddy Odille for the considerable time and effort helping me through the projects' hiccups, the writing of papers and finally the completion of this thesis.

I am grateful to the management team in Biosense France for their support in this project. This was a first for the team and thank you for your time and energy in making sure I had the best possible conditions for this project. Special thanks to Thibault Pugeat, Loic Masson, Anthony Ouvrard, Deborah Zaffuto, Matthieu Taufour and Wislane Ambri. Thank you for your trust and continued belief in this project.

I'm grateful to the entire Nancy Electrophysiology Unit for spending their precious time in their busy schedules to help me understand and take into account the numerous aspects of the world of electrophysiology: Isabelle, Jean-Marc, Alberto, Néfissa, Charles, Jerome, Arnaud, Pierre Yves, Damien, Fabien, Céline, Catherine, Laurence, Delphine, Myriam, Annick. Special thanks to my co-authors for their extra time in testing and assessing the novel methods developed.

I'd like to thank my family and friends for making sure I keep a balance and enjoy what I do, absolutely key for long-term success.

I couldn't finish without thanking Isa, your continuous support, your patience and your love.

Summary

Since the beginning of the 1990s and the use of radiofrequency to ablate cardiac arrhythmias, electrophysiologists treat increasing complex rhythm disorders. 3D mapping systems enable catheter locations to be known with high precision and therefore are very important tools for electrophysiology. Identifying zones of interest remains long and involves many steps based on indirect analyses of the heart's properties.

The main objective of the thesis is to develop new tools to locate the critical isthmus in post infarct ventricular tachycardia. The clear identification of the circuit components of the ventricular tachycardia enables the development of an ablation strategy to treat the patient. The studied methods do not require a 12-lead electrocardiogram (ECG) of the ventricular tachycardia and therefore have the advantage of being able to be used even if the tachycardia cannot be initiated during the procedure.

A major area of research is the development of an algorithm that automatically extracts the relevant data obtained during pace mapping. This facilitates the display of multi-parametric maps highlighting potential reentry circuits.

Another area of research is the development of a graph-based method to study the variations of the electrical properties of the ventricle. The paced points are considered as vertices of a graph. Each edge is given a weight and finding the path between two vertices of minimum weight allows the analysis of potential reentry circuits.

Abstract

Depuis le début des années 1990 et l'utilisation de l'énergie de radiofréquence pour l'ablation par voie endocavitaire des troubles du rythme rapide, les rythmologues interventionnels prennent en charge des troubles du rythme de plus en plus complexe. Des systèmes de cartographie 3D permettent une représentation précise dans l'espace du positionnement du cathéter et constituent donc un outil très important pour le rythmologue interventionnel. L'identification des zones d'intérêts reste néanmoins longue et sujet à des nombreuses étapes reposant sur des analyses indirectes des propriétés électriques du cœur.

L'objectif principal de la thèse est le développement de nouveaux outils afin de localiser l'isthme critique des tachycardies ventriculaires après infarctus du myocarde. L'identification précise des composantes du circuit de la tachycardie ventriculaire permet la mise en place d'une stratégie d'ablation pour traiter le patient. Les méthodes étudiées ne nécessitent pas un électrocardiogramme (ECG) à 12 dérivations de la tachycardie ventriculaire et présentent donc l'avantage de pouvoir être utilisées même en cas d'échec de déclenchement de la tachycardie pendant la procédure.

Un axe majeur de recherche est le développement d'un algorithme qui permet d'extraire de façon automatique les données pertinentes obtenus lors de la topo-stimulation. Cela permet de faciliter l'affichage des cartes multi paramétriques mettant en avant les circuits de réentrée.

Un autre axe de recherche est l'étude des variations des propriétés électriques du ventricule sous forme de graphe. Les points de stimulations sont considérés comme l'ensemble des sommets du graphe. Chaque arrête est associé à un poids et trouver le chemin entre deux sommets de poids minimum permet d'analyser les circuits de réentrée possibles.

Table of contents

Figures List

Abbreviations/Symbols

AP: Action Potential

ADP: Adenosine diphosphate

ATP: Adenosine triphosphate

DEEP: Decrement-evoked potential

ECG: Electrocardiogram

GRAAPH: Graph-based Reconstruction of Arrhythmic Activations by Pacing the Heart

IADI: Diagnosis and Interventional Adaptive Imaging – Imagerie Adaptative Diagnostique et Interventionnelle

LAVA: Local abnormal ventricular activity

LV: Left Ventricle

MRI: Magnetic Resonance Imaging

PPI: Postpacing Interval

RV: Right Ventricle

S-QRS: stimulus-QRS

TCL: Tachycardia Cycle Length

VT: Ventricular Tachycardia

Introduction

After myocardial injury, the disruption in blood supply to the heart infarction can modify the electrical pathways and lead to the formation of re-entrant circuits. These circuits possess an entrance, core and exit and can result in regular and fast heart rates, episodes that are named ventricular tachycardia (VT). Electrophysiology is the study of the electrical functioning and the electrical properties of the heart. This can be done by equipping catheters with electrodes to record the electrical data of the heart. The catheters can be used in conjunction with mapping systems to create precise electro-anatomical 3D maps.

The field of catheter ablation has progressed with the development of new tools to best analyze the electrophysiological data available. Activation mapping is the sampling of the local electrical activity during tachycardia from different sites of the ventricle and the most direct technique to identify the activation pattern of the tachycardia. Unfortunately, failure to induce tachycardia is common and other indirect methods are needed, such as pace mapping. Pace mapping consists of stimulating the myocardium and analyzing the induced signal. This signal reflects the pacing site location and electrical properties. Bundles of surviving myocytes within heterogeneous scar and areas of block are key components of the tachycardia substrate and the analysis of abnormal electrographic findings have increased our understanding of ventricular arrhythmias. Once the reentry circuit is clearly identified, catheter ablation is used to treat the tachycardia.

This thesis by publication at the Diagnosis and Interventional Adaptive Imaging (IADI) unit focused on improving the identification of reentry tachycardia with pace mapping by exploring 5 axes: a reference-less method, electrocardiogram signal quality, isthmus entrance calculator, automating the workflow and a graph-based reconstruction of activation patterns.

The reference-less pace mapping is a novel method based solely on the analysis of the electrocardiogram (ECG) data obtained during pace-mapping. This approach does not require a reference VT recording of the tachycardia and is particularly useful when the tachycardia cannot be induced. An increasing number of procedures are done with remote magnetic navigation and the quality of the ECG signal collected in the modifying magnetic field setting was studied with a new acquisition device. A multi-parameter electrogram automatic calculator was developed to determine the likelihood that a given site is located at a VT isthmus entrance, a key component of the circuit. Automatic detection was developed because pace mapping analysis is currently limited because of the time-consuming steps that the interventional

cardiologist needs to do to visualize the information of interest. A method to automatically extract the key information and facilitate the use of pace-mapping data was developed. A graph-based method GRAAPH (Graph-based Reconstruction of Arrhythmic Activations by Pacing the Heart) was implemented to take full advantage of all the available information obtained by pace mapping. The connections between each pacing site during pace-mapping was analyzed to generate a suggested activation pattern of the VT circuit.

The main contributions are that the reference-less pace mapping accurately identifies the same target zones as conventional pace mapping as well as additional zones that may cause other VT circuits. The automatic processing reduced the need for manual annotations and facilitated the visualization of the multi-parametric maps identifying the location of the entrance, core and exit of the VT circuit. The GRAAPH method successfully highlights possible activation patterns without the need of the reference VT. These three techniques highlight the electrical connections of the ventricle and could provide further insights to help the physician determine the most effective ablation strategy.

Publication list

1. Hoyland P, Odille F. Computer assisted electrophysiological intervention for reentrant circuit identification. Provisional US patent, application number 63179054.

2. Hoyland P, Hammache N, Battaglia A, Oster J, Felblinger J, Chillou C de, et al. A Paced-ECG Detector and Delineator for Automatic Multi-Parametric Catheter Mapping of Ventricular Tachycardia. IEEE Access. 2020;8: 223952–223960. doi:10.1109/ACCESS.2020.3043542.

3. Battaglia A, Odille F, Magnin-Poull I, Sellal JM, Hoyland P, Hooks D, et al. An efficient algorithm based on electrograms characteristics to identify ventricular tachycardia isthmus entrance in post-infarct patients. Europace : European pacing, arrhythmias, and cardiac electrophysiology : journal of the working groups on cardiac pacing, arrhythmias, and cardiac cellular electrophysiology of the European Society of Cardiology. 2020;22: 109–116. doi:10.1093/europace/euz315.

4. Dos Reis JE, Soullié P, Battaglia A, Petitmangin G, Hoyland P, Josseaume L, et al. Electrocardiogram Acquisition During Remote Magnetic Catheter Navigation. Ann Biomed Eng. 2019;47: 1141–1152. doi:10.1007/s10439-019-02214-3.

5. Odille F, Battaglia A, Hoyland P, Sellal J-M, Voilliot D, de Chillou C, et al. Catheter Treatment of Ventricular Tachycardia: A Reference-Less Pace-Mapping Method to Identify Ablation Targets. IEEE Transactions on Biomedical Engineering. 2019;66: 3278–3287. doi:10.1109/TBME.2019.2903631.

Part 1: Ventricular tachycardia and catheter ablation

1. Electrical activity of the heart

Cells in the normal human heart possess excitatory properties. Indeed, the electrical activity of the heart is responsible for its beating properties. Ions passing through the transmembrane ion channels of the heart cells generate action potentials, then leading to tissue contraction. The ventricle is a fiber-wound of interconnecting muscle fibers[1]. The orientation of fibers varies and its structure is characterized by a smooth transition of fiber angle from endocardium to epicardium.

A first common diagnostic tool for having a quick overview of the electrical activity of the heart is the analysis of the electrocardiogram: electrodes placed on the skin record the electrical variation over time of the cardiac muscle.

A normal electrocardiogram is composed of a P wave, representing the depolarization of the upper part of the heart, the atria, then a QRS wave representing the depolarization of the ventricles, the lower part of the heart followed by a T wave, representing the repolarization of the ventricles (figure 1).

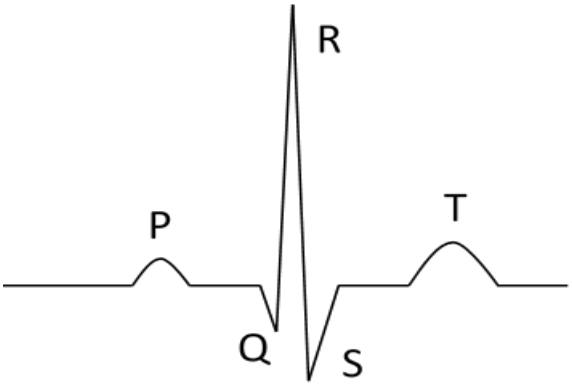

Figure 1. P, QRS and T wave representing the activation of the heart.

2. Ventricular tachycardia

A disruption in blood supply to the heart can lead to infarction, scarring and death of areas of tissue of the cardiac muscle. After myocardial injury, the myocardium can be divided into three areas, the necrotic zone, the peripheral intermediate scar zone and the healthy zone. Patients having had an infarction are likely to have modified electrical pathways that can lead to the formation of re-entrant circuits. These circuits can result in regular and fast heart rates, episodes that are named ventricular tachycardia (VT).

One method for stratifying this risk is by measuring the duration of the QRS wave. The longer it is, the higher the risk of having a cardiovascular related death[2], [3].

3. Electrophysiology

Electrophysiology is the study of the electrical properties of the heart. A common practice of this field is to insert a catheter containing multiple electrodes into the heart to record its electrical activity. Electrophysiologists puncture the femoral vein and then insert catheters through this vein to the heart. The catheters possess a handle that enable the electrophysiologist to move the tip of the catheter to the desired location inside the heart. The catheter can be connected to a radiofrequency generator, enabling the creation of ablation lesions. The unipolar and bipolar signals recorded from the electrodes on the catheter, can be visualized in real time on a recording system. Moving the catheter and recording the corresponding signal (e.g. activation mapping, see section 7) during tachycardia is a useful tool to facilitate the identification of the circuit[4]. The catheters also allow pacing from the electrodes, thus exciting the nearby tissue. Pacing from one site and recording from surrounding sites is also useful to analyze how electricity propagates in the heart[5]. Currently, several multielectrode catheters are available such as the flower shape 5 spline catheter, with 4 electrodes on each spline, the PENTARAY™ catheter (Biosense Webster Inc., Diamond Bar, USA). This catheter can be used in conjunction with the CARTO® mapping system that enables the creation of precise electro-anatomical 3D maps. Indeed, Biosense Webster's catheters can be equipped with a small magnetic sensor enabling the location of the catheter to be known at all times. This location, as well as the recorded electrical data is processed to be visualized on 3D maps. A 3D mapping system facilitates the detailed analysis of the electrical properties of the heart and helps direct delivery of ablation lesions.

4. Impulse propagation

Cardiac excitation involves generation of the action potential (AP) as shown in figure 2 and is the result of the interactions between the membrane ionic currents and the ionic milieu of the cell[6].

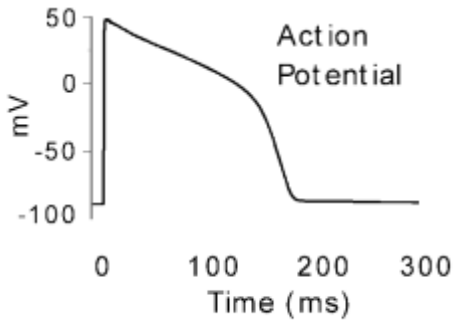

Figure 2. Action potential of a cell over time[6].

For a single cell under space-clamp conditions, the transmembrane potential V_m can be determined by the total transmembrane ionic current I_{ion} and the membrane capacitance C_m :

$$\frac{dV_m}{dt} = {}^{-1}/_{C_m} * I_{ion} \quad (1)$$

The movement of ions across the membrane occurs via voltage-gated ion channels, pumps and exchanges. Once the cell's activation threshold is reached, the fast inward sodium current I_{NA} depolarizes the membrane and generates the fast AP rise. When the V_m reaches -25 mV, the inward L-type calcium current $I_{Ca(L)}$ is responsible for the AP plateau and reduces the repolarizing action of outward delayed potassium currents I_K. L-type calcium channels slowly inactivate and the potassium current I_K increases during the plateau leading to the repolarization of the membrane towards its resting potential.

If we now consider cells to be part of a continuous chain, current flows from an individual cell to its neighboring cells through intercellular gap junctions. In a linear cell chain, the AP propagation follows:

$$C_m * \frac{\partial V_m}{\partial t} + I_{ion} = {}^{a}/_{2r_i} * \frac{\partial^2 V_m}{\partial x^2} \quad (2)$$

With a the fiber radius, $r_i$the axial resistance per unit length. Under space-clamp conditions, $\frac{\partial^2 V_m}{\partial x^2}$ is null and so $equation\ (2)$ reduces back to $equation\ (1)$. In this multicellular model, the I_{ion} charge of a given cell is now divided between discharging the membrane capacitance and also depolarizing the membrane of neighboring cells. The resistance r_i is not a constant and varies depending of the electrical coupling of the different cells. For example cardiac fiber orientation has an impact with a more rapid conduction in the direction parallel to the myocardial fiber axis than in the transverse direction[7]. Moreover, different layers of connective tissue lead to variations in resistance.

5. Myocardial infarction

Myocardial infraction and the subsequent block of oxidative metabolism and the fall in adenosine triphosphate/adenosine diphosphate (ATP/ADP) have many effects on ion concentrations channels and carriers[8]. For example, external potassium and internal sodium concentrations are increased whereas both internal and external pH becomes more acid. Some myocardial cells die while others survive because they continue to receive some blood supply. When the necrotic myocardial cells are replaced by fibrous tissue, the surviving cells in the subendocardium can be trapped in the scar[9]. Histologically, five dominant patterns can be defined: 1) contiguous areas of viable myocardium, 2) small confluent areas of fibrosis surrounded by viable myocardium, 3) confluent areas of fibrosis containing only strands of viable

cardiomyocytes, 4) confluent areas of fibrosis containing solitary viable cardiomyocytes, and 5) transmural confluent fibrosis[10]. Preparations from infarcted canine hearts have shown that as time passes, fibrosis increases, muscle fibers in the border zone are separated by increasing amounts of connective tissue and can change directions[11].

For the surviving cells, each ionic current change has its own time course of remodeling and can continue to vary several years after the onset of the infract[12]. The remodeling can also be consequences of the continuous changes during infarct healing such as increased wall stress, hypertension and medication[10].

These changes can lead to a reduced membrane excitability and a prolonged effective refractory period[6], [13], [14]. Tension and an increase in volume due to osmotic changes lead to cell stretching[8]. Stretching causes opening of stretch-sensitive channels that lead to enhanced inward and outward currents. This can lead to the shortening of the plateau of the action potential. In the myocardium associated with healed canine infarcts, each myocyte is connected to fewer cells. A great reduction (of up to 75%) in side-to-side cell interconnections has been found as well as a decreased number of gap junctions[15].

After infraction, the distribution of the nerve fibers in the ventricles is also altered. The necrotic myocardium is associated with denervation, whereas the peripheries of myocardial scar and perivascular regions are richly innervated[16], [17]. Sympathetic nerve activation have effects on a series of electrophysiological properties such as automaticity, refractoriness, and conduction velocity of myocardial cells[17]–[20].

The duration of the coronary artery occlusion is also proportionally correlated to the size and transmural extent of the myocardial scar[21]. Early reperfusion results in interstitial fibrosis of the inner third of the wall extending toward the midmyocardium, whereas late reperfusion or permanent occlusion results in more uniform transmural necrosis[10], [22], [23].

These combined effects result in changes in action potential, cell coupling and structure that can eventually lead to the development of VT substrate and occurrences of arrhythmias[24], [25].

6. Abnormal electrical circuits

a. Slow conduction

One of the main consequences of ischemia is slowed conduction. This decrease in conduction velocity can be due to reduced cell excitability, decrease in cell-to-cell coupling and tissue structure.

i. *Due to reduced cell excitability*

After ischemia, the reduced availability of sodium channels lead to a decrease in the fast inward sodium current I_{NA}, reducing excitability and conduction velocities between cells[6]. When the sodium channel availability falls below 11%, the generated depolarizing charge is no longer sufficient to depolarize the membrane above the excitation threshold and the overall conduction ceases, a conduction block has been created. Simulations have determined that the lowest conduction velocity prior to failure is 17 cm/s, a third of the velocity (54 cm/s) at full membrane excitability[6].

ii. *Due to reduced cell-to-cell coupling*

After ischemia, changes in the average conductance of gap junctions due to progressive interstitial fibrosis reduces cell-to-cell coupling[6], [11], [15]. Conduction velocity then decreases with increasing coupling resistance. Slowing of conduction is direction dependent and mainly occurs in a direction transverse rather than longitudinal to fiber orientation[6], [11], [26], [27]. The characteristic histological pattern in zones of slow conduction is of parallel muscle fibers oriented transversely to the activation wave front.

Lower conduction velocities can be sustained with reduced intercellular coupling compared to reduced cell excitability[6]. The lower the coupling, the slower the conduction but also the higher the conduction safety. Low coupling leads to very slow, robust, and discontinuous conductions. Indeed, as coupling is reduced, there is greater confinement of the depolarizing current to the remaining coupled and depolarized cells. As a result, individual cells depolarize with a high margin of safety, but much slower.

iii. *Due to tissue structure*

Reduced conduction velocities can also be caused by the complex structures of viable myocardium[6], [11]. Side-to-side electrical coupling among fibers can be absent over several millimeters, only interconnections further away can transfer the activation to neighboring bundles[11]. Long conduction times are due to increased path lengths and zig-zagging patterns of conduction.

b. Unidirectional block

Another consequence of ischemia is unidirectional block, a particular type of block that stops the conducting wave in one direction but does not if the propagation comes from the opposite direction. The blocking properties depend on the direction of the conducting wave.

i. *Asymmetry of excitability*

The electric asymmetry of the cardiac AP can lead to unidirectional block. Indeed, if local cardiac excitation interacts with the repolarization phase of a preceding wave, the development of a unidirectional block is

possible. The AP can propagate incrementally in the retrograde direction but block in the antegrade direction. The incremental AP response in the retrograde direction reflects the residual voltage due to the underlying progressive recovery from inactivation of sodium channels whereas in the antegrade direction the current can be not sufficient to conduct[6].

ii. Tissue structure

The tissue structure can also lead to unidirectional block. After ischemia, small areas of dense scars are interspersed within areas of preserved voltages[10]. Each patch has different conducting properties that can lead to slow, unidirectional, bidirectional or non conducting zones. During premature stimulation, unidirectional conduction block can occur in a certain direction but not in all directions because of the gradual conducting properties of the region[28], [29]. That conduction block is considered as functional, not anatomic, if it is only present at the short activation coupling intervals of premature stimulation and ventricular tachycardia but not at the longer cycle lengths of normal sinus rhythm[28].

Moreover, block can occur when the conducting wave exits a narrow path. After crossing a narrow path the propagating wave becomes curved. A decrease in the width of the path leads to a decrease in the radius of the curved wavefront. Beyond a critical curvature, unidirectional block will arise[6].

c. Reentry mechanisms

Many factors influence the conduction of electrical impulses and excitation waves can be slowed as well as impacted by a unidirectional block. When possible, the propagating wave will rotate around these zones, and reenter the site of original unidirectional block. As shown in figure 3, if sufficient time for recovery of excitability has elapsed, the merged impulse can cross the unidirectional block line from the opposite side to reenter the previously excited region and thus a repetitive cycle can be initiated. This is facilitated when the initial unidirectional block area is bounded laterally by arcs of non-conducting zones, either functional or anatomical[6], [28], [30].

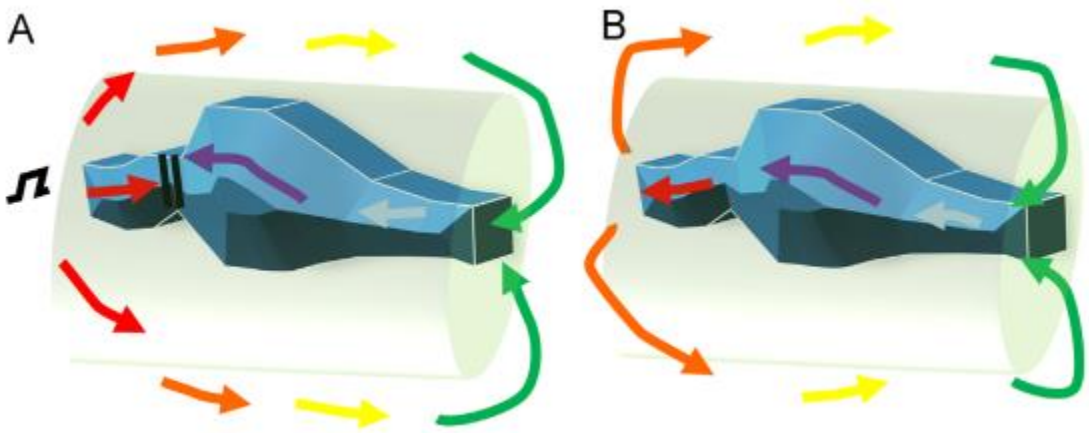

Figure 3. Structure of the reentrant circuit mechanism. The abnormal conducting zone (in blue) is surrounded by non-conducting zone (in green) that is in turn surrounded by healthy myocardium (in white). The color-coded arrows represent the propagation o of the conducting wave (the wave is first located by the red arrows, then orange, yellow, green, grey and purple). In A) the wave is blocked in the abnormal conducting zone but continues to propagate around the non-conducting zone to then reenter the abnormal area from the opposite side. In B) the impulse crosses the unidirectional block line from the opposite side and repetitive cycle is initiated[28].

This mechanism is called reentry. For maintaining reentrant activation, the circuit length must be long enough to enable tissue in each part of the circuit to restore its excitability sufficiently to respond to the next impulse. The higher the velocity, the larger the circuit. Although slow conduction is not a prerequisite for reentry, it reduces the minimal length of reentrant circuits and therefore enhances the likelihood that a circuit can be contained within an area of myocardial scar[11]. The central common pathway of conductive myocardial tissue is called the isthmus or diastolic pathway. The isthmus of the reentrant circuit, is bounded laterally by nonconductive tissue. This nonconductive tissue can either be zones of block, scar area, or an anatomic obstacle such as the mitral valve[28], [29], [31]. In the majority of cases, the barriers consist of zones of block, characterized by continuous lines of double potentials[31]. When the mitral valve is involved, the isthmus is always activated parallel to the mitral annulus in either direction[32].

The reentrant circuit is mostly likely to be endocardial, but can also be mid-myocardial, intramural, subepicardial or transmural[29], [33], [34]. In some rare cases, the circuit is biventricular[35]. In the majority of patients, a given isthmus is associated with a single VT morphology[31]. Extensive sheet of surviving myocardial fibers with multiple entry and exit points allow for different reentrant paths at different times, all in the same heart[30]. Multiple entrances and exits from the slowly conducting tissue allow for a variety of reentry circuit configurations to form[36]. For example, in[37], five tachycardias with different QRS morphologies were initiated in the same patient during intraoperative mapping. An area of

slow conduction that is a bystander relative to one tachycardia circuit can participate in another circuit[38]. On average, isthmi were 31 mm long and 16 mm wide[31].

An isthmus that the depolarization wavefront must cross to perpetuate the tachycardia is defined as the critical VT isthmus[31]. Critical isthmi always correspond to a slow conduction zone, with 57% to 81% of the VT total cycle length being recorded in the critical isthmus. Conduction velocity in the critical isthmi ranged from 6.9 to 19.5 cm/s and is not linked to isthmus width[31]. The same critical isthmus can be shared by multiple tachycardias. Up to 4 different VT morphologies have been reported to share the same critical isthmus[31].

This "figure of eight" reentry mechanism seems to be the most common pattern[4]. In[31], 76% of VTs exhibited a double-loop figure-8 reentrant circuit. The onset and the stability of a given reentrant circuit is determined by a combination of cell excitability, coupling and tissue structure influencing the overall conducting properties of the circuit[12]. There is often a long delay between infarction and the occurrence of VT[39], [40]. This suggests an important role for continued late remodeling and changes in the electrophysiological properties of surviving myocardial cells occurring long after myocardial infarction[41].

The reperfusion strategy also has an impact. Reperfused patients have smaller areas of dense scar but larger areas of scar border zone[10]. This patchy pattern characterized by small areas of dense scar and thicker border zones may result in shorter isthmus length, faster conduction, and therefore shorter VT cycle length. More aggressive reperfusion strategies for acute myocardial infarction reduce the number of infarct survivors that eventually require ablation[40].

Myocardial remodeling results in enhanced arrhythmogenicity with reentry being responsible for a number of clinically important chronic tachyarrhythmias[6], [39], [42].

7. Identification of the VT circuit

a. Surgery

Despite antiarrhythmic drug and pacemaker therapy 40% of patients continue to have recurrent tachycardia episodes[43]. This initially led to the development of a surgery-based method of treatment, subendocardial resection, which removes a 1 to 2 mm thick sheet of endocardium[43]. This technique with the removal of between 2 and 40 cm^2 of subendocardial tissue had success rates approaching 90% in terms of VT elimination[44], [45]. However, some areas were particularly challenging to cure[43]. In the inferior free wall, the endocardium is particularly trabeculated and the proximity of the mitral valve further

hindered surgery. Moreover, disparate sites of origin of ventricular tachycardia further increased failure rates of surgery. The mortality rate above 5% limited the use of surgery to a few patients[43], [45].

b. Catheters

Although the surface electrocardiogram enables a quick overview of the overall electrical activity of the heart, electrophysiologic guided mapping with catheters was developed to analyze in more detail the activation wave fronts that are involved in ischemic ventricular tachycardia[46].

Catheters are long tubes containing multiple electrodes that are inserted into the heart to record its electrical activity. They are generally 7 or 8 Fr wide and possess a handle to help guide the recording electrodes to the desired position. Catheters can be deflectable, unidirectionally or bidirectionally. Electrodes come in multiple shapes, size and spacing. Figure 4 is an example of a flower shape 5 spline catheter, the PENTARAY™ catheter (Biosense Webster Inc., Diamond Bar, USA). The catheter can also provide temperature and impedance monitoring, particularly useful during energy delivery by radiofrequency.

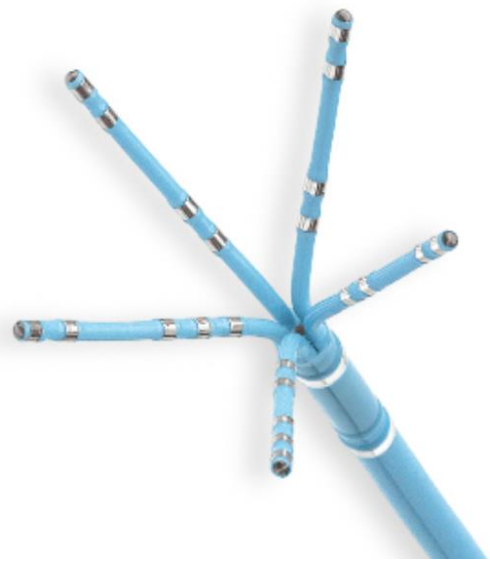

Figure 4. PENTARAY™ catheter (Biosense Webster Inc., Diamond Bar).

Radiofrequency directly transfers electromagnetic energy into thermal energy to the tissue by resistive heating. Durable lesions will form when the tissue temperature exceeds 50°C with irreversible loss of cellular depolarization. Radiofrequency also delivers energy to the tissue by conductive heating, with deeper tissue layers destroyed by passive heat transfer[47].

An increase in ablation power will lead to an increase in lesion size due to both the increase in the source temperature and the increase in diameter of the heat source. However, the tissue temperatures must remain below 100°C to prevent intramyocardial steam from forming and dissecting tissue for release. These “steam pops,” can result in cardiac perforation and tamponade[47], [48].

The size of an RF lesion depends on a great number of factors. On top of power and duration of energy delivery, catheter stability, lesion contiguity and continuity, contact, electrode-tissue orientation, cooling from the surrounding blood pool and anatomic wall thickness all influence lesion formation[44], [47], [48]. For example, lesions are larger with the electrode in parallel position than in perpendicular position[49].

Monitoring tip-electrode temperature can help maximize power delivery. For example, in the “temperature-control” mode, the output of the radiofrequency generator is adjusted to keep the electrode temperature below a target value. Using a very large ablation electrode (8 mm in length) leads to a greater volume of direct resistive heating and a greater convective cooling of the electrode by the blood. However, a large ablation electrode has reduced mobility and flexibility as well as a lower resolution of recordings[48].

i. Irrigated

Additionally, the electrode can be irrigated with saline for convective cooling to maintain a low electrode temperature[49]. This can prevent the electrode-tissue temperature reaching 100°C and developing coagulum[48], [49], [50].

As convective cooling from the bloodstream is no longer required, an irrigated electrode is capable of delivering more energy at sites of low blood flow, such as ventricular trabecular crevasses[48].

Moreover, the additional energy delivered increases the depth of direct resistive heating and therefore the diameter of the effective source. With an irrigated catheter, the highest temperatures occur 3 to 4 mm below the tissue surface, producing deeper and larger lesions without increasing the diameter of the endocardial surface of the lesion[47], [48].

Irrigating an electrode enables the reduction in electrode size while maintaining a sufficient lesions size. A smaller irrigated electrode also has the benefit of being more flexible and enabling higher-resolution electrogram resolutions[48], [50].

Electrode temperature or electrode-tissue interface temperature do not reflect the temperature of the underlying tissue and therefore cannot be used to predict lesion size[48]. This greatly limits the value of

electrode temperature monitoring as irrigated catheter tip temperatures are a poor indicator of lesion formation[47].

ii. Half-normal saline

Saline has an ionic charge and conducts electrical current with lower impedance than blood or tissue. Radiofrequency current therefore preferentially disperses to the saline cloud in contact with the ablation electrode created with irrigation. Half-normal saline is an irrigant that has the particularity of possessing a lower ionic irrigation and thus a higher electrical impedance and therefore enables radiofrequency to preferentially be focused to the targeted cardiac tissue[51], [52]. This method of decreasing the irrigant ionic concentration leads to deeper ablation lesions[51], [52]. This may be a useful strategy to improve radiofrequency current delivery for myocardial circuits, especially arrhythmogenic cardiac tissue refractory to standard ablation[51]. Moreover, the use of higher-impedance fluid also has advantages for the pericardial space. Half-normal saline may further protect parietal pericardium by acting as insulation and may also obviate the need for the continuous evacuation of fluid[52]. However, pushing the reasoning further was not successful as using an irrigant with absolutely no ionic components does result in even larger lesions but with a much higher steam pop rate[51].

c. 3D system

Initially, electrophysiological catheters were navigated and localized in the heart with the use of multiple 2D fluoroscopy x-ray planes. A major limitation of fluoroscopy is its inability to accurately link local electrograms to their spatial position and orientation[46]. It is not possible to accurately associate (tag) a specific spatial position in the heart with its specific electrogram. Moreover, the position of a catheter cannot be accurately determined in respect to a site that has already been mapped[46].

The CARTO® system (Biosense Webster Inc., Diamond Bar, USA) enables the generation of 3D electroanatomical maps[46]. The entire heart can be reconstructed in real time with color-coded electrophysiological information projected on the electroanatomical map. A miniature passive magnetic field sensor is located at the tip of the catheter. As shown in figure 5, an external ultralow ($5 * 10^{-6}$ to $5 * 10^{-5}$ T) magnetic field emitter (locator pad) is located beneath the operating table. It contains three coils with each coil generating a magnetic field that decays as a function of distance. The signals received by the sensor located in the catheter measure the strength of the magnetic field, thus enabling the distance from each coil to be precisely determined. These distances determine the radii of theoretical spheres around each coil. The intersection of the three spheres determines the location and orientation of the sensor in six degrees of freedom (x, y, z, roll, pitch, and yaw)[46].

This mapping method enables the determination of the location of catheters with high precision (mean relative distance error of 0.73±0.03 mm) and good reproducibility (standard deviation of 0.74±0.05 mm). The high spatial resolution (<1 mm) enables the construction of very detailed electroanatomical maps. The location of the catheter can be determined with reference to any previously created electroanatomical map, further helping the selection of the best target site for ablation[46].

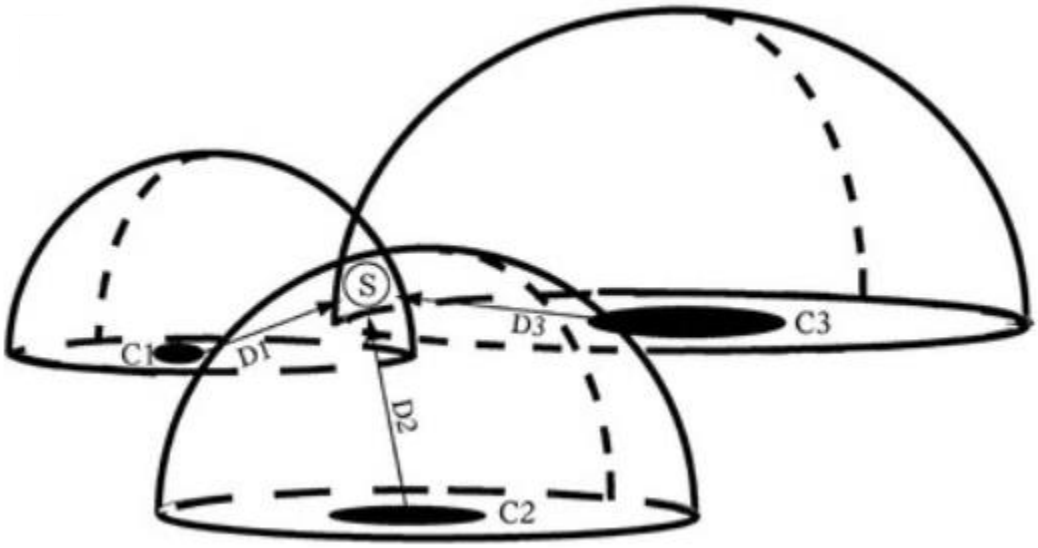

Figure 5. The CARTO® system. Three coils C1, C2, C3 each generate a magnetic field that decays as a function of distance. The signals received by the sensor S located in the catheter enables the distance D1, D2, D3 from each coil to be determined. These distances determine the radii of theoretical spheres around each coil. The intersection of the three spheres determines the location and orientation of the sensor in six degrees of freedom (x, y, z, roll, pitch, and yaw)[46].

i. X-ray exposure

The use of a 3D system reduces x-ray exposure to both the staff and the patient[46]. This is important as cardiovascular imaging and intervention represent nearly 40% of medical radiation exposure to the US population[53].

There are two main biological effects of radiation. A deterministic effect provoking predictable changes in tissue when the radiation exceeds a specific threshold and a stochastic effect, linked to the potential for future harm. For any given radiation exposure, the cancer risk is higher in females than in males and differs among individuals[54]. The cancer risk is three to four times higher in children than in adults[54]. Children are at a higher risk than adults because they have more rapidly dividing cells and a greater life expectancy. The decrease in radiation exposure is especially important in children[54], [55]. The medical staff are also impacted even if they wear radioprotection. Cardiologists have a typical cumulative lifetime attributable risk on the order of magnitude of 1 cancer per 100[54], [56]. They therefore need to make every effort to give 'the right imaging exam, with the right dose, to the right patient' by implementing the ALARA (as low as reasonably achievable) principle[45], [54].

ii. Integration of fluoroscopy images

The CARTOUNIVU™ Module (Biosense Webster Inc., Diamond Bar, USA) enables the integration of previously acquired fluoroscopy images and cine loops into the current 3D electroanatomical maps[57]. Using CARTOUNIVU™ can lead to an operator independent reduction 52% reduction in fluoroscopy time and 63% in radiation dosage for VT ablation procedures[57].

A near-zero fluoroscopy procedure can be achieved in up to half of the VT ablation procedures[58]. The percentage is particularly high in ischemic patients with endocardial ablation[58]. For epicardial mapping, CARTOUNIVU™ is particularly useful to visualize the coronary arteries within the epicardial voltage map, helping the development of safer ablation strategies[58].

d. Remote magnetic navigation

In addition to 3D mapping systems, another important method is remote magnetic navigation. Instead of directing the catheter with the catheter's handle, the orientation of the tip of the catheter is controlled by modifying a magnetic field (0.08–0.1 Tesla) generated by two permanent magnets[59]. The catheter possesses small magnets that are drawn by the desired magnetic field vector. The catheter deflects to align parallel to the magnetic field[45], [60], [65]. Figure 6 shows the electrophysiology room in Nancy equipped with such a system, the Niobe® system (Stereotaxis Inc., St. Louis, USA).

Figure 6. Electrophysiology room in Nancy equipped with the remote magnetic navigation Niobe® system (Stereotaxis Inc., St. Louis, USA). The two permanent magnets are located on both sides of the table.

The main advantage of this technique is the increased catheter movement and the ability to steer the flexible distal portion of the catheter in any direction. In contrast to manually controlled catheters that deflect in a single plane, the tip of the magnetic catheter can be deflected toward any direction in 3D space[61]. This is particularly valuable for complex situations and unknown cardiac anatomies[62]. The force applied by the catheter with this technique is modest but stability is high[47], [60], [63]. Finally, the electrophysiologist is usually located in the next door room and can take off his radioprotection equipment. This reduces physical stress and radiation exposure for the operator[64].

Remote magnetic navigation is safe and is an alternative approach to manually performed ablation in the treatment of ischemic tachycardias with clinical outcomes being at least equivalent to manual ablation[47], [63], [65], [61].

e. Contact catheters

A major improvement in catheters' design was the added possibility to measure the contact applied between the tip of the catheter and the tissue. This has increased the quality of mapping, lesions as well as ablation safety.

In THERMOCOOL SMARTTOUCH® catheters, (Biosense Webster Inc., Diamond Bar, USA), the ablation tip electrode is connected to the rest of the shaft by a small spring. The movement of the spring is detected. The distal portion of the spring is connected to a transmitter coil that emits a reference signal that is then detected by location sensor coils located in the proximal portion of the spring. Once the movement is determined, the associated force is deduced based on the spring characteristics[66], [67]. In bench testing, the resolution of the contact measurements was less than 1 gram[66]. This technology is integrated to the CARTO® system enabling force measurements to be visualized directly in real time during mapping and ablating[68]. Moreover, on top of the quantity of force applied, the orientation of the contact can also be visualized with a 3D vector[68].

i. Mapping

During catheter mapping, electrogram characteristics are collected and analyzed. Poor contact can lead to misinterpreted data. Indeed, an area might be wrongly identified as a low-voltage zone because of lack of contact. Collecting data with a catheter having a minimum forces of 9 grams can reduce misinterpretations[47], [69]. Moreover, contact force catheters can lead to a decrease in radiation use[68]. As we have previously discussed, this is beneficial for the patient as well as the medical team.

ii. Ablation efficacy

Before contact catheters, electrophysiologists could not directly measure contact force. They relied on fluoroscopy, tactile feedback, electrogram amplitude, impedance and temperature drop to estimate contact[66]. However, these measures have been shown to be inaccurate with up to 22% of radiofrequency applications in the ventricle using such estimates not resulting in any lesion formation[70], [66], [67].

Indeed, pure tactile feedback can be influenced by contact, torque and deflection of the catheter shaft. An impression of contact on the distal part of the catheter might be in fact due to contact somewhere else along the catheter. The tactile feedback can also be influenced by the presence of a sheath[68]. Concerning the impedance drop during ablation, the major limitation is that this measure is only available during radiofrequency applications. It cannot be used to position the catheter before the application[66]. Moreover, the impedance drop does not predict the magnitude of the contact force[66]. A decrease in electrogram amplitude is not able to predict lesion size. This may be due to the fact that the electrode can continue to record the electrical activity outside the lesion thus limiting the use electrogram reduction[70]. As we have previously seen, irrigation can alter electrode temperature[47], [48]. Irrigated catheter tip temperature monitoring is therefore a poor indicator of contact. Directly measuring contact force

therefore decreases the number of radiofrequency applications that do not lead to any lesions, avoiding ablations that do not have sufficient contact and can lead to reduced overall procedure times[70], [68].

iii. Ablation safety

It is possible to perforate cardiac tissue with a contact force as low as 77 grams and ablation can lead to a decrease the perforating force of 23%[67]. Being able to measure the contact force can help the physician to safely navigate the catheter in the heart. Moreover, the visualization of the direction of the force applied can increase safety. Indeed, during epicardial ablation, if the force is not applied towards the myocardium and towards the lung, the radiofrequency applications may result in pulmonary lesions[70]. Without force vector information, up to 50% of the lesions could be towards the wrong direction[47], [71].

iv. Metrics beyond contact

Contact force alone is not sufficient to guarantee high quality lesions[47]. On top of absolute contact force quantity, a combination of factors influence lesion formation including radiofrequency power and time, orientation between the catheter and tissue, catheter stability, constant force and energy delivered during ablation. Moreover, lesion continuity with small interlesion distances improve ablation lines. Wall thickness also has an important impact on transmural lesions. All these parameters need to be taken into account to deliver optimal lesions[47].

f. Multielectrode mapping

Another major evolution in catheters' design is multielectrode catheters. Understanding the electrical propagation of the heart depends on the ability for the electrophysiologists to create accurate maps of this electrical activity[72]. The electrograms collected by the electrodes on the catheter are distance-weighted averages of the activity of an area of heart tissue located underneath each electrode. Bipolar electrograms correspond to the difference between the signals collected by two electrodes and thus limits the far-field electrical contribution to the collected bipolar signal. The spatial resolution is increased as the distance between the electrode and the analyzed tissue is decreased, further highlighting the importance of tissue contact[72]. Regarding the electrode design, the resolution of the electrogram is increased the smaller the electrode width and the interelectrode spacing.

Conventional catheters possess a 3.5 mm tip electrode as well as a more proximal 1 mm electrode. The center-to-center spacing between the two electrodes is 3.25 mm. The bipolar signals collected are estimated to correspond to an area of tissue that can represent up to 2.4 cm^2[73].

Multielectrode catheters have been developed to increase mapping resolution[74]. They have a higher number of electrodes (10 or above) with smaller electrode size and closer center-to-center interelectrode distance enabling each signal collected to correspond to the electrical activity of a smaller tissue area[72], [73]. Smaller electrodes have an increased electrogram resolution. Each electrode records the electrical activity of a smaller portion of the tissue. The overlap of the bipolar electrogram between the two unipolar signals is therefore smaller, leading to an overall larger bipolar electrogram[75]. This electrode configuration enables the recording of lower amplitude signals[30]. This can be particularly useful in areas with low voltage and scar, facilitating the identification of small preserved myocardial bundles. These structures could otherwise remain invisible with conventional catheters[74]. Multielectrode catheters enable the recording of distinct diastolic activity and have been found to have sufficient sensitivity to map the heterogeneous and complex post myocardial scar structures[45], [74], [76]. Moreover, the increased substrate definition due to the reduced far field participating of the neighboring healthy tissue can lead to larger low voltage areas[77].

Another advantage of the smaller electrodes of multielectrode catheters is the lowered pacing threshold. The increased electric current density of smaller electrodes can achieve capture of lower-voltage tissue than conventional catheters[45], [74]. This can be particularly useful for pace mapping, an important technique to identify ablation targets that will be developed in depth later.

Furthermore, the increased number of electrodes leads to more data points being collected at each beat, resulting in increased mapping density and speed[74]. This has been shown to shorten the overall duration of mapping as the electrophysiologist often terminates the mapping phase as soon as the density of points is sufficient to understand the circuit[31]. The increase number of data collected at each beat is particularly useful during the mapping of ventricular tachycardias that can only be sustained for a short period of time[45]. High-density mapping has been defined as over 25 points acquired per cm^2 and can allow precise characterization of patchy fibrotic areas by limiting potential errors due to interpolation between points[4], [76]. Overall, the use of multielectrode catheters has a positive impact and can lead to increased patient outcomes and lower VT recurrence rates[78].

ORION™

An example of such a multipolar catheter currently used in clinical practice is the INTELLAMAP ORION™ 64-electrode catheter (Boston Scientific Inc., Cambridge, USA). It is an 8F minibasket catheter with 8 splines, each containing 8 electrodes. Each electrode has an area of 0.4 mm^2 and a center to center interelectrode spacing of 2.5 mm[4]. During each beat, an average of 2 splines are in contact with the

myocardium enabling the catheter to acquire on average 12 electrograms[4]. The remaining 6 splines are facing the blood pool. Although mechanical ectopy can occur while moving the catheter inside the chamber, the number of data points that can be acquired is significant (up to 148 per cm^2)[4], [45]. However, it's design is ill suited for mapping papillary muscles or the epicardium[45].

g. Microelectrode mapping

Recent catheter developments have looked into incorporating microelectrodes on an ablation catheter to take advantage of the increased mapping resolution and pacing capabilities. Microelectrodes enable the detection of smaller channels of surviving myocardial bundles and when incorporated on an ablation catheter can further improve the positioning of the catheter for radiofrequency delivery[75]. Furthermore, microelectrodes facilitate pacing with capture in low-voltage areas and the lower pacing thresholds reduce the impact of noise and artifacts[75].

The latest ablation catheter, the QDOT MICRO® (Biosense Webster Inc., Diamond Bar, USA) has 3 microelectrodes embedded along the circumference of the distal electrode. Each electrode measures 0.086 mm^2 with a center to center interelectrode spacing of 1.5 mm. The innovative design of the microelectrodes located at the circumference of the distal electrode facilitate the recording of bipolar electrograms in a parallel orientation to the chamber wall. The two microelectrodes are more spatially and temporally distant from one another in a parallel than in a perpendicular configuration. This feature further improves electrogram resolution by reducing the cancelling effect between the two electrodes, leading to an overall larger bipolar electrogram amplitude. The QDOT MICRO® microelectrodes size, spacing as well as design enhance the detection of surviving myocardial bundles[75].

h. Automated mapping

The development of novel catheters with its ever-increasing number of electrograms recorded has led to the fact that manual annotation by the electrophysiological team of all the electrograms is time-consuming, tedious and no longer feasible[79]. Another limit of manual annotation is that presumption and bias can lead to misconceptions[79]. Algorithms, directly implemented in the navigation system, have been developed to automatically detect and annotate the collected points. They are based on user-defined acceptance criteria with each point passing through a series of preassigned filters[80], [81]. For example a tissue proximity indicator can be defined to only mark points that are in close proximity to surface tissue[81]. The multiple point collection filters and the large selection of parameters limit erroneous point acquisition. Once acquired, the annotation of the point has also been automatized. Algorithms that use a combination of the maximum negative slope in the unipolar signal as well as the corresponding bipolar

signal are the most used to determine the local activation time. Manual correction is rarely needed with operator intervention representing as little as 0.17% of the total accepted electrograms[82]. The latest versions of navigation systems offer fast and fully-automatic acquisition with accurate annotation that help to better localize the tachycardia circuit[81], [83].

i. Signal analysis in sinus rhythm

The mapping, catheter and software capabilities were developed to best analyze the electrophysiological data available. Bundles of surviving myocytes within heterogeneous scar and areas of block are key components of the tachycardia substrate and the analysis of abnormal electrographic findings identified during sinus rhythm may help to identify isthmuses during VT[84]. By predicting from sinus rhythm analysis the location at which a reentrant circuit is most likely to form, targeted ablation can then be performed to prevent the tachycardia[85]. The following section will evaluate the use of voltage, scar, fragmented and double potential sinus rhythm mapping to help identify reentrant circuits.

i. Bipolar voltage

Bipolar voltage is a measure of amplitude (usually in mV) of the peak-to-peak deflection.

The mean left ventricle (LV) bipolar electrogram amplitude recorded with a 4 mm tip and a 2 mm-ring electrode separated by 1 mm mapping catheter and filtered at 10–400 Hz was 4.8 mV with 95% of normal LV endocardial electrograms with a peak-to-peak amplitude above 1.55 mV[45], [86]. The infarct zone presents electrograms with lower bipolar amplitudes (1.26 mV) and longer duration (74.26 ms) compared to electrograms recorded from the rest of the ventricle[87]. Figure 7 is an example of a left ventricle bipolar map. The lower limit is set at 0.50 mV, all areas under this value are in red. The upper limit is set at 1.50 mV, all areas above this value are in purple.

The analysis of electrographic amplitude depends on multiple factors and therefore must be interpreted with caution.

Bipolar voltage is a not an absolute measure of the underlying tissue but rather a metric to quantify conduction between 2 electrodes of a given catheter design and technology. Electrode size, interelectrode spacing and filtering all influence voltage measurements[5]. Bipolar recordings reduce far-field interferences and this effect is maximized as interelectrode distance is decreased[74]. Electrogram amplitude not only depends on catheter design but also on relative wavefront orientations. The orientation of the activation wavefront relative to the two electrodes and the orientation of the activation wavefront relative to myocardial fiber orientation both influence voltage measurements[5], [77], [88],

[89]. For example, voltage measurements in the septal area can be more difficult to determine because of the complex nature of the conduction system[88]. Multielectrode catheters enable the collection of more data points with a greater variability of the angle between the activation wavefront and the two electrodes and may be less subjective[74].

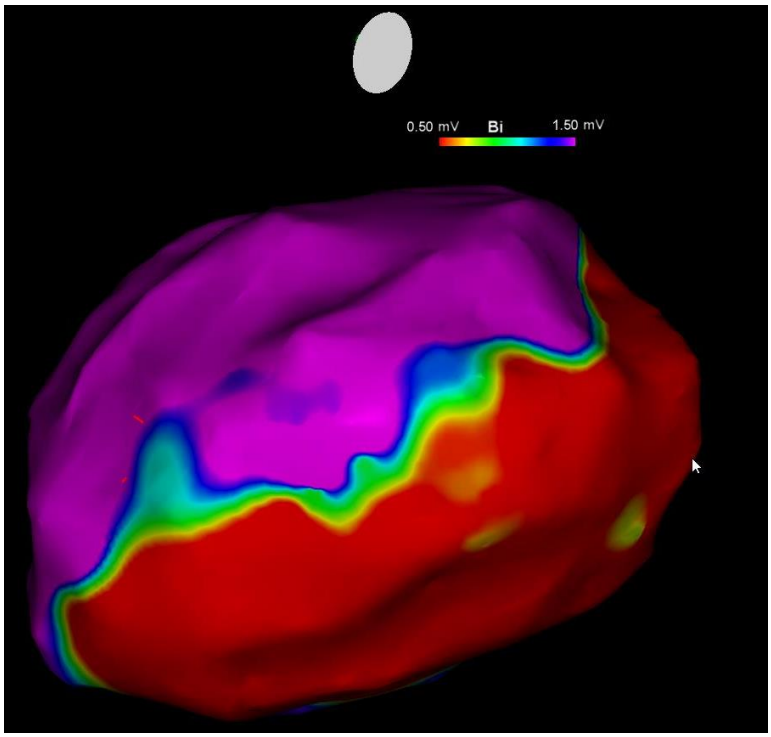

Figure 7. Bipolar map of a left ventricle (Biosense Webster Inc., Diamond Bar).

ii. Scar

While keeping these voltage limitations in mind, bipolar voltage <0.5 mV has been used to define "dense scar" zones[45], [86], [90]. Low voltage does not equal electrically silent nonconductive zones.

These voltage defined regions can overestimate the area of scar by still containing viable myocytes[5], [45], [90]. The total low-voltage area can be large reaching over 200 cm^2 hindering complete encirclement with catheter ablation[90]. Mapping with smaller electrodes and lower interelectrode distances has helped by identifying healthy sharp and high-voltage signals in areas previously considered as "dense scar" when mapped using standard mapping catheters with larger electrodes[4], [5].

Voltage mapping can also underestimate the area of scar as contrast-enhanced magnetic resonance imaging has shown that surviving myocardium as little as 2 mm can produce a bipolar electrogram amplitude above 1.5 mV, preventing the identification of the local scar due to a higher far-field signal[91],

[92], [93]. This is particularly true in the case of non transmural scar, where viable myocardium overlying the subendocardial scar generate high-voltage signals[93].

Voltage amplitude alone should not be used to define nonconductive barriers and pacing maneuvers to define the lack of electrical excitability can be used to provide additional information. Pacing stimulus from the pacing electrode directly attempts to depolarize the neighboring tissue. Local capture suggests the presence of viable myocardium and can limit voltage based scar regions overestimations[4], [5], [90]. However pacing does not help to identify small scar areas. These areas may still create important conduction block, but can escape both voltage and pacing based detection[90]. Up to 17% of isthmuses can include areas with normal voltage amplitude[84]. Moreover, up to 15% of ablation sites were outside the bipolar low voltage area[91], [94]. VT termination by ablation outside the low voltage area has also been reported[88], [93].

Using different voltage scar definitions can help highlight areas of higher voltage “channels”, regions of relatively preserved voltage within denser scar areas[95], [96]. These sites may serve as the protected VT isthmus but with only 30% of channels containing a clinical VT isthmus, many are not critical to the VT circuit[96]. This low specificity highlights the fact that the majority of channels are “bystanders”, hindering the use of voltage based channel identification to guide ablation[96].

The limitations of using bipolar voltage alone to identify reentrant circuits has led to the development of other metrics especially regarding the analyses of abnormal electrogram characteristics.

iii. Double potential

Double-potential electrograms are defined by at least 2 separate ventricular bipolar potentials with peaks separated by an isoelectric interval. The minimum length of the interval varies from 30 ms[4] to 50 ms[31]. Split electrograms frequently show opposite unipolar electrogram polarity. This difference in vector orientation indicates the presence of a first wave propagating in a given direction and a second wave propagating in another direction[4]. Double potentials can represent desynchronized activation sequences of multiple wave fronts and can account for 5% of total mapped sites[97].

A VT isthmus is defined as a conductive myocardial tissue delineated by nonconductive tissue. In addition to an anatomical obstacle or a scar area, a line of double potentials can also represent this nonconductive tissue[31].

In 31 out of 33 VTs, at least one isthmus boundary was represented by a double potential line. A mean of 1.8 zones of block per patient was identified by a continuous 32 mm line of double potentials[31].

Double potentials represent desynchronized activation of tissue and further help to identify reentrant circuits. These split electrograms are recorded at fewer sites and in fewer patients than the fractionated electrograms that we will now look into[97].

iv. Fragmented signals

Electrograms that are the most abnormal are defined as fractionated. They consist of multiple high-frequency components with low amplitudes and long durations (figure 8). Unfortunately the lack of a standardized definition limits comparisons between studies. Most authors agree that fractionated electrograms are composed of multiple components (5 or above in[4]) crossing the isoelectric baseline with an amplitude less than 0.5 mv and duration longer than 50 ms (reaches 133 ms as in[91])[97], [98]. An amplitude to duration ratio below 0.005 V/s has also been used to further characterize fractionated electrograms[98], [99], [100] while others have looked into a fractionation index defined by number of peaks/width of local electrogram[101].

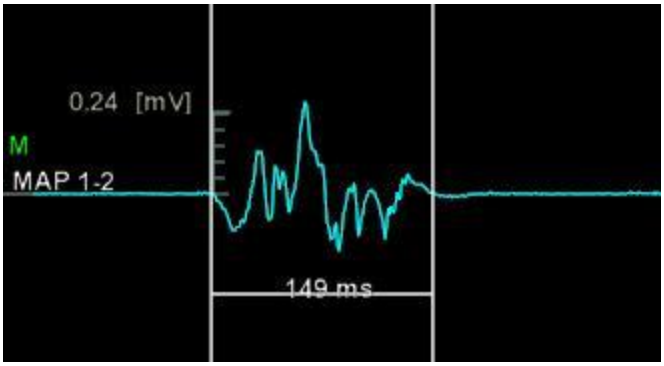

Figure 8. Fractionated signal (Biosense Webster Inc., Diamond Bar).

Quantitative characterization is limited by the fact that electrogram amplitude and width vary depending on multiple factors such as electrode design and wavefront orientation. Electrode size has a direct effect on electrogram complexity. Fractionated electrograms recorded by an electrode with a larger diameter are associated with smaller amplitude[102]. Wavefront direction in relation to the recording dipole will also impact signal amplitude[89]. Changes in wavefront activation or catheter orientation lead to changes in signal amplitude and complexity[5]. Electrogram morphology may also change because of artifacts induced by electrode movement and filter settings[98], [100].

Fractionated electrograms are caused by surviving myocardial cells that have been uncoupled and electrically isolated by intervening fibrous tissue. The slow and desynchronized depolarization is responsible for the high-frequency multicomponent long duration electrogram[97], [100]. The multiple

components reflect the depolarization of different surviving muscle bundles at different times[98]. The electrical wavefront travelling perpendicular to the fiber long axis activate the muscle bundles across high-resistance intercellular connections resulting in conduction delay and multiple components being recorded[9], [100], [102], [103]. The fiber axis variations prevent a consistent wavefront direction that maximizes the detection of fragmented signals in a given ventricle to be identified[88]. More severe micro fibrosis can lead to reduce transverse conduction and an increased number of electrogram deflections[102]. Fractionated electrograms also increase with time because of growing connective tissue during infarct healing[100]. Increased spatial resolution helps to determine the different bundles responsible for fractionated electrograms[72].

Patients with ventricular tachycardia have more numerous and longer fractionated electrograms[97], [100]. Fractionated sites may represent non uniform anisotropic conduction and help delineate regions where reentry occurs[97], [100]. Fractionated electrograms that persist regardless of different electrical activation sequences are even more likely to be associated with reentry circuit isthmuses[103]. The electrogram duration is longer in the reentry circuit but fractionation is most common (up to 69%) outside of the circuit[103]. Fractionated activity can even occur without the presence of reentrant circuits[98], [99]. This low specificity prevents the use of fractionation sites identified in sinus rhythm as targets for ablation[103].

v. Late potentials, LAVA and DEEP

Late potentials are defined as low voltage (<1.5 mV) local ventricular potentials occurring at least 20 ms after the end of the surface QRS[103]–[109]. An example is shown figure 9.

Figure 9. Late potential (Biosense Webster Inc., Diamond Bar).

Late potentials can either be isolated potentials or continuous fragmented activity. Very late potentials describe potentials that occur at least 100 ms after the QRS[105], [107]. Late potentials are found in most post infarct VT ablation patients, with a rate ranging from 66%[109] to 88%[108]. The average area containing late potentials for each patient is 22.2 cm^2[108]. Patients without late potentials seem to have smaller and less-dense scars[93], [107], [110]. Moreover, very late potentials are usually clustered in 1 or 2 regions[105].

Local abnormal ventricular activity (LAVA) are any sharp high-frequency potentials distinct from the far-field ventricular electrogram. These potentials can be high or low amplitude and occur at any time before, during, or after the QRS[93], [111]. LAVAs can be hidden in the QRS far-field signal making their identification challenging[91]. Different pacing maneuvers can be used to help identification. Pacing at a fixed rate from the right ventricle (RV) apex changes the direction of the electrical wavefront and can help to identify otherwise undetected local activity[94], [103], [104]. Moreover, the addition of a single coupled extra stimulus with a low coupling interval has been used to exhibit the decremental conduction properties of LAVAs and facilitate their identification from far-field ventricular electrograms[91], [93], [111]. Local ectopic activity can similarly be used to help identification[111]. LAVAs are found in 96% of ischemic patients and occupy an average area of 39 cm^2[111].

Decrement-evoked potential (DEEP) mapping technique consists of annotating the latest sharp, near-field component of the bipolar signals during the pacing train and on the first extra stimulus. If the delay between the two is over 10 ms, the site is categorized as DEEP[112], [113]. Double or triple extra stimulus can also be similarly used to highlight these zones of slow conduction and functional block[91]. DEEP display areas with decremental conduction that can be hidden during sinus rhythm. DEEP sites can allow the time for blocked regions to recover excitability and then initiate reentry[112]. DEEPs are more specifically associated with VT circuits and are localized more frequently in the diastolic pathway of the VT than late potentials[93], [112], [113].

In addition to endocardial mapping, epicardial mapping has also been used for late potential or LAVA mapping[108], [111], [114]. Compared to the endocardium, the pericardium has the advantage of possessing less obstacles to catheter movement, making it easier to reach a particular area. However, adequate contact can be more challenging to achieve increasing the risk of falsely identifying low voltage values[114]. The onset of local epicardial electrograms is further delayed due to additional transmural conduction facilitating their identification[105]. During combined endocardial-epicardial mapping, the scar borders of the two areas are close[114]. Moreover, patients without any endocardial substrate can be

explored with epicardial mapping. Overall, endocardial LAVAs were present in 90% patients whereas epicardial LAVAs were present in 81% patients[111].

Color-coded activation delay maps of late potentials have been used to highlight the localization of late potentials[108]. This representation facilitates the identification of conduction channels[115]. This technique can be easily coupled with previously described voltage map analysis and seem to increase the specificity of predicting a clinical channel[96], [104]. Moreover, very late potentials seem to be more specific but less sensitive in predicting critical conducting channels[101], [104]–[107]. Late, LAVA and DEEP potentials have been used as a guide for targeting ablation in numerous studies[93], [99], [103]–[106], [109], [111], [112], [116]. Conceptually this enables to address all actual as well as potential circuits while keeping the advantage of a more selective intervention than the complete encircling of the scar[76], [108]. However, some patients still have clinical isthmus circuits that are not linked to the identified channels[96]. For example, late potentials can only be recorded in as little as 30% of isthmus sites[84], [89]. Late potential sites being not specific to the clinical VT, this strategy can still result in an extensive ablation, especially in patients with large myocardial infarctions[86], [96]. Late potential ablation has been shown to limit VT inducibility, with late potential abolition having a positive predictive value of 75%, negative predictive value of 90.4%, sensitivity of 60.0%, and specificity of 95.0% for arrhythmia recurrence[108]. Overall, there is currently no consensus about the best sinus rhythm signal morphology to target during ablation[99], [116].

vi. Activation gradients

On top of localizing low-voltage regions, electrically unexcitable scar and abnormal electrogram components, activation gradients during sinus rhythm have been used to further identify abnormal conduction properties[84], [85]. The electrical propagation is expected to be slowed at the isthmus location during sinus rhythm, causing delayed activation between closely located points[85]. Areas with the most significant activation gradients during sinus rhythm can therefore represent zones that are vulnerable for conduction slowing or block during re-entry. These critical zones can be combined with other sinus rhythm techniques to reach a sensitivity of 83.8% and specificity of 89.2% in estimating the isthmus location[85]. This suggests that activation gradients during sinus rhythm can be used as an additional tool to better understand and characterize the location of the reentrant circuit and improve reentrant VT ablation accuracy in post-infarct patients[84], [85].

vii. Limitations of sinus map

The main limitation of all the substrate-based mapping techniques is that an isthmus during ventricular tachycardia is not always present during sinus rhythm[4]. Lines of block may be at least partially functional and therefore remain undetectable during sinus rhythm[117]. The conditions required for re-entrant circuits to occur tend to depend on functional rather than fixed abnormalities[5]. Furthermore, electrogram characteristics are influenced by wavefront activation and catheter orientation[5]. This explains why neither the type, duration, nor timing of electrograms recorded during sinus rhythm are completely reliable in localizing the reentry circuit and may in fact represent characteristics unrelated to the reentrant activity[97], [118]. For example, late electrograms during sinus rhythm can represent slow conduction into dead end pathways[119]. Artifacts resulting from catheter movement or filter settings can also hinder analysis[97], [118]. The different sinus rhythm mapping techniques lack in standardization mostly in regard quantitative description of signal characteristics and filter settings leading to difficulty in comparing results[99], [118]. The confusion also hinders the use of sinus rhythm mapping. Finally, the ablation of all sinus-rhythm identified targets can lead to ablating large areas, representing up to one-third of the surface of the left ventricle[97]. Overall, sinus rhythm based mapping techniques need to be interpreted with caution when used to define the mechanisms of ventricular tachyarrhythmia in post infarct patients[54], [118].

j. Activation mapping during tachycardia

i. Definition

Mapping the activation pattern during tachycardia is a widespread technique to localize the reentry circuit. Activation mapping consists of sampling the local electrical activity during tachycardia from different sites[120]. The unipolar and bipolar signals are recorded and the relative timing between the sites is determined[4]. The display of the different timings on 3D mapping systems allow patterns of activation to be identified[45], [120]. Figure 10 shows an example of an activation map during VT. The color coding (red-yellow-green-blue-purple) enables the quick identification of the activation sequence.

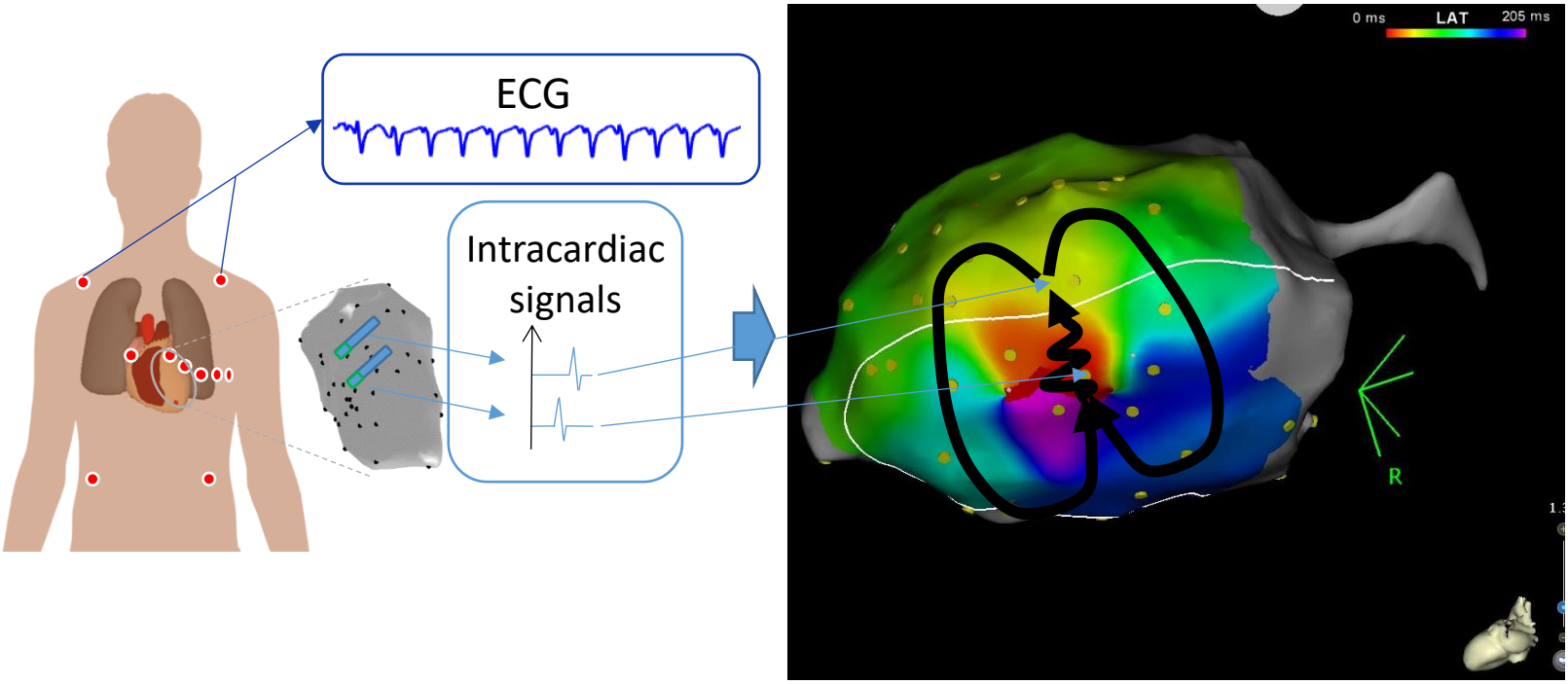

Figure 10. Activation map in tachycardia (Biosense Webster Inc., Diamond Bar).

ii. Induction

Most patients are not in tachycardia when the electrophysiology study starts. A programmed electrical stimulation is used to induce the ventricular tachycardia. An external stimulator is connected to the catheter and delivers 2 ms pulses at a 600 ms basic cycle length followed by an extra stimulus pulse with a shorter coupling. If the stimulation fails to induce the VT, the coupling of the extra stimulus is gradually reduced. Up to 3 extra stimuli can be added and a basic cycle length of 400 ms can be used to try to induce VT. The sensitivity of programmed stimulation rises and the specificity drops as the number of extra stimuli is increased[108], [121]. If the VT cannot be induced, the catheter is moved and the programmed

stimulation is started again at another location[31], [122]. The stimulation protocol often starts via the catheter positioned at the right ventricular apex before moving to the right ventricular outflow tract or the left ventricle. Induction of a VT is highly dependent on the stimulation protocol and lacks in reproducibility[108], [123]. The induced tachycardia is considered sustained if it lasts more than 30 seconds or results in loss of consciousness[43]. Recordings of previous VTs help determine the clinical relevance of the induced tachycardia[122]. The mean number of VTs induced in a patient varies between 2.4 and 3[105], [124], [125]. General anesthesia limits the ease of inducing VTs[105].

iii. Reference and annotation

The timings of the signals of the different catheter locations are all compared to the same electrical reference. The electrical reference is chosen as a morphologically stable and regular electrogram. The electrogram can either be endocardial (from a fix catheter) or a surface lead. If a surface QRS is selected, a sharp and easily identifiable feature is selected (maximum). The window of interest is often centered on the reference with a width equal to the VT cycle length minus 20 ms[31]. For each pair of electrode, the local activation time is determined by taking into account both unipolar and bipolar signals. Automatic annotation algorithms are based on selecting the timing of the largest rapid deflection of the unipolar signal corresponding to a bipolar signal above a certain threshold. The time interval to the electrical reference is then calculated and is used if the value can be reproduced on at least two consecutive beats[120].

iv. Activation

After the catheter has been positioned all over the cavity, the overall activation pattern can be analyzed. The critical isthmus corresponds to a slow conducting zone and represents a large proportion, between 57% and 81%, of the total VT cycle length[31]. The conduction velocity is slowed both at the isthmus entrance (0.28 m/s) and isthmus exit (0.40 m/s)[4]. The curved wave front propagation in these two areas can also explain the slowed propagation. Indeed, conduction speed is greatly influenced by fiber orientation. Conduction that is perpendicular to the fiber direction can be reduced up to 10 times[4]. The onset of the QRS complex occurs when the impulse exits the scar and activates the large mass of healthy myocardium[4], [45], [120], [126]. It is important to carefully interpret the activation map in order to understand the circuit. For example, diastolic potentials can also be present outside the isthmus location, adding complexity to the analysis[45]. Furthermore, the complete circuit is not always entirely localized on the left ventricular endocardium and some tachycardias have subepicardial or intramural components[28], [33]. These usually exhibit a gap in the activation sequence as part of the circuit is

concealed on the endocardial map[45]. In these cases, epicardial mapping may help to further understand the circuit by mapping these hidden features[34]. After detailed review, an activation map enables the distinct identification of the entrance, isthmus, and exit sites of the circuit.

Activation mapping during VT is very valuable to identify isthmuses for patients with hemodynamically stable monomorphic tachycardia[45], [127]. It can localize in detail reentry circuits and isthmuses formed by either fixed or functional lines of conduction block[4], [5]. Activation mapping is a valuable mapping strategy.

v. Limitations of activation map

Failure to induce tachycardia is the main limitation of activation mapping during tachycardia[97]. At least 20% of the time patients have no inducible clinical tachycardia[104], [108], [127]. Even when induced, the VT can be unstable and factors such as hemodynamic collapse, changing morphology and termination of tachycardia during mapping greatly limit the utility of activation mapping[97], [99], [112], [129]. Mapping during VT can be performed in only between 30% and 40% of cases[88], [130]. Even when the targeted VT is stable, inability to delineate the entirety of the circuit (intramural components) can further limit activation mapping[131]. Mapping only during VT does not able to determine whether the conduction blocks are anatomical or functional[31]. To reduce the impact of these limitations, activation mapping is often coupled with other techniques such as substrate, entrainment, or pace mapping[45].

k. Entrainment mapping

i. Definition

Entrainment involves applying during tachycardia, via the mapping catheter, an electrical stimulus with sufficient strength to capture. This stimulus produces the continuous resetting of the reentry circuit and can help determine the pacing site location relative to the tachycardia circuit[126]. If the stimulus is applied at a site in the circuit and during the excitable gap after the preceding wavefront but before the next wavefront, the pacing stimulus will capture the underlying myocardium. The stimulated orthodromic wavefront will travel in the same direction as the tachycardia wavefronts and will propagate through the circuit, resetting the tachycardia[126]. If a train of several stimuli is applied with an appropriate strength and rate, the reentry circuit is continuously reset. If the pacing site is outside the circuit, the stimulated wavefront propagates through a portion of the myocardium before reaching the reentry circuit. Then, the stimulated wavefront enters the circuit and resets the tachycardia[126]. Through the analysis of the measured postpacing intervals, the QRS morphology and the recorded electrograms, the entrainment technique can be used to help identify the critical sites of the arrhythmia circuit. Entrainment mapping is useful for understanding the different components of VT circuit[85], [126], [134].

ii. Postpacing interval

The postpacing interval (PPI), measured between the start of the last captured stimulus and the first local potential of the pacing electrode represents the conduction time from the pacing site to the circuit, through the reentry circuit and then back to the pacing site. When pacing does not alter conduction velocity nor the propagation pathway, this delay, especially when subtracted by the circuit cycle length, can be used as an indication of the proximity of the pacing site to the reentry circuit[38]. Indeed, if the pacing site is located in the reentry circuit, the postpacing interval represents the delay for one revolution through the reentry circuit and will be equal to the tachycardia cycle length (TCL). If the pacing site is outside the circuit, the postpacing interval will be greater than the cycle length and the difference will represent the conduction time from the pacing site to and back from the circuit[126]. A postpacing interval within 30 ms of the tachycardia cycle length is used to determine close proximity to the reentry circuit[126].

iii. QRS morphology

The morphology of the QRS complex during entrainment also provides useful information on the proximity of the pacing site to the reentry circuit[126]. When the pacing site is located outside the reentry circuit, the paced QRS complex is due to the fusion of wavefronts propagating directly away from the pacing site

with those emerging from the tachycardia circuit. This is called classic entrainment[45]. When the pacing site is within a protected region in the reentry circuit or a bystander site that is connected with the isthmus, pacing during tachycardia will not change the QRS morphology. This is called concealed entrainment or entrainment with concealed fusion[45]. The analysis of the QRS morphology helps determine whether a pacing site is located outside the circuit.

iv. S-QRS interval

The stimulus-QRS (S-QRS) interval, measured between the start of the captured stimulus and the beginning of the QRS complex, can provide further information regarding the location of the pacing site. Entrainment with concealed fusion indicates that the pacing site is either in the common pathway of the reentry circuit or in a bystander site. If the site is located in the common pathway, the stimulus-QRS interval is equal to the electrogram-QRS interval during VT[38], [45]. A difference in stimulus-QRS and electrogram-QRS of 30 ms has been used to distinguish bystander sites from common pathway sites[45].

During entrainment with concealed fusion, the S-QRS interval represents the conduction time from the pacing site to the reentry circuit exit. For pacing sites that are in the circuit, this indicates the distance from the pacing site to the reentry circuit exit[45], [126], [132]. The location of the pacing site within the critical zone is determined by its S-QRS/VT cycle length ratio. An exit site is defined as a stimulus-QRS/VT CL ratio below 0.3, the common pathway and entry sites have a stimulus-QRS/VT CL ratio between 0.3 and 0.7, and the inner loop sites have a stimulus-QRS/VT CL ratio above 0.7[4], [38], [45].

v. Limitations of entrainment

Entrainment mapping has numerous limitations, the main one being failure to induce hemodynamically well tolerated tachycardia stable enough to allow pacing[126]. This can represent half of scar based reentrant VTs[133].

Moreover, several aspects can limit interval comparisons. The technique is only valid if pacing does not alter conduction velocities and conduction paths in the reentry circuit[38], [126]. Indeed, if the conduction velocity slows or the length of the reentry path increases, the postpacing interval will be prolonged, and entrainment produced by pacing at such a reentry circuit site would then have a postpacing interval longer than the tachycardia cycle length, further complicating the analysis[126]. Pacing rates only slightly faster than the tachycardia cycle length are used in clinical practice to limit these negative effects[126]. The timing of the local signal needed for postpacing interval measurements can also be difficult to determine. The presence of far-field potentials and low-amplitude fractionated electrograms can complicate interval measurements[38], [126], [134]. During high stimulus pacing, part of the circuit can be captured that does

not correspond to the to the area producing the local electrogram, rendering the post pacing interval difficult to analyze[38].

Entrainment mapping can overestimate the size of the isthmus by up to 50%[4]. The technique has been found to exaggerate the exit area of the isthmus with concealed QRS fusion combined with PPI-TCL below 30 ms occurring beyond the distal curvature of the isthmus[4]. After taking into account these limitations, entrainment mapping remains an important technique to improve our understanding of ventricular reentry circuits and its critical components[4], [38], [85], [126], [134].

l. Pace Mapping

i. Definition

Pace mapping consists of stimulating the myocardium and analyzing the induced ECG signal, the 12-lead morphology and the S-QRS interval. The conduction delay and QRS configuration reflects the pacing site location and electrical properties[129], [135]. It is important to take into account waveform amplitude as well as QRS morphology when comparing two signals[133], [136]. This comparison is quantified with a dedicated software[136]. A commonly used metric is the correlation calculation $CORR$ as shown in $equation\ (3)$ between vectors X and Y, each composed of 12 leads X_i and Y_i[136]. The software is designed to find the best possible match by sliding the two signals over each other and then selecting the position that provides the highest score. The maximum correlation score is 1 and represents a perfect match whereas the minimum possible is -1 and represents the worst possible match for example in case of similar amplitude but with opposite polarity[137]. Initially, the two waveforms were only compared visually by human interpretation but an objective quantitative approach was developed to provide a metric reducing operator bias and subjectivity especially by enabling the quantification of subtle amplitude or precordial lead transition differences between two ECG patterns[136], [138]. Before the use of correlation scores, visual comparisons could lead to the conclusion that pacing over an area up to 4 cm2 produced similar QRS patterns[139]. Subtle changes can now be precisely quantified and more recent studies have shown that correlation values decrease with distance, even when pacing sites are separated by just a few mms[136], [140].

$$CORR = \frac{\sum_{i=1}^{12}(X_i-\bar{X})\times(Y_i-\bar{Y})}{\sum_{i=1}^{12}(X_i-\bar{X})^2\times\sum_{i=1}^{12}(Y_i-\bar{Y})^2} \quad (3)$$

The PASO™ Module (Biosense Webster Inc., Diamond Bar, USA) enables the visualization of 3D pace maps, the correlation value of the paced signal with the tachycardia QRS being associated via a color code to the 3D localization of each pacing site. This technique of generating color coded maps of correlation values between the paced signal and the tachycardia is widely used when the targeted arrhythmia is hemodynamically unstable, preventing activation or entrainment techniques. Standard pace mapping only requires one QRS complex of the tachycardia[45].

ii. Pacing parameters

Pacing is generally performed by bipolar rather than unipolar pacing[45], [90]. The advantage of bipolar pacing is smaller stimulus artifacts simplifying the analysis of the early portion of the QRS complex[141]. The drawback of bipolar pacing is the potential and unmeasurable shift of the effective site of stimulation away from the catheter tip and towards the proximal electrode as the activation at the anode may coexist or merge with the distal cathodal excitation[141]. This shift can modify the effective area of impulse and thus slightly change the paced QRS morphology[139]. The shift is increased as the pacing current and interelectrode spacing increases but remains minor when the interelectrode distance is 5 mm[141].

The pacing parameters generally used are 10 mA with a 2 ms pulse width at a pacing cycle length similar to that of the clinical VT[45], [90], [137]. Pacing thresholds depends on the underlying tissue as they increase in scar areas and decrease in healthy myocardial tissue. To avoid capture over a too large area, some studies involve checking the pacing threshold at each site to then set the stimulus strength either slightly greater or at twice the threshold[45], [90], [137]. This increases accuracy and may better simulate a point source but at the cost of time-consuming less practical pacing maneuvers for each pacing point. Some studies pace at strong current strengths depolarizing large areas to better simulate a propagating wave front emerging from an exit site[142], [143]. Overall, major current dependent differences are uncommon[141]. The pacing rate has an influence on the QRS morphology and pacing at a rate close to the tachycardia is desirable[45], [144]. If the pacing cycle length differs by more than 80 ms, the accuracy of the pace map will be reduced as the QRS morphology can be rate dependent[136].

iii. Identifying the VT circuit

When a site inside a defined isthmus is paced, the wavefront propagates along the protected channel and follows at least two directions, the orthodromic and antidromic direction of the VT. If the pacing site is located near the exit, the orthodromic wave leaves the channel first and depolarizes the region close to the exit area of the isthmus, resulting in a similar QRS morphology to the VT. If the pacing site is located near the entrance, the antidromic wave leaves the channel first, producing a very different QRS morphology[45], [132], [135], [145], [146].

Pace-mapping is very helpful in identifying the critical sites of the isthmus[45], [106], [137]. The high correlation sites, with an average correlation score of 89%, best matching the VT morphology are located in the exit zone of the isthmus whereas the neighboring sites with much lower correlation values, with an average of 39%, are located in the entrance zone (figure 11)[137]. The speed of change in correlation values provides further information on the VT isthmus location. A gradual change is seen when moving

from the exit zone to the outer exit zone along the direction of the tachycardia circuit. The abrupt change from good to poor values further helps in determining the isthmus orientation by defining the transition from the exit to the entrance zone[137]. This abrupt change cannot be seen during concealed entrainment maneuvers during VT. Indeed, regardless of the pacing position along the isthmus, the activation will propagate in the orthodromic direction leading to a similar QRS morphology to the VT. In the antidromic direction, the wave collides with the orthodromic wavefront of the previous cycle. The propagation does not take the shortest path to the healthy myocardium but will reach the myocardium at the exit zone of the tachycardia[137], [139]. This is consistent with the fact that the S-QRS interval during pacing in sinus rhythm is shorter than during VT[132].

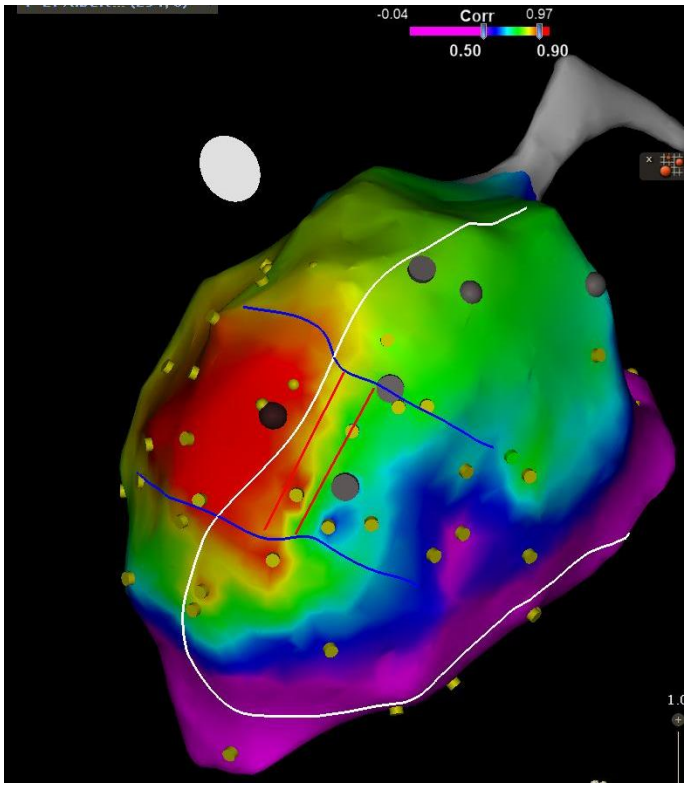

Figure 11. Pace-mapping helps identify the isthmus. High correlation sites are marked in red and are located in the exit zone. Neighboring sites with much lower correlation are located in the entrance zone (Biosense Webster Inc., Diamond Bar).

A suggested workflow to determine the VT isthmus through pacemapping is to first identify the sites with the highest correlation values corresponding to the isthmus exit. Then neighboring sites (10–15 mm) are paced to find the low correlation zone corresponding to the isthmus entrance[137]. A voltage map and all the information it contains can further guide the pacing strategy. The exit site is likely to be located in a

border zone between low and high amplitude points[106], [108]. Isolated and very late potentials with long electrogram durations are more likely to be located in the isthmus[105], [106], [132].

Pace mapping in sinus rhythm also provides a measure of slow conduction, determined by the interval between the stimulus and the QRS complex, the S-QRS interval. Pacing sites with long S-QRS values slowly conduct to healthy myocardium and can be located in a potential isthmus or adjacent to regions of conduction block[135], [146]. S-QRS intervals above 40 ms are associated with critical sites and have been used to help identify reentry circuits[129]. The reentry circuit exit zone, close to the infract border, will exhibit low S-QRS intervals[146].

Pacing also enables the identification of unexcitable scar that creates conduction block, a critical component for reentry circuit. The lack of capture with a high stimulus strength (20 mA) and a large virtual electrode radius marks the zone as unexcitable[90]. Pacing provides complementary information to electrogram amplitude in defining likely conduction block areas, potentially facilitating the identification of reentry circuits.

Pacing provides valuable information to identify the VT isthmus, facilitating targeted ablation[86], [137]. RF lesions can be deployed to transect the isthmus, interrupting a critical portion of the reentrant circuit [137]. One the ablation has been performed, pacing maneuvers can be used to confirm the block. If the exit zone has been successfully ablated, pacing form a neighboring site within the isthmus after ablation will exhibit a very different QRS morphology and a longer SQR interval compared to before ablation[137], [147]. If a second ablation line along the entrance zone is also made, both lines can be checked by making sure that the stimulation pacing from a site between the entrance and the exit does not reach healthy myocardium.

iv. Limitations of pace mapping

One limitation of interpreting pacing information is when multiple different QRS morphologies are produced during the same pacing drive. The multiple morphologies complicate the analysis of the activation pattern from the site. A single study in 2012 reported that multiple QRS morphologies in a given pacing site were observed in 57% of patients[143]. This high percentage not reported in other studies might be in part due to the intermittent contact at the tip of the catheter, leading to intermittent capture. The study was done before the introduction of contact catheters. Another challenge to pacing maneuvers is to fully understand the electrical properties of the analyzed myocardium to then unmask potential VT circuit mechanisms. Pacing from a point source may not mimic a broad wavefront of a reentrant tachycardia[146]. For example, functional blocks present during tachycardia need to be also identified

during pacemapping in sinus rhythm. The differences between the two mechanisms need further study. Moreover, it is difficult to estimate the virtual pacing electrode of a given pacing site, complicating the differentiation between near and far myocardial capture[143]. Pace mapping technique is currently time consuming but future multielectrode catheter designs will facilitate and accelerate the creation of pace maps[137]. A final limitation that has been reported is the induction of the tachycardia itself during pacing maneuvers[145]. This is not an issue as an activation map can then be created to further understand the arrhythmia. The initiation of the tachycardia is most frequent when pacing close to the exit zone, the late and slowed conduction along the isthmus facilitating VT induction[143].

Part 2: Novel reference-less pace-mapping methods for identifying VT circuits

Ischemia modifies the conduction of electrical impulses in the ventricle and can create the necessary conditions for reentry tachycardia. The onset and the stability of a given reentrant circuit is determined by the overall conducting properties of the circuit. Signal analysis in sinus rhythm, activation, entrainment and pace mapping have been developed to identify the tachycardia circuit but are considerably hindered when the tachycardia cannot be induced. The following section will look into novel methods to take the most advantage of the available information to identify the critical components of VT circuit mechanisms. These methods are reference-less mapping, improving signal quality, analyzing isthmus entrance characteristics, automating the workflow and graph-based reconstruction of activation patterns.

1) Correlation gradient mapping

In current clinical practice, the conventional pace mapping technique consists of stimulating the myocardium and comparing the 12-lead morphology of the induced ECG signal with a reference VT recording. The main challenge of the conventional technique is that a reference VT recording is required. Moreover, this technique highlights the circuit of the VT recording. Additional secondary circuits may occur that also warrant study. The following paper studies a novel reference-less pace-mapping method based solely on the analysis of the ECG data obtained during pace-mapping[148]. A local correlation map is defined by analyzing pairwise correlations between the paced QRS signals from a network of neighboring pacing sites. This reference-less method is proposed in order to quantify local changes in activation pathways. The electrical properties of the electric influx between two points does not depend on the selected reference VT recording. Abnormal points are identified by high correlation gradient values.

My main contribution to the paper was the acquisition of all the relevant pacing information into the CARTO® system. The current version of the CARTO® software only includes the correlation map so for each procedure I helped the cardiologist to “mentally” reconstruct the correlation gradient map. I was also responsible for anonymizing and exporting the data from the CARTO® to the in-house SMARTIS software, and provided support for interpreting all the exported CARTO® data (vendor-generated meshes, catheter positions, ECG data in sinus rhythm and pace-mapping, ablation data etc.). The work described later in this manuscript aimed at improving and extending the SMARTIS software, and the results of this first study were used as input data for the last two chapters in particular.

The conventional and reference-less method was evaluated retrospectively in 24 VT ablation procedures. The reference-less pace-mapping can accurately identify the same target zones as conventional pacemapping, plus additional zones that may cause other VT circuits. The abrupt change from good to poor values also helps in determining the isthmus orientation by defining the transition from the exit to the entrance zone. The reference-less method can be used in addition to the conventional method, and is especially useful to treat patients in whom VT cannot be induced during the intervention.

This article has been accepted for publication in a future issue of this journal, but has not been fully edited. Content may change prior to final publication. Citation information: DOI 10.1109/TBME.2019.2903631, IEEE Transactions on Biomedical Engineering

Catheter treatment of ventricular tachycardia: a reference-less pace-mapping method to identify ablation targets

Freddy Odille, Alberto Battaglia, Philip Hoyland, Jean-Marc Sellal, Damien Voilliot, Christian de Chillou, Jacques Felblinger, *Member, IEEE*

***Abstract*—*Objective*: A novel method is developed to identify ablation targets for the catheter treatment of ventricular tachycardia (VT). *Methods*: The method is based on pace-mapping, which is a validated technique to determine the catheter ablation targets. Conventionally, it consists of stimulating the heart ventricle from various sites and comparing the resulting activation pathways to that of a clinical VT, by analysis of surface electrocardiograms (ECG). In this work a novel pace-mapping method is presented, that does not require a reference ECG recording of the VT. A 3D correlation gradient map is reconstructed by semi-automatic analysis of ECG morphological changes within the network of pace-mapping sites. In these maps, abnormal points are identified by high correlation gradient values (i.e. corresponding to slow propagation of the electric influx, as in the core of the reentrant VT circuit). The relation between the conventional and reference-less method is described theoretically and evaluated in a retrospective study including 24 VT ablation procedures. *Results*: The "reference-less" method was able to identify normal points with a high accuracy (negative predictive value: NPV=97%) and to detect more abnormal points, as predicted by the theory. Correlation gradients computed by the proposed method were significantly higher in ablation zones than in other zones of the ventricle ($p<10^{-12}$), indicating excellent prediction of the ablation targets. *Significance*: The reference-less method might either be used in complement of the conventional method, or to treat patients in whom VT cannot be induced during the intervention.**

***Index Terms*—Arrhythmia, radiofrequency catheter ablation, cardiac interventional electrophysiology, electrocardiography.**

I. Introduction

PATIENTS who go through a myocardial infarction have a significant risk of developing, after several years, a ventricular tachycardia (VT), which is a life-threatening arrhythmia. The infarcted heart region indeed undergoes a remodeling process during which damaged myocardial tissue is replaced by fibrosis and evolves into a scar. This remodeling process impacts the conduction of electric currents, with the scar area containing zones of conduction block and slow conducting zones when surviving myocardial fibers are present. This heterogeneous setup has been shown to be the cause of VT through the creation of reentrant circuits in the ventricles [1]–[3]. The mechanism underlying a reentrant circuit is that an electric current comes out of the slow conduction zone with a delay greater than the myocyte refractory period, so that it can excite healthy myocytes again.

Catheter interventions have been developed for the treatment of VT. The procedure comprises a diagnosis part where the likely origin of the VT circuit is identified, and a treatment part where radiofrequency heating is applied locally in order to ablate the core of the reentrant circuit. The diagnosis part is crucial and can be performed by several approaches. Activation mapping is the most direct technique [4]–[7]. It consists of acquiring intra-cardiac electrical signals, termed electrograms, by moving the catheter to different points of the ventricles during a sustained VT. A 3D map of propagation delays between electrograms can then be reconstructed, which represents the activation pathway of the VT. Unfortunately, activation mapping can only be performed in a small number of patients who can tolerate a sustained VT for the whole duration of the mapping. Alternative methods, referred to as substrate mapping [8]–[12], attempt to identify the critical, slow conduction zones by studying the local electrical characteristics of the ventricle. This can be done by detecting abnormal electrograms (i.e. presence of late or fragmented potentials on electrograms acquired in normal sinus rhythm and/or after stimulation of the ventricles from various sites) [10], [12]. However the presence of such abnormal electrograms at a given site does not mean that this site can support a reentrant VT circuit. Besides, it is difficult with this technique to distinguish low amplitude electrograms from noise in dense fibrotic scar areas.

This study was funded by the French "Investments for the Future" program under grant number ANR-15-RHU-0004. The authors also thank INSERM, CPER 2007-2013, Région Lorraine and FEDER for the funding of the Niobe Magnetic Navigation System, Stereotaxis Inc. F. Odille and A. Battaglia contributed equally to this work. C. de Chillou and J. Felblinger contributed equally to this work.

F. Odille and J. Felblinger are with IADI, Inserm and Université de Lorraine, Nancy, France, and with CIC-IT 1433, Inserm, Université de Lorraine and CHRU Nancy, Nancy, France (e-mail: freddy.odille@inserm.fr and j.felblinger@chru-nancy.fr).

A. Battaglia and D. Voilliot are with CIC-IT 1433, Inserm, Université de Lorraine and CHRU Nancy, Nancy, France, and with Pôle Cardiologie, CHRU Nancy, Nancy France.

P. Hoyland is with with IADI, Inserm and Université de Lorraine, Nancy, France, and with Biosense Webster France, Johnson & Johnson, Issy-lès-Moulineaux, France.

J.-M. Sellal and C. de Chillou are with IADI, Inserm and Université de Lorraine, Nancy, France, and with Pôle Cardiologie, CHRU Nancy, Nancy France.

This article has been accepted for publication in a future issue of this journal, but has not been fully edited. Content may change prior to final publication. Citation information: DOI 10.1109/TBME.2019.2903631, IEEE Transactions on Biomedical Engineering

Pace-mapping is another technique which has been shown to be a good surrogate for activation mapping [13], [14]. Pace-mapping consists of stimulating the heart with the catheter from different sites of the ventricular cavity, in order to produce activation pathways originating from each of these sites. The exit site of the VT circuit is identified when the activation pathway best matches that of the clinical VT (previously recorded for that patient), i.e. when the surface electrocardiogram (ECG) obtained during pacing best matches the surface ECG recorded during the clinical VT. The core of the circuit was also shown to correspond to a zone of abrupt changes of the activation pathway [4]. The correlation coefficient between the QRS complexes is used as an objective metric for comparing VT morphologies recorded by a surface 12-lead ECG. In summary, the pace-mapping technique has several key advantages: (i) only a short ECG recording of the VT is necessary; (ii) the actual VT circuit can be reconstructed and visualized; (iii) after radiofrequency ablation, the ventricles can be stimulated again near the entrance of the circuit in order to demonstrate that the electric current cannot enter this circuit any longer, thus providing a feedback on the efficiency of the ablation lesion that was applied.

Despite all advantages of the pace-mapping technique, there are remaining challenges or disadvantages: (i) a reference VT recording is required, yet in some patients VT cannot be induced during the procedure or it is poorly tolerated, even during a short period of time; (ii) after a VT circuit is ablated by pace-mapping, in some cases a secondary circuit can occur (sometimes still during the procedure, sometimes after a few months).

In this work, a "reference-less" pace-mapping method is proposed in order to identify the target zones for ablation, relying solely on the ECG data recorded during pace-mapping. The rationale is to search for regions corresponding to abrupt changes of the activation pathway, by looking at surface ECG correlations between neighboring pacing sites, rather than looking at correlations between each pacing site and a clinical VT. Our hypothesis is that reference-less pace-mapping can accurately identify the same target zones as conventional pace-mapping, plus additional zones that may cause other VT circuits. The relation between conventional and reference-less pace-mapping is studied both theoretically and experimentally, by retrospective analysis of 24 VT ablation procedures performed with the conventional pace-mapping technique. The reference-less method was thereby compared to the conventional method in terms of performance for detecting ablation target zones, using a specially developed software tool providing semi-automatic analysis.

II. Theory

In this section we give a formal description of the conventional and proposed pace-mapping methods to identify ablation targets in macro-reentrant VT circuits, as those that can occur in ischemic VT patients.

A. *Conventional pace-mapping: ventricular tachycardia correlation mapping*

In the conventional pace-mapping method, a correlation map with the clinical VT, $\mathcal{C}_{PacedQRS/VT}$, is generated. The process for generating this map has been published previously [13] and is implemented in the CARTO system (PASO™ module of CARTO3®, Biosense Webster, Inc., Irvine, USA). We describe this process more formally in the following.

The correlation score at each point $\boldsymbol{x} = [x\ y\ z]$ is calculated as the Pearson correlation coefficient $c(.,.)$ between the QRS signal, $S^{lead}_{PacedQRS}(\boldsymbol{x})$, recorded right after pacing at site $\boldsymbol{x}$, and the QRS of the clinical VT, S^{lead}_{VT} (i.e. one user-selected cycle of the clinical VT recording), averaged over the 12 leads:

$$\mathcal{C}_{PacedQRS/VT}(\boldsymbol{x}) = \frac{1}{12}\sum_{lead=1}^{12} c\left(S^{lead}_{PacedQRS}(\boldsymbol{x}), S^{lead}_{VT}\right) \quad (1)$$

Areas of abrupt changes of the activation pathway can be identified by large values of the spatial gradient of the VT correlation map defined above. For a neighboring point located at $\boldsymbol{x}+\boldsymbol{\delta x}$, with $\|\boldsymbol{\delta x}\|$ sufficiently small ($\|\boldsymbol{\delta x}\| < 20$ mm in this study), the magnitude of the spatial gradient, by definition, can be estimated by:

$$\mathcal{G}_{PacedQRS/VT}(\boldsymbol{x}) = \left|\nabla \mathcal{C}_{PacedQRS/VT}(\boldsymbol{x})\right| \simeq \frac{\left|\mathcal{C}_{PacedQRS/VT}(\boldsymbol{x}+\boldsymbol{\delta x}) - \mathcal{C}_{PacedQRS/VT}(\boldsymbol{x})\right|}{\|\boldsymbol{\delta x}\|} \quad (2)$$

In the remainder, the correlation map $\mathcal{C}_{PacedQRS/VT}$ is expressed in percent units (%) and its gradient $\mathcal{G}_{PacedQRS/VT}$ in %/mm. Mathematically, the correlation gradient at a given point x of the heart surface represents the infinitesimal change that will be observed in the VT correlation score in response to moving the pacing catheter by an infinitesimal distance. A singularity is expected when the catheter is in a zone from where two distinct electrical pathways are equally possible. When pacing from the center of the VT circuit core zone, termed mid-isthmus line in the literature, the activation wavefront can propagate in either direction of the VT circuit (towards its entrance or towards its exit), as demonstrated and visualized in figure 3 of Ref. [14]. Note that this mid-isthmus line can even be met in practice by the cardiologist: when the catheter happens to be located exactly on the mid-isthmus line, changing the amplitude of the stimulation pulse can result in the activation wavefront to travel towards the entrance or towards the exit. This is because a larger pulse will stimulate of broader area, including cardiomyocytes across the mid-isthmus line, which is likely to give rise to the other possible pathway.

B. *Reference-less pace-mapping method*

A reference-less method is proposed in order to study changes in activation pathways, based solely on the ECG data obtained during pace-mapping. For each pacing site $\boldsymbol{x}$, a local correlation map $\mathcal{C}_{PacedQRS(\boldsymbol{x})}$ is defined that represents the correlation between paced QRS signals at site $\boldsymbol{x}$ and paced QRS signals in a small neighborhood of $\boldsymbol{x}$, i.e. any site $\boldsymbol{x}+\boldsymbol{\delta x}$, with $\|\boldsymbol{\delta x}\|$ sufficiently small ($\|\boldsymbol{\delta x}\| < 20$ mm as well):

This article has been accepted for publication in a future issue of this journal, but has not been fully edited. Content may change prior to final publication. Citation information: DOI 10.1109/TBME.2019.2903631, IEEE Transactions on Biomedical Engineering

$$\mathcal{C}_{PacedQRS(\boldsymbol{x})}(\boldsymbol{x}+\boldsymbol{\delta x}) = \frac{1}{12}\sum_{lead=1}^{12} c\left(S^{lead}_{PacedQRS}(\boldsymbol{x}), S^{lead}_{PacedQRS}(\boldsymbol{x}+\boldsymbol{\delta x})\right) \quad (3)$$

The spatial gradient of this local correlation map can be estimated between each pair of neighboring sites $\boldsymbol{x}$ and $\boldsymbol{x}+\boldsymbol{\delta x}$ by:

$$\begin{aligned}\mathcal{G}_{PacedQRS/PacedQRS}(\boldsymbol{x}, \boldsymbol{x}+\boldsymbol{\delta x}) &= \left|\nabla \mathcal{C}_{PacedQRS(\boldsymbol{x})}(\boldsymbol{x}+\boldsymbol{\delta x})\right| \\ &\simeq \frac{\left|\mathcal{C}_{PacedQRS(\boldsymbol{x})}(\boldsymbol{x}+\boldsymbol{\delta x}) - \mathcal{C}_{PacedQRS(\boldsymbol{x})}(\boldsymbol{x})\right|}{\|\boldsymbol{\delta x}\|} \\ &= \frac{\left|\mathcal{C}_{PacedQRS(\boldsymbol{x})}(\boldsymbol{x}+\boldsymbol{\delta x}) - 100\%\right|}{\|\boldsymbol{\delta x}\|} \\ &= \left|\left(\frac{1}{12}\sum_{lead=1}^{12} c\left(S^{lead}_{PacedQRS}(\boldsymbol{x}), S^{lead}_{PacedQRS}(\boldsymbol{x}+\boldsymbol{\delta x})\right)\right) - 100\%\right| / \|\boldsymbol{\delta x}\|\end{aligned} \quad (4)$$

In the equation above, $\mathcal{C}_{PacedQRS(\boldsymbol{x})}(\boldsymbol{x})$ is the correlation between pacing site $\boldsymbol{x}$ and itself, i.e. 100%.

There is a relation between the correlation gradient maps obtained by the conventional method, $\mathcal{G}_{PacedQRS/VT}$, and by the reference-less method, $\mathcal{G}_{PacedQRS/PacedQRS}$. This relation can be explained by the following thought experiment. Let us consider two neighbor pacing sites $\boldsymbol{x_1}$ and $\boldsymbol{x_2}$ that give rise to a highly similar activation, i.e. $\mathcal{C}_{PacedQRS(\boldsymbol{x_1})}(\boldsymbol{x_2}) \simeq 1$. Then the respective correlation of $\boldsymbol{x_1}$ and $\boldsymbol{x_2}$ with the reference VT must be similar, i.e. one must have $\mathcal{C}_{PacedQRS/VT}(\boldsymbol{x_1}) \simeq \mathcal{C}_{PacedQRS/VT}(\boldsymbol{x_2})$ (and consequently $\mathcal{G}_{PacedQRS/VT}(\boldsymbol{x_1}) \simeq 0$). Conversely, if $\boldsymbol{x_1}$ and $\boldsymbol{x_2}$ give rise to a different activation, i.e. $\mathcal{C}_{PacedQRS(\boldsymbol{x_1})}(\boldsymbol{x_2}) \ll 1$, then one cannot conclude about their similarity to the clinical VT, e.g. one could have $\mathcal{C}_{PacedQRS/VT}(\boldsymbol{x_1}) \simeq \mathcal{C}_{PacedQRS/VT}(\boldsymbol{x_2})$ (the morphology of paced QRS no.1 and paced QRS no.2 are equally similar/dissimilar to that of the VT) or $\mathcal{C}_{PacedQRS/VT}(\boldsymbol{x_1}) \neq \mathcal{C}_{PacedQRS/VT}(\boldsymbol{x_2})$ (the morphologies of paced QRS no.1, paced QRS no.2 and the VT are all different from one another).

In practice, in healthy myocardium, i.e. away from the core of a reentrant VT circuit, subtle changes in the depolarization wavefront are expected when moving the pacing catheter from one site to its neighbors. Therefore one should have $\mathcal{G}_{PacedQRS/VT} \simeq 0$ and $\mathcal{G}_{PacedQRS/PacedQRS} \simeq 0$. Only within the core of the VT circuit (called isthmus in the literature), marked transitions have been observed in the VT correlation map [13]. As a result, such transition zones, identified by large values in the $\mathcal{G}_{PacedQRS/VT}$ map, must also show large values in the $\mathcal{G}_{PacedQRS/PacedQRS}$ map. However the converse of this statement is not true, so it is expected that large values in $\mathcal{G}_{PacedQRS/PacedQRS}$ are present which may or may not correspond to large values in $\mathcal{G}_{PacedQRS/VT}$.

III. METHODS

A. Patient population

Nineteen consecutive patients (13 men, mean age = 59 ± 12 years) referred for post-infarct VT catheter ablation between March 2016 and October 2017 were included in this retrospective, non-interventional study. Inclusion criteria were: (i) presence of a spontaneous sustained monomorphic VT documented by a 12-lead ECG which was subsequently inducible during the electrophysiological study; (ii) identification of the VT isthmus by the pace-mapping technique [13] using the CARTO3® PASO™ software (Biosense Webster, Inc., Irvine, USA) and (iii) confirmation that radiofrequency catheter ablation lesions applied across the VT isthmus prevented further VT induction. The study was granted a waiver by our institutional review board due to its retrospective, non-interventional nature. The storage of anonymized data was declared to the French data protection authority (CNIL).

All 24 procedures were performed with the Niobe® robotic magnetic navigation system (Stereotaxis Inc., St. Louis, USA). The electrophysiologic mapping and the radiofrequency ablation were performed as previously described[5], [13], [15].

In all procedures, at least one scarified area was detected (<1.5mV bipolar voltage). Its mean area was 38.1 ± 28.4 cm^2, representing 16.7% (± 10.9%) of the total left ventricle surface. VT was induced by programmed electrical stimulation, with the catheter placed in the right ventricular apex. This was done by application of up to 3 extrastimuli during spontaneous rhythm (600-ms and then 400-ms basic cycle length). Failure to induce a sustained VT promoted the same protocol from another site (alternatively right ventricle outflow tract or left ventricle). Pace-mapping was performed in a bipolar configuration (600 ms cycle length) with the output delivered at twice the diastolic threshold.

B. Automated software processing

Anonymized data were exported from the CARTO3® workstation and were processed using an in-house software for smart isthmus identification (SMARTIS) written in MATLAB language (The Mathworks, Natick, USA). Electro-anatomic data were first loaded into the software, including: 12-lead ECG data acquired during sinus rhythm, during the induced clinical VT, and during pace-mapping (2.5 s of ECG recording at each pacing site); catheter positions corresponding to all these recordings; high-resolution vendor-generated 3D meshes of the ventricular cavity, as well as 3D meshes of the bipolar and unipolar voltage maps derived from the electrograms acquired in sinus rhythm. All correlation gradient maps used in this study (conventional and reference-less method) were generated offline with the MATLAB software, as described hereafter.

This article has been accepted for publication in a future issue of this journal, but has not been fully edited. Content may change prior to final publication. Citation information: DOI 10.1109/TBME.2019.2903631, IEEE Transactions on Biomedical Engineering

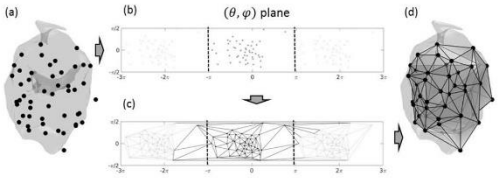

Fig. 1. Raw points where catheter stimulation is applied (i.e. pacing sites) (a); conversion to polar coordinates and planisphere representation (b); Delaunay triangulation in $(\boldsymbol{\theta}, \boldsymbol{\varphi})$ plane (c); raw triangular surface mesh identifying connections between neighboring pacing sites (d).

1) Raw mesh generation

First a 3D surface mesh was generated from the raw pace-mapping sites, which will be called raw mesh. As illustrated in Fig. 1, the coordinates $\boldsymbol{x} = [x\ y\ z]$ of the pacing sites were converted into polar coordinates $[r\ \theta\ \varphi]$ (with the origin being the center of gravity of all pacing sites). Then a 2D Delaunay triangulation was performed in the (θ, φ) plane in order to establish connections between neighboring pacing sites. To ensure circular continuity of the connections in the "longitude" direction θ, the (θ, φ) plane was extended at its edges with $(\theta \pm 2\pi, \varphi)$. The resulting list of triangle connections was used to connect the pacing sites in the 3D space and form the raw 3D surface mesh. On average, there were 61 pacing sites per procedure, and 179 pairs of connected pacing sites, including 121 pairs of sites separated by a distance below the distance threshold defined for our analysis, $D_{max} = 20\ mm$.

2) Correlation and correlation gradient meshes

The generation of correlation and correlation gradient maps is illustrated in Fig. 2 and Fig. 3.

The VT correlation mesh generation from the raw mesh is straight-forward. Provided correlation scores have been calculated between each pacing site and the clinical VT (details in the next paragraph), a color is assigned to each vertex of the raw mesh in order to form the VT correlation map. For better visualization, this map is finally projected onto the high-resolution anatomical mesh provided by the vendor (using nearest-neighbor interpolation), as illustrated in Fig. 2. For final visualization of the 3D map, the rendering engine (still within MATLAB in this study) was set to use linear interpolation of values defined at each vertex of the high resolution mesh, as it is done in the vendor's CARTO3® software.

Correlation gradient maps were calculated on an intermediate mesh, defined by subdivision of the triangles in the raw mesh: each triangle of the raw mesh identifies connections between 3 pacing sites, and is further divided into 3 subtriangles (see Fig. 2d and Fig. 3d). Each subtriangle is mapping an area between 2 neighboring pacing sites and is then assigned a color code corresponding to the correlation gradient between these two sites (either $\mathcal{G}_{PacedQRS/VT}$ or $\mathcal{G}_{PacedQRS/PacedQRS}$, using formulas in equations (2) and (4)). When the distance between two pacing sites is greater than D_{max} ($D_{max} = 20\ mm$), a neutral color is assigned (white). Finally, the correlation gradient map is projected onto the high-resolution anatomical mesh and visualized in the same way as described for the VT correlation map.

3) Automated alignment of ECG signals

Automatic ECG alignment was proposed in order to compare the morphology of a paced QRS signal with either the reference VT recording or paced QRS signals from its neighboring sites.

This alignment is necessary because there a variable delay between the stimulation spike and the QRS onset (i.e. the start of ventricular activation), depending on the presence of slow conducting zones. The automatic alignment procedure consisted of the following steps: (i) automatic detection of stimulation spikes in the ECG using basic signal processing techniques (convolution of the ECG signal with a spike template, thresholding to produce a binary signal, and front edge detection); (ii) QRS peak detection after each spike, by a maximum search in the module of a synthetic vectorcardiogram reconstructed from the 12-lead ECG, using inverse Dower transformation [16], [17] (www.mit.edu/~gari/CODE/DOWER/idowerT.m); (iii) initial alignment of the two QRS signals based on the detected QRS peaks; (iv) refined alignment by maximization of the cross-correlation function [18]; (v) calculation of the correlation coefficient, averaged over the 12 ECG leads, using either equation (1) or (3). It should be noted that, in the reference-less method, several QRS complexes are present in each 2.5 s recording (i.e. at one given pacing site). Therefore all possible combinations of QRS complexes from the two pacing sites were computed, and finally the paced QRS pair providing the highest correlation score (in absolute value) was selected. For all QRS correlation calculations, a temporal window needed to be defined: for the conventional method, it was set to the duration of the clinical VT cycle (one user-selected cycle of the sustained VT recording); for the reference-less method, it was set to 300 ms.

The software tool allowed visualization of all aligned signals. An experienced interventional cardiologist was asked to review all aligned ECG signals (paced QRS against clinical VT, and paced QRS against their neighbors) and to correct the alignment when necessary (thereby updating the correlation scores).

C. Validation

1) Automated processing

The efficiency of the automated processing was assessed by statistics of QRS signals that needed manual correction by the cardiologist. The correction was considered to be necessary when a mismatch greater than 10% in the correlation score was found between the automatic and the manual QRS alignment.

2) Comparison with activation mapping

In one of the patients (patient 1) the VT was hemodynamically well tolerated. Therefore an actual activation map was also acquired by mapping the delay between a reference time in the VT cycle and the local activation time, as detected by a signal peak on the electrograms, for each location of the catheter within the ventricle. The proposed reference-less correlation gradient map was then visually compared to the reconstructed activation map. In particular the location of the abnormal zone, as detected by the proposed method, was superimposed to the trajectory of the activation wavefront, shortly before entering the core of the reentrant circuit, during traversal of the core and shortly after.

This article has been accepted for publication in a future issue of this journal, but has not been fully edited. Content may change prior to final publication. Citation information: DOI 10.1109/TBME.2019.2903631, IEEE Transactions on Biomedical Engineering

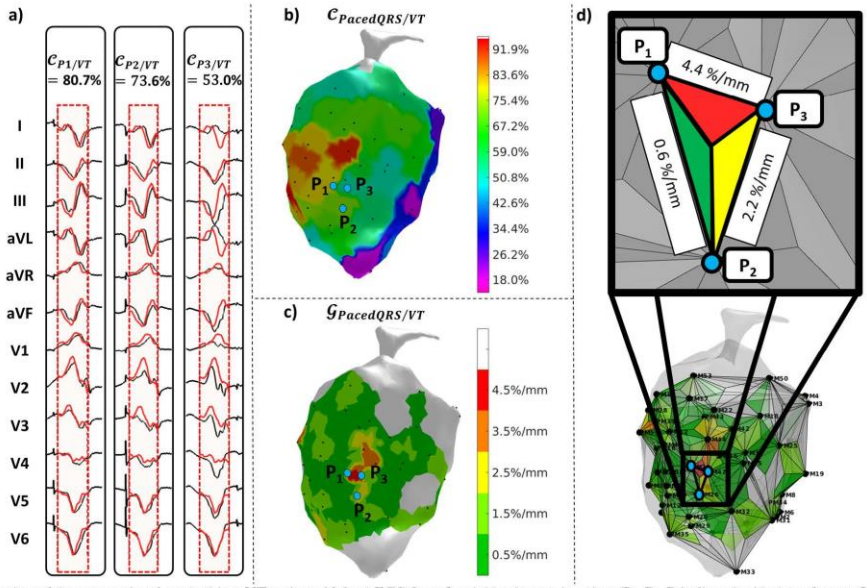

Fig. 2. Illustration of the conventional method in a VT patient: 12-lead ECG from 3 neighboring pacing sites (P_1, P_2, P_3) aligned with the reference VT signal (red signals) for correlation coefficient calculation (a); VT correlation map $C_{PacedQRS/VT}$, i.e. a surrogate for the VT activation map (b); VT correlation gradient map $G_{PacedQRS/VT}$, highlighting marked transitions in the VT correlation map (i.e. slow propagation zones in the core of the VT circuit) (c); intermediate mesh (with triangle subdivision) used to generate the gradient correlation map from equation (2) (d).

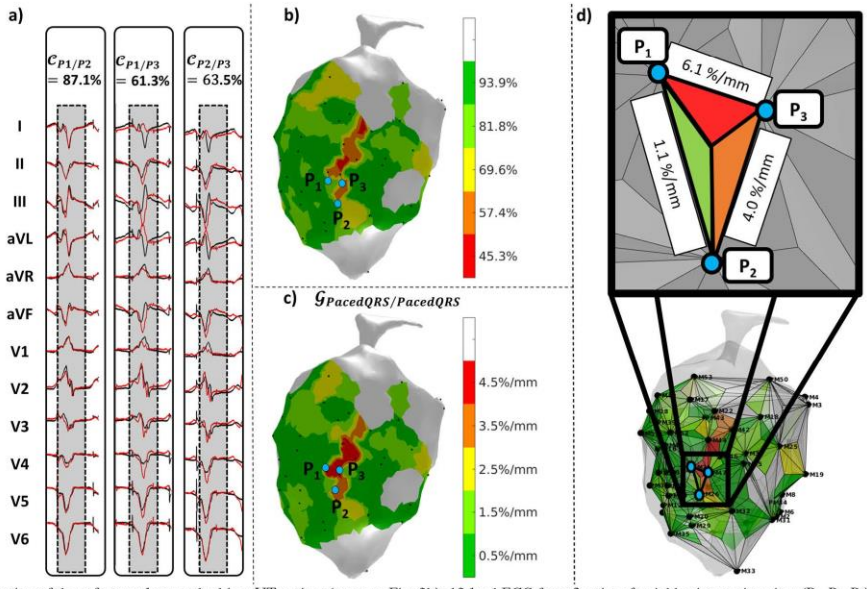

Fig. 3. Illustration of the reference-less method in a VT patient (same as Fig. 2h): 12-lead ECG from 3 pairs of neighboring pacing sites (P_1, P_2, P_3) aligned with each other for pair-wise correlation coefficient calculation (a); pair-wise correlation map representing correlation between neighboring pacing sites (b); reference-less correlation gradient map $G_{PacedQRS/PacedQRS}$, highlighting marked transitions corresponding to slow propagation zones in the core of the VT circuit (c); intermediate mesh (with triangle subdivision) used to generate the gradient correlation map from equation (4) (d).

This article has been accepted for publication in a future issue of this journal, but has not been fully edited. Content may change prior to final publication. Citation information: DOI 10.1109/TBME.2019.2903631, IEEE Transactions on Biomedical Engineering

3) Comparison of the conventional and reference-less methods

In order to compare the reference-less method with the conventional method, areas showing abnormal correlation gradients with the two methods were identified and compared. Cut-off values needed to be defined in order to discriminate between normal and abnormal correlation gradient values.

Normal correlation gradient values were determined for both methods using data measured in healthy myocardium only (sites where bipolar voltage was greater than 2 mV and unipolar voltage greater than 8 mV) using the same patient population. This was done by calculating the histogram of correlation gradient values and by calculating the 95th percentile, corresponding to the value below which 95% of correlation values in healthy myocardium lied. Correlation values above these cutoffs were considered abnormal. The ability of both methods to detect normal/abnormal regions was compared using common statistics for binary classifiers (using $\mathcal{G}_{PacedQRS/VT}$ as the ground truth), including the negative predictive value (NPV), the positive predictive value (PPV), the sensitivity (Se) and specificity (Sp).

4) Agreement between identified zones and actual ablation sites

Finally, the relevance of the identified zones (from both methods) was assessed by retrospective analysis of the sites that were actually targeted by radiofrequency ablation during the procedure. The mean value of correlation gradients ($\mathcal{G}_{PacedQRS/VT}$ and $\mathcal{G}_{PacedQRS/PacedQRS}$) in the areas that were subsequently ablated (called ablation sites) was compared to that in the non-ablated areas (all other sites in the ventricle) and in the non-ablated areas within the scar region (identified as regions with bipolar voltage < 1.5 mV or unipolar voltage < 8 mV). The actual ablation zone was in general larger than the transition zone identified on the conventional VT correlation map, depending on the chosen ablation strategy. However it is expected that the ablation zone comprises a larger proportion of areas with abnormal correlation gradients. Differences in correlation gradients between ablated and non-ablated regions were tested for statistical significance using two-sample t-test, with a significance level set to 5%.

5) Sensitivity analysis

The proposed method relies on several key parameters which may impact the generated maps and thereby the identified target zones. We analyzed the sensitivity of the method to the following parameters: (i) sampling density of the pacing sites; (ii) distance threshold (above which correlation gradients are considered unreliable); (iii) ECG alignments errors; (iv) ECG lead averaging mode used in the correlation calculation process (average of the 12 leads, or various other lead combinations). The detailed methods for the sensitivity analysis are given in a supplementary file.

IV. Results

A. Automated processing of ECG data

Before and after correction of the automated ECG alignment, correlation scores showed differences, expressed as mean ± standard deviation, of -3.5% ± 23.3% (conventional method, i.e. correlation between paced QRS and clinical VT) and -2.3% ± 13.9% (reference-less method, i.e. correlation between paced QRS and their neighbors). Manual correction was necessary in 28.5% of cases with the conventional method and in 12.5% of cases with the reference-less method. The automatic alignment was more reliable when the QRS complexes to be compared had similar morphologies, as indicated by the lower correlation scores in datasets for which correction was necessary (average correlation of 19.3%/32.1% for the conventional/reference-less method) compared to datasets for which the automatic alignment was satisfactory (average correlation of 60.5%/81.1%).

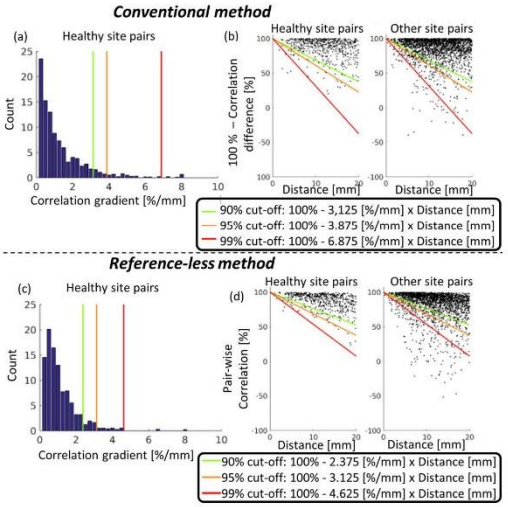

Fig. 4. Histogram showing the distribution of correlation gradient values in pairs of healthy myocardium pacing sites, as computed with the conventional (a) and proposed (c) method. Relation between correlation and distance in healthy pacing site pairs and in other pacing site pairs (b and d). The green (respectively orange and red) slope on (b) and (d) graphs indicate cutoff values above which 90% (respectively 95% and 99%) of healthy site pairs lie. Conversely, pacing site pairs below these cutoffs are considered to be abnormal.

B. Normal values of correlation gradients

The distribution of correlation gradient values in healthy myocardium, computed with both methods, is shown in Fig. 4. The histograms show very low values in general with both methods (Fig. 4a and 4c). Cutoff values are shown on the histograms, below which 90% (respectively 95% and 99%) of the pairs lie. Another representation of this distribution is shown in Fig. 4b and 4d, where correlation values are further plotted against the distance between pacing sites. In these graphs, the correlation gradient cutoff values correspond to the slope of a linear function. When plotting other (i.e. non-healthy) pacing site pairs, a small portion of pairs appear below the defined cutoff values and can be considered as abnormal.

The 95% cutoff values were used in the remainder of the study to classify normal/abnormal correlation gradient values: $\mathcal{G}^{normal}_{PacedQRS/VT} = 3.875\ \%/mm$ and $\mathcal{G}^{normal}_{PacedQRS/PacedQRS} = 3.125\ \%/mm$.

This article has been accepted for publication in a future issue of this journal, but has not been fully edited. Content may change prior to final publication. Citation information: DOI 10.1109/TBME.2019.2903631, IEEE Transactions on Biomedical Engineering

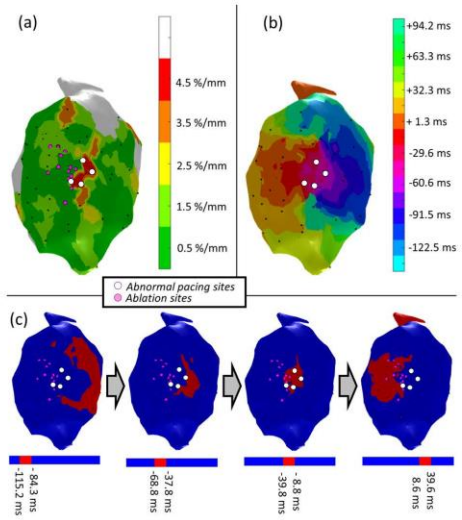

Fig. 5. Comparison between the reference-less correlation gradient map (a) and the actual VT activation map (b) obtained in patient 1. The activation map is representing the local activation time in ms. The activation wavefront (c) is derived from the activation map and shows the activated areas at different time windows of the VT cycle, from left to right: before entering the core zone of the reentrant circuit, during its entrance and traversal, and shortly after. The precise location of four pacing sites surrounding the target zone, as identified by the proposed method, is indicated by the four white spots on all maps. Ablation sites that actually terminated the VT were determined by conventional pace-mapping and are indicated as pink spots.

C. *Validation of the reference-less method against activation mapping*

The reference-less correlation gradient map generated for patient 1 is shown in Fig. 5, together with the actual activation map of the VT. On the proposed map, one region is identified as abnormal (i.e. above the threshold given in the previous section) and is color-coded in red. Four pacing sites are located in the direct neighborhood of this abnormal region and are highlighted as white spots. On the activation map, it can be seen that the region between the four spots precisely corresponds to the entrance into the core of the reentrant VT circuit. Indeed on the activation map (Fig. 5b), the blue regions are first activated, corresponding to the entrance into the circuit, then a narrowing of the activation wavefront is observed towards the purple and red regions, corresponding to the core of the VT circuit. Finally, the activation wavefront evolves faster towards the orange region, corresponding to the exit of the circuit. Note that the activation time is relative to the exit of the VT circuit (activation time t=0), which corresponds to the onset of the QRS complex of the VT. The narrowing of the activation wavefront may be better observed in Fig 5c, were the region of activated myocardium is shown at different times of the VT cycle. A full video of this activation sequence is provided as supplementary material. These show that the identified abnormal region precisely corresponds to the critical part of the VT circuit, i.e. to its core entrance.

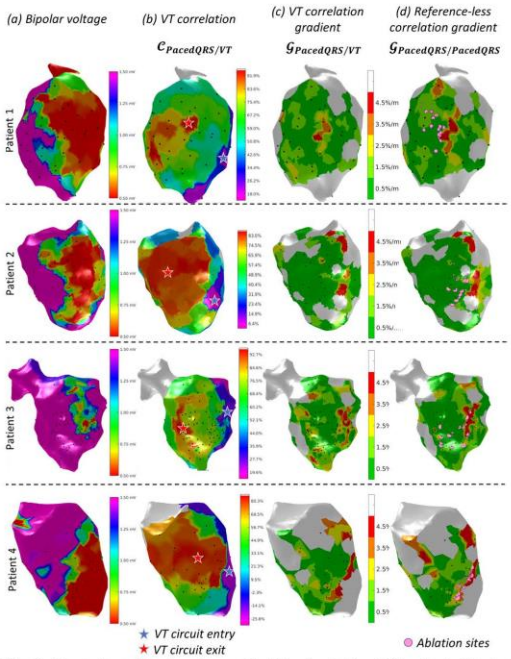

Fig. 6. Illustration of the target zone identification in four VT patients: bipolar voltage map, with low voltage (red) representing the scar region (a); VT correlation map, with highest correlation indicating the VT circuit exit (red star), and lowest correlation indicating the entrance (blue star) (b); VT correlation gradient map (c) and reference-less correlation gradient map (d) indicating critical zones of slow conduction (red), i.e. potential ablation targets identified by the conventional and proposed method respectively. Actual ablation sites that were destroyed to terminate the VT were determined by conventional pace-mapping and are indicated as pink spots.

D. *Comparison of the conventional and reference-less methods*

Example correlation gradient maps obtained in four representative patients with the conventional and reference-less method are shown in Fig. 6. Along with these maps, the bipolar voltage map is shown in order to visualize the scar area, as well as the VT correlation map which is used by the clinician. Visually, there was a good match between correlation gradient maps from the two methods, with most of the myocardium appearing with green color (low gradient values) and small portions of the maps (yellow to red color) showing larger correlation gradients with the two methods.

TABLE I
AGREEMENT BETWEEN THE CONVENTIONAL AND REFERENCE-LESS METHOD FOR CLASSIFYING NORMAL/ABNORMAL CORRELATION GRADIENT VALUES (MAPS FROM 24 PROCEDURES, 9739 MESH VERTICES IN TOTAL).

Conventional* \Reference-less	Normal	Abnormal
Normal	TN=8193	FP=753
Abnormal	FN=244	TP=549

TN=true negative ; FN=false negative ; FP=false positive ; TP=true positive

*The conventional method is used as the reference standard here

This article has been accepted for publication in a future issue of this journal, but has not been fully edited. Content may change prior to final publication. Citation information: DOI 10.1109/TBME.2019.2903631, IEEE Transactions on Biomedical Engineering

TABLE II
CORRELATION GRADIENT VALUES MEASURED RETROSPECTIVELY AT THE ABLATION SITES AND AT OTHER SITES OF THE VENTRICLE (DATA FROM 24 PROCEDURES). RESULTS ARE EXPRESSED AS MEAN (± STANDARD DEVIATION).

	Ablation sites[1]	All non-ablation sites (whole ventricle)	All non-ablation sites within scar
Total number of mesh vertices	1382	77228	74924
VT correlation gradient [%/mm]	1.64 (± 3.14)	1.38 (± 1.85) $p=8.10^{-6}$ *	1.40 (± 1.87) $p=3.10^{-5}$*
Reference-less correlation gradient [%/mm]	1.80 (±2.73)	1.41 (± 1.69) $p=7.10^{-14}$ *	1.42 (± 1.70) $p=9.10^{-13}$ *

[1]Values measured at the spatial coordinates of ablation sites, before actual ablation
*Statistically significant difference with the 'Ablation sites' column

Quantitative comparison of the correlation gradient maps, using the 95% cutoff values defined in the previous section to classify normal/abnormal values, is summarized in Table I. As expected, more abnormal points were detected with the reference-less method (1302) than with the conventional method (793). Other relevant metrics derived from these raw data, include: the negative predictive value, NPV=97% (i.e. 97% of point classified as normal with the proposed method are indeed normal with the conventional method); the positive predictive value, PPV=42% (i.e. 42% of point classified as abnormal with the proposed method are indeed abnormal with the conventional method); sensitivity, Se=69%; specificity, Sp=92%.

E. Agreement between identified zones and actual ablation sites

The correlation gradients values measured retrospectively in the ablation sites and in other sites are given in Table II. Gradient values in the ablation sites were higher than in the rest of the ventricle and higher than in non-ablation sites within the scar. These differences were significant with both the conventional method ($p<10^{-4}$) and with the reference-less method ($p<10^{-12}$).

F. Sensitivity analysis

Detailed results of the sensitivity analysis are given in the supplementary material. To summarize, the method was found to be relatively robust to the parameters that were tested. Spatial resolution seems to be the most important parameter, and a sampling with a mean distance below 20 mm seems adequate to identify potential abnormal regions. A denser sampling (around 10 mm) seems a better choice in order to define more accurately the extent and contours of the abnormal region. In our experiments, changing the distance threshold did not seem to change the identified region. Nevertheless, using a reasonable threshold (e.g. < 20-30 mm) seems fairer as the user is explicitly shown that in some regions, computing correlation gradient values is questionable. In terms of ECG alignment, a variability up to 6 ms seemed to have a mild impact on the generated maps. Finally, a correlation score combining the information from all 12 leads seems preferable, such as the mean correlation over the 12 leads used in this study.

V. DISCUSSION

A novel method has been proposed to identify target zones for catheter ablation of VT that does not require a reference (spontaneous or induced) VT recording. The method proceeds by analyzing pairwise correlations between surface ECG signals from the network of pacing sites. The generated correlation gradient maps can identify abnormal points which are potential targets for radiofrequency ablation. The resulting map can be easily integrated into the vendor's system (e.g. using the mesh integration module of the CARTO3® system). In one patient who went through an actual VT activation mapping, the identified region has been shown to correspond precisely to the VT circuit core entrance. The relation between correlation gradient maps calculated with/without a VT reference has been described formally and evaluated experimentally. The reference-less correlation gradient map, in %/mm units, can be interpreted as follows: low values efficiently identify normal zones (NPV=97%, considering the VT correlation gradient map as the ground truth); high values identify abnormal zones which may or may not be confirmed by the VT correlation gradient map (PPV=43%). The reference-less method indeed identified 1.6 times more abnormal zones. This result was expected, as explained earlier, because some abrupt transitions can only be identified by a direct comparison of the QRS signals from two neighboring pacing sites, rather than comparing each of them to a third QRS signal (i.e. the reference VT signal). It could be hypothesized that the additional abnormal zones correspond to other, "hidden" or "silent" reentrant VT circuits. In practice, a good qualitative agreement was found between the two gradient maps. Differences between the values measured in the actual target ablation sites and in other sites were significant with both methods. The reference-less method seemed to be better at discriminating between regions which were subsequently ablated and other regions in the ventricle, and the mean correlation gradient value found in the ablation sites was also closer to the cutoff $\mathcal{G}^{normal}_{PacedQRS/PacedQRS} = 3.125\ \%/mm$. In practice the ablation zone covers a larger area than theoretically required, due to all sources of inaccuracies in the localization process (discussed hereafter) and in the ablation process (little feedback on the created lesion is available to the cardiologist). However the inability to induce a VT after ablation, as checked

in the final stage of the clinical procedure, is a strong evidence that the ablated region did contain the core of the reentrant VT circuit.

Sources of inaccuracies in the target localization process should be mentioned. The intrinsic accuracy of the catheter navigation system is vendor-dependent, and depends on the localization technique (GPS-like or bio-impedance-based) and on the patient motion compensation system. The density of pacing sites, however, is controlled by the user. A high density is desirable as it allows more reliable correlation gradient values to be obtained. The gradient values are indeed computed by estimation formulas given in equations (2) and (4), which hold when the distance between pacing sites is small. In this study the threshold of $D_{max} = 20\,mm$ was used, above which gradient estimates were considered unreliable. The drawback of increasing the pacing site density is that a compromise has to be found between data acquisition time and processing time. Finally it should be noted that the current version of the CARTO software only includes the correlation map $C_{PacedQRS/VT}$, and not the correlation gradient map $G_{PacedQRS/VT}$. Instead, the cardiologist reconstructs this gradient map "mentally" in order to identify the abrupt transition zone. This may also partly explain spatial inaccuracies when choosing target ablation sites.

We have tested the proposed method in macro-reentant VT circuits that occurred in ischemic cardiomyopathies. Ablation of VT in non-ischemic cardiomyopathies would also be of great interest. The mechanisms underlying VT in the latter case is not completely understood. However macro-reentrant circuits have been mapped in non-ischemic cardiopathies, including arrhythmogenic right ventricular dysplasia [19] and dilated cardiomyopathy [20]. The reference-less pace-mapping method should also be applicable in such macro-rentrant circuits. However there is still a lack of knowledge about VT circuits other than monomorphic macro-reentries, including polymorphic VT and micro-reentrant circuits. Such circuits have not been reconstructed by activation mapping, so there is no data indicating that the reference-less method could be applied in such cases.

In order to optimize the trade-off between spatial accuracy and duration of the procedure, both data acquisition and processing time should be optimized. With regard to data acquisition, automated catheter navigation systems such as the Niobe magnetic navigation system (Stereotaxis, St. Louis, USA) can improve the efficiency of the procedure. Data processing time is constrained by the need for manual correction of ECG alignments, which can be reduced using efficient automated ECG alignment as proposed in this study. To save even more time, new acquired pace-mapping site pairs could be identified during the course of the procedure, so that the cardiologist would be able to check and correct the alignment of paced-QRS signals on-the-fly. Fully automatic post-processing may be difficult to achieve, as it may necessitate perfectly "clean" data recordings, i.e. containing only paced-QRS signals at each site. In practice, some heart beats need to be ignored as the stimulation spike does not always induce a paced QRS, thereby the amplitude of the stimulation spike has to be adjusted, especially within the scar region. Interestingly, the automatic ECG alignment was more reliable with the reference-less method than with the conventional method. This is because the reference-less method directly compares QRS signals from neighboring sites, so this comparison is easier in pacing sites located far away from the VT circuit, where the paced QRS morphology is very different from that of the reference VT.

The main limitation of this study is that it is retrospective and involved a small number of patients (19). The determination of cutoff values to classify normal/abnormal points may be adjusted by considering a larger cohort. A prospective study will be necessary in order to evaluate the true clinical benefit of choosing ablation target sites with the proposed method. In particular, the success rate of the procedure obtained with either ablation method will need to be evaluated with patient follow-up data, in order to prove that the recurrence rate can be reduced. This would provide a clinical evidence that the additional areas detected by the reference-less method do correspond to other (secondary or hidden) VT circuits. Nevertheless, in this study, there are indices supporting this hypothesis: (i) although the reference-less method was blind to the clinical VT, it was able to correctly identify proven VT isthmuses (as identified by conventional pace-mapping and by successful ablation); (ii) as the method is based on pace-mapping, the abnormal areas are identified by analysis of experimentally feasible activation pathways in a given patient, which is of utmost importance since the aim is to identify a macro-reentrant circuit, which is an abnormal activation pathway. This is different from substrate methods, as the presence of abnormal (e.g. late/fragmented) potentials locally does not tell anything about the resulting activation pathways macroscopically, i.e. it does not tell whether it can support a macro-reentrant circuit.

In the clinical workflow, the proposed method might be used as a surrogate of the conventional pace-mapping method to identify the ablation targets. The remainder of the procedure might remain unchanged. This means the procedure would still begin with programmed electrical stimulation to try and induce a clinical VT. Pace-mapping data would be collected as with the conventional method, preferably with a higher sampling density in the scar area, i.e. in areas with low values in the voltage maps. Only the processing of the pace-mapping data would change. The reference-less method would be blind to the clinical VT and would identify one or multiple zones as potential ablation targets, instead of a single zone with the conventional method. One might also use both methods to check that the targets identified by the reference-less method do contain the targets identified by the conventional method. After ablation of all identified sites, programmed electrical stimulation would still be performed again to check that no VT can be induced (end-point of the procedure). It is expected that the reference-less method would reach the end-point faster in complex cases, e.g. when multiple VT circuits are present. Indeed with conventional pace-mapping, new pacing sites might be needed after ablation of the primary VT circuit, and a new correlation map has to be generated with the new VT recording as a reference.

When a VT reference is available, the method can be used in combination with the conventional method. Indeed if a clinical VT recording can be easily obtained, the decision could be made by the cardiologist based on all available information (VT

This article has been accepted for publication in a future issue of this journal, but has not been fully edited. Content may change prior to final publication. Citation information: DOI 10.1109/TBME.2019.2903631, IEEE Transactions on Biomedical Engineering

correlation map, VT gradient correlation map and reference-less correlation gradient map). In that case the new method may help speeding-up the procedure, as automated processing is more reliable than with the conventional method. Another way of shortening the intervention would be to use ECG imaging [21]–[23] to guide the procedure, since it has the potential of reconstructing the source of the arrhythmia (i.e. here the exit site of the VT circuit) directly from multi-channel surface ECG data recorded during VT, and even potentially from the standard 12-lead ECG recording [24]. Alternatively, artificial intelligence has shown promising results to predict the exit site of the VT circuit from the 12-lead ECG of the VT, based on machine learning [25] or deep learning [26]. In particular, in Ref. [25], it was shown that the relation between pacing location and the lead-wise QRS energy distribution can be learnt (using a population-based and/or patient-specific training) and used to predict the location of the VT exit site. Both ECGI and artificial intelligence necessitate a VT reference ECG. However it is also desirable to localize VT circuits without having a reference ECG recording of the VT, because (i) in some patients the VT cannot be induced during the procedure; (ii) secondary or "hidden" VT circuits may occur after ablation of the primary VT circuit, and should be detected as well. Alternatives to the proposed reference-less pace-mapping include substrate mapping methods [7]–[9], [11], [12] (in particular those methods detecting regions with late/fragmented potentials). A drawback of substrate mapping is that it may identify a large number of abnormal sites (i.e. with late/fragmented potentials) which may not necessarily lead to a VT circuit; conversely, pace-mapping experimentally identifies the feasible activation pathways for a given patient. Having said that, substrate mapping may also be used in combination with the proposed method in such cases. Recent progress in biophysics-based simulation, e.g. incorporating magnetic resonance imaging of scar tissue, may also help improving our understanding and interpretation of such substrate mapping data [27], [28].

VI. Conclusion

A method was proposed to identify ablation targets in macro-reentrant VT circuits, such as those occurring in ischemic patients. It is based on the pace-mapping mapping technique in that it uses surface ECG recordings during electrical stimulation of the ventricle from multiple sites. However if differs from conventional pace-mapping in that the localization of the critical zone to be ablated does not require a reference ECG recording of the VT. The results of this retrospective study support the hypothesis that the detected regions correspond to critical regions as those found in the core of VT reentrant circuits, as assessed by the comparison to (i) regions detected by conventional pace-mapping, (ii) the location of ablation sites (ablation terminated VT in all 24 procedures of the study) and (iii) activation mapping (performed in one patient). This reference-less technique is of particular interest for patients in whom VT cannot be induced during the intervention. It might also help detecting secondary VT circuits that may occur after ablation of a primary VT circuit.

References

[1] N. El-Sherif, B. J. Scherlag, R. Lazzara, and R. R. Hope, "Re-entrant ventricular arrhythmias in the late myocardial infarction period. 1. Conduction characteristics in the infarction zone," *Circulation*, vol. 55, no. 5, pp. 686–702, May 1977.

[2] H. Klein, R. B. Karp, N. T. Kouchoukos, G. L. Zorn, T. N. James, and A. L. Waldo, "Intraoperative electrophysiologic mapping of the ventricles during sinus rhythm in patients with a previous myocardial infarction. Identification of the electrophysiologic substrate of ventricular arrhythmias.," *Circulation*, vol. 66, no. 4, pp. 847–853, Oct. 1982.

[3] J. M. de Bakker *et al.*, "Reentry as a cause of ventricular tachycardia in patients with chronic ischemic heart disease: electrophysiologic and anatomic correlation," *Circulation*, vol. 77, no. 3, pp. 589–606, Mar. 1988.

[4] W. G. Stevenson *et al.*, "Identification of reentry circuit sites during catheter mapping and radiofrequency ablation of ventricular tachycardia late after myocardial infarction," *Circulation*, vol. 88, no. 4 Pt 1, pp. 1647–1670, Oct. 1993.

[5] C. de Chillou *et al.*, "Isthmus characteristics of reentrant ventricular tachycardia after myocardial infarction," *Circulation*, vol. 105, no. 6, pp. 726–731, Feb. 2002.

[6] W. G. Stevenson *et al.*, "Exploring Postinfarction Reentrant Ventricular Tachycardia With Entrainment Mapping," *J. Am. Coll. Cardiol.*, vol. 29, no. 6, pp. 1180–1189, May 1997.

[7] K. Soejima *et al.*, "Catheter Ablation in Patients With Multiple and Unstable Ventricular Tachycardias After Myocardial Infarction: Short Ablation Lines Guided by Reentry Circuit Isthmuses and Sinus Rhythm Mapping," *Circulation*, vol. 104, no. 6, pp. 664–669, Aug. 2001.

[8] F. E. Marchlinski, D. J. Callans, C. D. Gottlieb, and E. Zado, "Linear Ablation Lesions for Control of Unmappable Ventricular Tachycardia in Patients With Ischemic and Nonischemic Cardiomyopathy," *Circulation*, vol. 101, no. 11, pp. 1288–1296, Mar. 2000.

[9] H. Kottkamp *et al.*, "Catheter Ablation of Ventricular Tachycardia in Remote Myocardial Infarction:," *J. Cardiovasc. Electrophysiol.*, vol. 14, no. 7, pp. 675–681, Jul. 2003.

[10] A. Arenal *et al.*, "Ablation of electrograms with an isolated, delayed component as treatment of unmappable monomorphic ventricular tachycardias in patients with structural heart disease," *J. Am. Coll. Cardiol.*, vol. 41, no. 1, pp. 81–92, Jan. 2003.

[11] A. Arenal *et al.*, "Tachycardia-Related Channel in the Scar Tissue in Patients With Sustained Monomorphic Ventricular Tachycardias: Influence of the Voltage Scar Definition," *Circulation*, vol. 110, no. 17, pp. 2568–2574, Oct. 2004.

[12] P. Jaïs *et al.*, "Elimination of Local Abnormal Ventricular ActivitiesClinical Perspective: A New End Point for Substrate Modification in Patients With Scar-Related Ventricular Tachycardia," *Circulation*, vol. 125, no. 18, pp. 2184–2196, May 2012.

[13] C. de Chillou *et al.*, "Localizing the critical isthmus of postinfarct ventricular tachycardia: the value of pace-mapping during sinus rhythm.," *Heart Rhythm Off. J. Heart Rhythm Soc.*, vol. 11, no. 2, pp. 175–181, Feb. 2014.

[14] C. de Chillou, J.-M. Sellal, and I. Magnin-Poull, "Pace Mapping to Localize the Critical Isthmus of Ventricular Tachycardia," *Card. Electrophysiol. Clin.*, vol. 9, no. 1, pp. 71–80, Mar. 2017.

[15] M. Pauriah *et al.*, "A stepwise approach to the management of postinfarct ventricular tachycardia using catheter ablation as the first-line treatment: a single-center experience," *Circ. Arrhythm. Electrophysiol.*, vol. 6, no. 2, pp. 351–356, Apr. 2013.

[16] G. E. Dower, "A lead synthesizer for the Frank system to simulate the standard 12-lead electrocardiogram," *J. Electrocardiol.*, vol. 1, no. 1, pp. 101–116, Jan. 1968.

[17] G. E. Dower, H. B. Machado, and J. A. Osborne, "On deriving the electrocardiogram from vectoradiographic leads," *Clin. Cardiol.*, vol. 3, no. 2, pp. 87–95, Apr. 1980.

[18] S. Abboud and D. Sadeh, "The use of cross-correlation function for the alignment of ECG waveforms and rejection of extrasystoles," *Comput. Biomed. Res.*, vol. 17, no. 3, pp. 258–266, Jun. 1984.

[19] J.-M. Sellal, I. Magnin-Poull, A. Battaglia, D. Hooks, and C. de Chillou, "First Simultaneous Endocardial and Epicardial Mapping of a Ventricular Tachycardia in an ARVD/C Patient," *JACC Clin. Electrophysiol.*, vol. 4, no. 9, pp. 1265–1267, Sep. 2018.

[20] V. Swarup, J. B. Morton, M. Arruda, and D. J. Wilber, "Ablation of Epicardial Macroreentrant Ventricular Tachycardia Associated with Idiopathic Nonischemic Dilated Cardiomyopathy by a Percutaneous Transthoracic Approach," *J. Cardiovasc. Electrophysiol.*, vol. 13, no. 11, pp. 1164–1168, 2002.

[21] J. E. Burnes, B. Taccardi, P. R. Ershler, and Y. Rudy, "Noninvasive Electrocardiographic Imaging of Substrate and Intramural Ventricular Tachycardia in Infarcted Hearts," *J. Am. Coll. Cardiol.*, vol. 38, no. 7, pp. 2071–2078, Dec. 2001.

[22] W. H. W. Schulze *et al.*, "ECG imaging of ventricular tachycardia: evaluation against simultaneous non-contact mapping and CMR-derived grey zone," *Med. Biol. Eng. Comput.*, vol. 55, no. 6, pp. 979–990, Jun. 2017.

[23] C. Han, S. M. Pogwizd, C. R. Killingsworth, and B. He, "Noninvasive imaging of three-dimensional cardiac activation sequence during pacing and ventricular tachycardia," *Heart Rhythm*, vol. 8, no. 8, pp. 1266–1272, Aug. 2011.

[24] P. M. van Dam, R. Tung, K. Shivkumar, and M. Laks, "Quantitative localization of premature ventricular contractions using myocardial activation ECGI from the standard 12-lead electrocardiogram," *J. Electrocardiol.*, vol. 46, no. 6, pp. 574–579, Nov. 2013.

[25] J. L. Sapp *et al.*, "Real-Time Localization of Ventricular Tachycardia Origin From the 12-Lead Electrocardiogram," *JACC Clin. Electrophysiol.*, vol. 3, no. 7, pp. 687–699, Jul. 2017.

[26] P. K. Gyawali, S. Chen, H. Liu, B. M. Horacek, J. L. Sapp, and L. Wang, "Automatic coordinate prediction of the exit of ventricular tachycardia from 12-lead electrocardiogram," in *2017 Computing in Cardiology (CinC)*, 2017, pp. 1–4.

[27] R. Cabrera-Lozoya, B. Berte, H. Cochet, P. Jaïs, N. Ayache, and M. Sermesant, "Image-Based Biophysical Simulation of Intracardiac Abnormal Ventricular Electrograms," *IEEE Trans. Biomed. Eng.*, vol. 64, no. 7, pp. 1446–1454, Jul. 2017.

[28] Z. Chen *et al.*, "Biophysical Modeling Predicts Ventricular Tachycardia Inducibility and Circuit Morphology: A Combined Clinical Validation and Computer Modeling Approach," *J. Cardiovasc. Electrophysiol.*, vol. 27, no. 7, pp. 851–860, Jul. 2016.

2) Improving ECG signal quality during remote magnetic navigation

In remote magnetic navigation, the orientation of the tip of the catheter is controlled by moving two magnets that in turn modify the magnetic field[59]. According to Faraday's law of induction, $\Phi(B)$ the flux of the magnetic field will also induce an electromotive force $\mathcal{E}$ in the various cables around the patient.

$$\mathcal{E} = -\frac{d\Phi(B)}{dt} \quad (4)$$

This force $\mathcal{E}$ can induce noise in the 12-lead ECG cables. The induced noise coupled with the presence of the high-pass acquisition filter can render the monitoring of the ECG challenging for up to 10 seconds after each magnet movement[149]. The pacemapping technique previously described relies on precise comparisons of ECG signals and such artifacts can hinder the physician's ability to analyze pacemapping data. Moreover, any movement induced noise in the acquisition circuit will be amplified because of the magnetic field, further hindering precise ECG comparisons. Possible causes of such movements can be the patient trembling or neighboring devices such as the pump. The following paper studies and tests a novel acquisition device based on optical transmission to limit the magnetic correlated distortions on the ECG.

My contribution to the paper was in highlighting the clinical and technical implications of this new device on pacemapping procedures. The original concept was first developed for MRI (Magnetic Resonance Imaging) and this study is a result of its adaption to the electrophysiology setting[150]. I highlighted the importance of using the correlation coefficient metric. I also designed the study protocol, especially regarding the simultaneous acquisition with the new and conventional setup, the selection of the different motion patterns and different arrhythmias. The acquisition and data export with the CARTO® system was also my contribution to this work.

The new acquisition device studied here improves the quality of the ECG signal collected in the magnetic navigation setting. This could help optimize workflow, result in higher density maps and reduce procedure times.

Annals of Biomedical Engineering, Vol. 47, No. 4, April 2019 *(© 2019)* pp. 1141 1152
https://doi.org/10.1007/s10439-019-02214-3

Electrocardiogram Acquisition During Remote Magnetic Catheter Navigation

JESÚS E. DOS REIS,[1,2] PAUL SOULLIÉ,[1] ALBERTO BATTAGLIA,[3,4] GREGORY PETITMANGIN,[2] PHILIP HOYLAND,[1,5] LAURENT JOSSEAUME,[6] CHRISTIAN DE CHILLOU,[1,4] FREDDY ODILLE,[1,3] and JACQUES FELBLINGER[1,3]

[1]IADI, INSERM, U1254 and Université de Lorraine, Nancy, France; [2]Schiller Medical SAS, Wissembourg, France; [3]CIC-IT 1433, INSERM, Université de Lorraine and CHRU Nancy, Nancy, France; [4]Department of Cardiology, CHRU de Nancy, Nancy, France; [5]Biosense Webster France, Johnson & Johnson, Issy-les-Moulineaux, France; and [6]Stereotaxis Inc., St. Louis, MO, USA

(Received 6 September 2018; accepted 18 January 2019; published online 30 January 2019)

Associate Editor Sriram Neelamegham oversaw the review of this article.

Abstract—Electrocardiogram (ECG) acquisition is required during catheter treatment of cardiac arrhythmias. The remote magnetic navigation technology allows the catheter to be moved automatically inside the heart chambers using large external magnets. Each change of position of the catheter requires fast motion of the magnets, therefore magnetic fluxes are created through the ECG cables, causing large distortions of the ECG signals. In this study a novel ECG sensor is proposed for reducing such distortions. The sensor uses short cables to connect the electrodes to the amplification and optical conversion circuit, using a technology similar to that used for magnetic resonance imaging. The proposed sensor was compared to the conventional 12-lead ECG device during various operation modes of the magnets. Quantitative morphological analysis of the different waves of the ECG was performed in two healthy subjects and on a conductivity phantom reproducing various cardiac pathologies. In healthy subjects the beat-to-beat correlation coefficients were improved with the proposed sensor for the PR interval (80–93% vs. 49–89%), QRS complex (93–96% vs. 74–94%), ST segment + T wave (95–98% vs. 67–99%), and whole PQRST wave (82–97% vs. 55–96%). Similar observations were made with the conductive gel in the whole PQRST wave in the pathological morphologies of the ECG for the VT (99% vs. 56–98%), AT (95% vs. 26–89%), ST_E (96–97% vs. 20–91%) and ST_D (96% vs. 28–90%). The new sensor might be used for better (uninterrupted) monitoring of the patient during catheter interventions using remote magnetic navigation. It has the potential to improve the robustness and/or duration of certain clinical procedures such as ventricular tachycardia ablation.

Keywords—Electrocardiography (ECG), Remote magnetic navigation (RMN), Cardiac electrophysiology, Electromagnetic compatibility, Optical sensor.

Address correspondence to Jacques Felblinger, IADI, INSERM, U1254 and Université de Lorraine, Nancy, France. Electronic mails: dosreisjesus@hotmail.com, j.felblinger@chru-nancy.fr

INTRODUCTION

Interventional cardiac electrophysiology (EP) is an emerging technique for the treatment of certain types of arrhythmia. The procedure consists of inserting a catheter in the cardiac chambers in order to identify areas of the myocardium at the origin of electrical disorders. Then the interventional cardiologist defines a target zone that needs to be destroyed, e.g. by radiofrequency catheter heating, in order to prevent the arrhythmia.

High quality surface electrocardiograms (ECG) are required during the whole EP procedure in order to monitor the patient and to analyze and treat the arrhythmia. As an example, in case of complex arrhythmia such as ventricular tachycardia (VT), the identification of the target zone can be performed using a technique called pacemapping,[4] which is based on the analysis of the QRS complex morphology. Pacemapping consists of stimulating the heart with the catheter from different sites of the intraventricular surface, in order to produce activation patterns originating from each of these sites. The site of origin of the arrhythmia is identified when the activation pattern best matches that of the spontaneous, clinical VT (previously recorded for that patient), i.e. when the surface ECG obtained during pacing best matches the surface ECG recorded during the clinical VT. The correlation coefficient between these QRS complexes is used as an objective metric for comparing VT morphologies recorded in a surface 12-lead ECG. Therefore, on the one hand, ECG is needed to continuously monitor the patient during pacing sequences. On the other hand, its

quality is also crucial for accurate identification of the ablation target and success of the procedure.

In the past 10 years, remote magnetic navigation (RMN) systems have been developed in order to remotely automate the displacement of the catheter inside the heart cavities and towards the target ablation zone.[5] Applications have been particularly useful for atrial fibrillation[14] and VT.[2,3] The aim is both to speed-up the procedure and to improve the accuracy of catheter positioning and targeting. One such system is commercialized by Stereotaxis (Niobe Magnetic Navigation System, Stereotaxis Inc., St. Louis, USA) and is composed of two permanent magnets that generate static magnetic fields from 0.08 T to 0.1 T which are moved around the patient in order to orientate and steer the catheter remotely. However this moving of the magnets generates low frequency magnetic field changes in time (in the range of Hz). Electric currents are therefore induced in conducting cables of the 12-lead ECG device (electromotive force $\varepsilon = -\mathrm{d}\Phi(B)/\mathrm{d}t$ [*V*], with $\Phi(B)$ the flux of the magnetic field throughout the closed conducting surface) and can disturb the ECG signals, as shown in Fig. 1. In worst-case scenarios, the added parasitic voltages can saturate the amplification stage of the acquisition device and the user has to wait for approximately 10 s until the ECG signal becomes stable again. Severe distortions of the ECG generally prevent the monitoring of the patient during the moving of the magnets, as well as the QRS morphological analysis. Additionally, since the magnetic field is spatially non-uniform, any motion of the long ECG cables within this magnetic field (e.g. patient trembling or any source of mechanical vibrations in the room) is also likely to cause induced currents and artifacts on the ECG. Such artifacts cause problems for all types of catheter interventions performed using an RMS system as the patient cannot be monitored during the periods of magnet motion. In addition to patient monitoring, the quantitative analysis of the ECG morphology is required by certain types of procedures, such as VT ablation using the pacemapping technique. The impact of such artifacts should therefore be quantified.

Similar concerns arise when recording ECG during magnetic resonance imaging (MRI). A design of the ECG sensor was proposed based on short wires between the electrodes and the amplification/optical conversion circuit[6] which is currently the basis of most MR-compatible ECG devices. Such systems do not completely eliminate high-frequency magnetic field switching artifacts (in the range of kHz), and additional post-processing may be necessary.[1,7,12,13] However they drastically reduce the area formed by conducting cables and thereby minimize distortions on the ECG, allowing patient monitoring and triggering of the MRI scanner.

In the present work we investigated whether a novel ECG device based on MRI-compatible technology can be used as an RMN-compatible ECG device, i.e. to reduce distortions of the ECG signals during remote magnetic navigation of the catheter in the EP room. We compared signals of the proposed sensor to those of the conventional ECG device used clinically. Quantitative evaluation was performed by morphological analysis of the different ECG waves (P, Q, R, S, T) in order to show the potential benefit for EP procedures.

MATERIALS AND METHODS

Proposed Electrocardiography Device for Remote Magnetic Navigation

The proposed device is a prototype based on a commercial MR-compatible ECG sensor, for use with MRI scanners up to 3 T (Maglife, Schiller Médical, Wissembourg, France).The architecture of the device is shown in Fig. 2a. The ECG device is composed of a triple-branch wire, connecting four surface electrodes (one common lead reference electrode + three measurement electrodes) to the sensor box. The sensor box is shielded but the wires are not. The analog signal is first pre-amplified and digitized in a front-end ECG module are built into the device (sampling frequency = 1 kHz, ADC 16 bits). Then real-time signal processing (QRS detection) is performed on a microcontroller also integrated into the device. The signals are finally modulated and transferred by optical fiber to a computer for recording (RS232 serial communication protocol at 460800 Baud).

According to vendor's technical data, the RMN system operates the magnets with rotational motion, at a speed between 19.37°/s and 76.9°/s (depending on the direction) and translational motion at a speed of 11.7 cm/s, and the artifacts due to magnet motion are in the range 0.054-0.5 Hz. The amplitude is large enough to saturate the acquisition device, as seen in Fig. 1. In comparison, MRI scanners operate with switching magnetic fields in the range 0 20 kHz. According to vendor's technical data, the amplitude of raw induced voltage during MRI sequences (without any filtering) can be up to 300 times higher than the QRS complex.

The proposed device provides three independent ECG leads with a 0.05 150 Hz bandwidth. Usually conventional MRI-compatible ECG devices use very restrictive analog filters (40 60 Hz) at the input of the operational amplifiers. Unlike the MRI-compatible

device, the proposed prototype has a bandwidth suitable for diagnostic use (0.05–120 Hz required). For post-processing, all ECG signals (conventional and proposed) were filtered offline to the diagnostic bandwidth (0.05–120 Hz) using Butterworth low-pass and high pass filters (4th and 2nd order respectively). In this study only one ECG device was used, however several such ECG devices can be placed on the patient in order to measure several spatially independent electrical projections.

The proposed device was compared to the default device that is used at our institution during EP procedures with the CARTO 3 system (Biosense Webster, Los Angeles, USA). This is a conventional 12-lead ECG device with long cables, providing signals with a 0.05–120 Hz bandwidth. The conventional ECG cable has a total length of 3.8 m and is divided into two segments. The signal form each electrode is first transmitted through a 1.8 m long shielded single line and then through a 2 m long shielded multiline up to

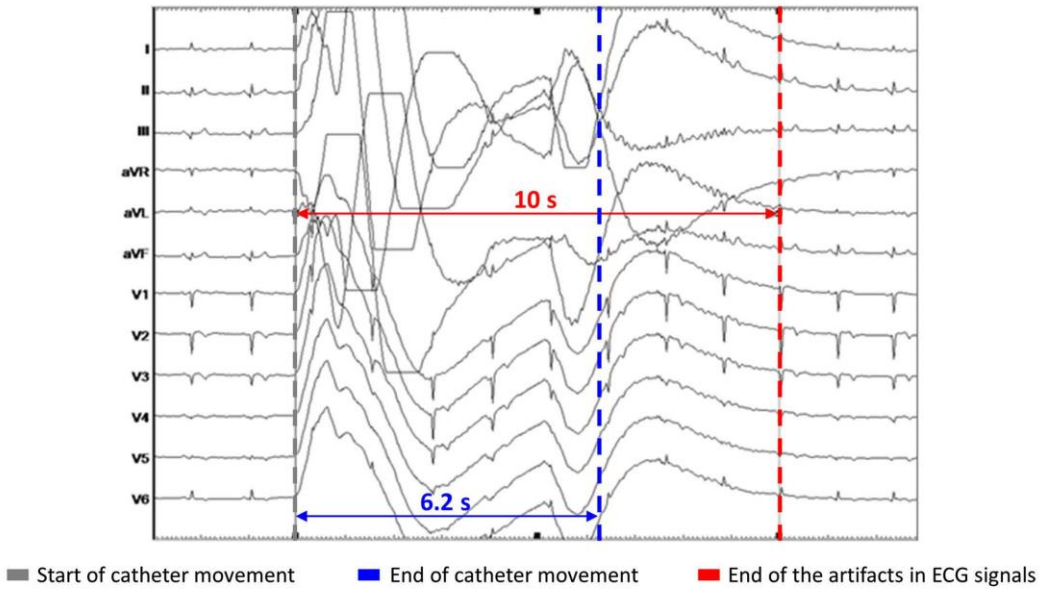

FIGURE 1. Example artifacts observed on the 12-lead ECG during a cardiac electrophysiology procedure using a magnetic navigation system for remote catheter steering. Catheter movement time was 6.2 s, and artifact duration was 10 s in the ECG signals.

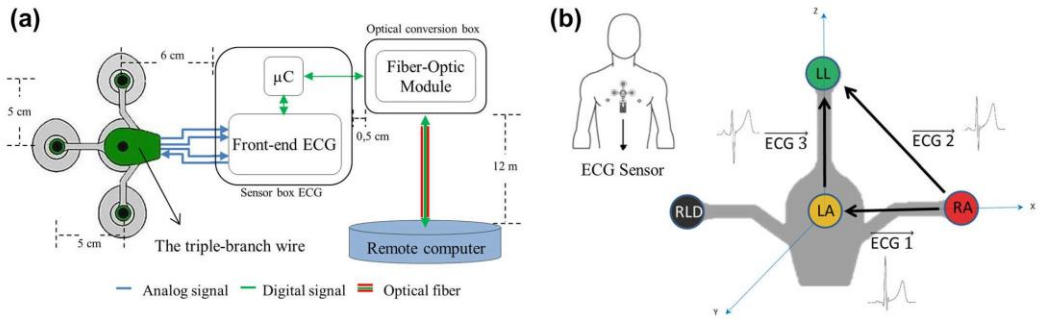

FIGURE 2. (a) Electronics design of the proposed ECG device. The copper (blue) conductor cables between the triple-branch wire and the front-end ECG system into the device are not shielded. The length of the cables is about 11 cm. The length of the optical fiber that connects the ECG sensor and the remote computer is 12 m. (b) Positioning of the RMN-compatible ECG sensor on the volunteer's chest, and measured ECG leads.

the amplifier. Signals from the conventional ECG device were recorded with the CARTO 3 system and were exported for subsequent analysis (sampling frequency = 1 kHz).

Experimental Protocol in Volunteers

ECG acquisitions were performed on two healthy male volunteers (age 37 and 55 years, weight 70 and 78 kg). The two subjects gave informed consent. The study complied with the declaration of Helsinki. It was submitted to the local ethics committee of CHRU Nancy our institution and was granted a waiver due to its non-interventional nature (no catheter was used in our volunteer experiments, only the driving magnets were operated).

The experimental setup was as follows. The subject was lying on the patient table of the EP room. Eight electrodes were placed on the subject's chest (above the sternum) for simultaneous acquisition with the RMN-compatible device (4 electrodes) and the conventional ECG (4 electrodes, located as close as possible to the previous ones), as shown in Fig. 2b. The 4 chosen cables of the conventional ECG (LA, RA, LL, RLD) were wired in a way to match the electrode combinations provided by the RMN-compatible ECG, i.e. providing three leads (named ECG1, ECG2, ECG3 in the remainder) with comparable morphologies for the different ECG waves (P, Q, R, S, T).

The acquisition protocol consisted of several recording sequences of one minute each. ECGs were first recorded with negligible magnetic field (approximately 175 μT at the center of the patient table), i.e. with magnets placed in the resting position, far away from the patient table. Then acquisition sequences were performed with a net magnetic field of 80 and 100 mT (maximum field strength, obtained when the magnets are closest to the table). For each of the two field strengths, six motion patterns of the magnets were applied, corresponding to magnetic field orientation changes of 90°, 180° or 360°, as shown in Fig. 3.

Simulated ECG in a Conductivity Phantom

In order to test both devices with a wider range of pathological ECG morphologies, we used a standard ECG simulator (MS 410, MedTec & Science GmbH, Ottobrunn, Germany) and a conductive gel (phantom). The phantom was made of a semi-rigid salty gel with similar electrical conductivity properties as human skin (~ 0.45 S m $^{-1}$). The recipe for this salty gel is described in ASTM F 2182A: 98.9% deionized water, 0.13% NaCl and 0.99% polyacrylic gel (commonly called PAA).

The ECG simulator was used to reproduce the following pathologic ECG signals: ventricular tachycardia (VT), atrial tachycardia (AT), ST-segment elevation (ST_E) and depression (ST_D), atrial fibrillation (AF) and ventricular fibrillation (VF). The signal from the ECG simulator was amplified and injected into the phantom. The amplification of the signal was carried out with an instrumentation amplifier of the AD620 type. The amplification gain was 5 and no additional digital/analog filter was used. In order to reduce the induction of parasitic noise in the electrical conductors (simulator/phantom), the injection of the ECG signal was achieved with a non-magnetic twisted cable. The length of the cable was long enough (65 cm) to move the simulator away from the magnetic field. The position and configuration of the electrodes of the conventional system and the proposed system was the same as in the volunteer experiments, with the electrodes stuck onto the phantom as explained in part b.

The conventional and proposed ECG devices were tested with this setup using the negligible magnetic (magnet rest position), and with maximum magnetic field strength (100 mT) using the worst case magnet motion sequence, as observed in the volunteer experiments (mode t_6, see Fig. 3). An additional acquisition was performed with the simulator set to reproduce a normal sinus rhythm ECG, while the support of the gel was manually tilted by the experimenter, in order to mimic breathing motion (slow and regular tilting) and abrupt patient motion (fast and sudden tilting). This mode is termed SR-PM (sinus rhythm, patient motion) is the remainder.

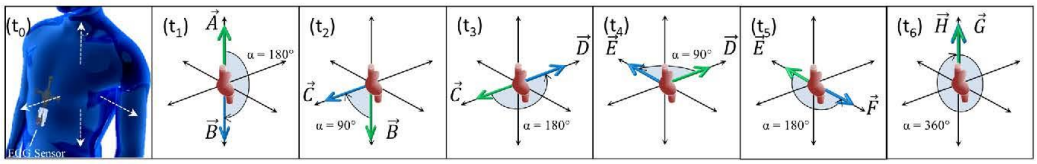

FIGURE 3. Motion sequences for the magnets of the magnetic navigation system. The heart of the patient with the ascending and descending aorta are symbolized at the center of the axes (red). The color of the arrows indicates the initial (green) and final (blue) position of the movement of the catheter. (t_0) ECG sensor position relative to motion axes, no movement and negligible magnetic field. (t_1) $\vec{A}$ to $\vec{B}$ (change of the magnetic field direction). (t_2) $\vec{B}$ to $\vec{C}$. (t_3) $\vec{C}$ to $\vec{D}$. (t_4) $\vec{D}$ to $\vec{E}$. (t_5) $\vec{E}$ to $\vec{F}$. (t_6) $\vec{G}$ to $\vec{H}$.

ECG Morphology Analysis

ECG signals were analyzed using Matlab (R2017a, Mathworks, Natick, USA). The morphology of the different ECG waves (P, Q, R, S, T) was assumed to be highly reproducible from heart beat to heart beat in our healthy subjects. A similarity metric was computed between the reference recording (t_0) with no magnetic field and each of the 60 s recordings acquired during magnet motion (t_1 t_6). The similarity between two given ECG recordings X and Y was computed using the processing workflow described hereafter and illustrated in Fig. 4a.

First an R-wave detection was performed on each recording. A set of N consecutive heart beats was manually selected on each of the two recording ($N = 6$ heart beats in the whole study). A window was then applied in order to select various subsets of the ECG signal, including PR interval, QRS complex, ST segment + T-wave, and the whole PQRST wave. The window location and width was determined in a subject-specific manner as described in Table 1. Then Pearson's correlation coefficients were computed in all possible pairs of windows from heart beats X_m and Y_n ($n = 1...N$ and $m = 1...N$), i.e.:

$$r(X_m, Y_n) = \frac{\sum_k \left(X_m[k] - \overline{X}_m\right)\left(Y_n[k] - \overline{Y}_n\right)}{\sqrt{\sum_k \left(X_m[k] - \overline{X}_m\right)^2 \sum_k \left(Y_n[k] - \overline{Y}_n\right)^2}}, \quad (1)$$

$$\text{where } \overline{X}_m = \frac{1}{N}\sum_{m-1}^{N} X_m[k] \text{ and } \overline{Y}_n = \frac{1}{N}\sum_{n-1}^{N} Y_n[k].$$

This metric was used in this study because it is used in clinical EP procedures for VT localization.[4] A global correlation coefficient was finally computed by averaging:

$$r(X, Y) = \frac{1}{N^2}\sum_{m-1}^{N}\sum_{n-1}^{N} r(X_m, Y_n) \quad (2)$$

Morphological analysis was applied using both the conventional ECG device and the proposed RMN-compatible device for each magnet configuration described in the previous section. The same heart beats and window selections were used for the two devices. We also compared the signals to those obtained after simple baseline correction of the conventional ECG by digital high-pass filtering (2nd order Butterworth filter). Two cutoff frequencies HPF were tested: 5 and 10 Hz. The reason for this choice is that the cutoff should be above the artifact frequency range of 0.054 0.5 Hz due to magnet motion, given by the vendor. In practice, we observed that the baseline is completely suppressed only when HPF is above 10 Hz. However the ECG morphology is severely distorted, therefore the intermediate cutoff of 5 Hz was also used, which better preserves morphology but does not completely remove the baseline drifts.

RESULTS

Volunteer Experiments

ECG signals were successfully recorded in all configurations with the two volunteers.

Example signals recorded simultaneously with the two devices are shown in Fig. 5. When no magnetic field was applied (t_0), the two devices provided a clean ECG. The morphology visually seemed highly reproducible from one heart beat to the other. When the

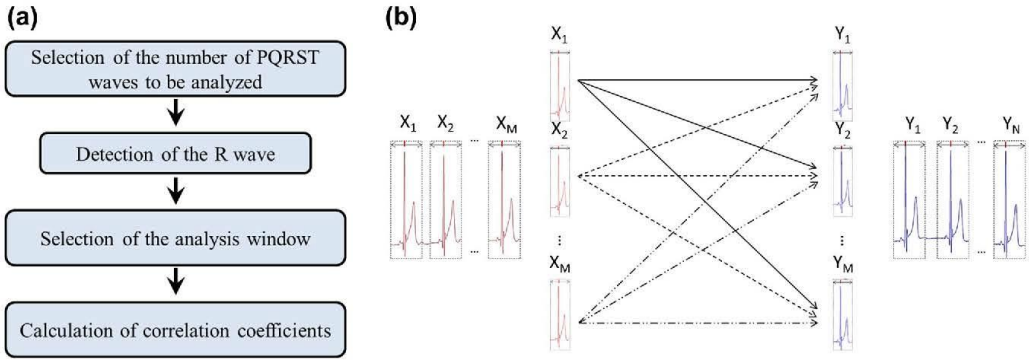

FIGURE 4. (a) Workflow of the ECG morphology analysis. (b) Example window selection for the pair-wise calculation of correlation coefficients between two recordings *X* (t_0, no magnetic field) and *Y* (during one of the magnetic field motion sequences t_1–t_6).

TABLE 1. Window width considered for signal analysis.

Volunteer	PR interval (ms)	QRS complex (ms)	ST segment + T wave (ms)	PQRST wave (ms)
V1	150	110	450	710
V2	140	130	430	700

magnets were operated (t_1 t_6), distortion of the ECG waveforms were observed. Distortions seemed more pronounced on the conventional device, with a large baseline drift observed during the moving of the magnets. The baseline drift was minimized with the proposed sensor. Furthermore, the signal-to-noise ratio seemed to be altered significantly with the conventional device, impacting the shape of the QRS complex and other waves. The worst case was observed with the 360° magnet motion (t_6). These higher-frequency distortions were not seen with the proposed sensor. In particular, in the t6 configuration, the P wave was clearly identified with the proposed device, whereas it was hardly distinguishable from noise with the conventional device.

Example signals obtained from the window-based morphological analysis are shown in Fig. 6. The superimposed signals from the $N = 6$ consecutive heart beats show the good reproducibility of the PQRST waves with the proposed device.

In this example, the signals from the conventional device were significantly distorted, impacting the subsequent morphological analysis.

Quantitative analysis of the morphological similarity is summarized in Tables 2 and 3 for various ECG waves and magnet configurations with volunteer 1 and 2. When no magnet was applied, the global correlation coefficient obtained with the proposed (respectively conventional) device was in the range 93 98% (respectively 89 99%) depending of the lead placement. The global PQRST shape was above 93% with the two sensors which shows excellent reproducibility of the normal cardiac activation from beat to beat. However when the magnets were operated, marked differences were observed between the two sensors. For volunteers V1 and V2, the similarity of the different waves was improved with the proposed sensor for the PR interval (80 93% vs. 49 89%), QRS complex (93 96% vs. 74 94%), ST segment + T wave (95 98% vs. 67 99%), and whole PQRST wave (82 97% vs. 55 96%).

For the whole PQRST wave, the improvement was much higher than that obtained by simple baseline correction: 72 96% for HPF = 5 Hz and 73 95% for HPF = 10 Hz. However it should be noted that the high-pass filters do introduce significant distortions of the ECG waves, especially the ST segment (see Fig. 7).

In summary, 97.61% (respectively 100, 100, 92.8, 100, 100 and 92.8%) of the correlation scores in Table 2 are improved with the proposed device. In Table 3 100% of the correlation scores are improved with the proposed device.

Pathologic ECG Signals

Results obtain with the different pathologic ECG signal generated by the simulator and conductive phantom are shown in Fig. 8. Morphologic analysis results are given in Table 4. Note that correlation scores between ECG without and with the magnets was only computed for the reproducible heart beats (SR-PM, VT, AT, ST_E and ST_D). For fibrillation signals (AF and VF), morphology fidelity was only performed visually since the electrical activation follows a randomized pattern.

In case of a simulated patient motion in sinus rhythm (SR-PM), low frequency variations of the baseline were observed with the conventional device, as well as abrupt transitions causing large artifacts on the ECG signal. With the proposed device these were not noticeable. In all pathologic signal (VT, AT, ST_E and ST_D, AF and VF), the pathologic patterns are much more easily read with the proposed device than with the conventional device. The same baseline oscillatory patterns as in the volunteer experiments are observed. Those visual results were confirmed by the average correlation metrics in Table 4, showing a clear improvement with the proposed device in all cases.

DISCUSSION

We have proposed a new device for ECG acquisition during remote magnetic catheter navigation. The design based on short cables was shown to minimize distortions on the ECG drastically during magnet operation. Possible causes of ECG signal distortion during EP procedures with the RMN system include motion of the magnets, patient motion and/or trembling, or mechanical vibrations in the exam room. Such distortions of the ECG can occur at any time during the EP procedure, although they are mainly observed during the motion of the magnets on the conventional ECG. Additionally, saturation of the

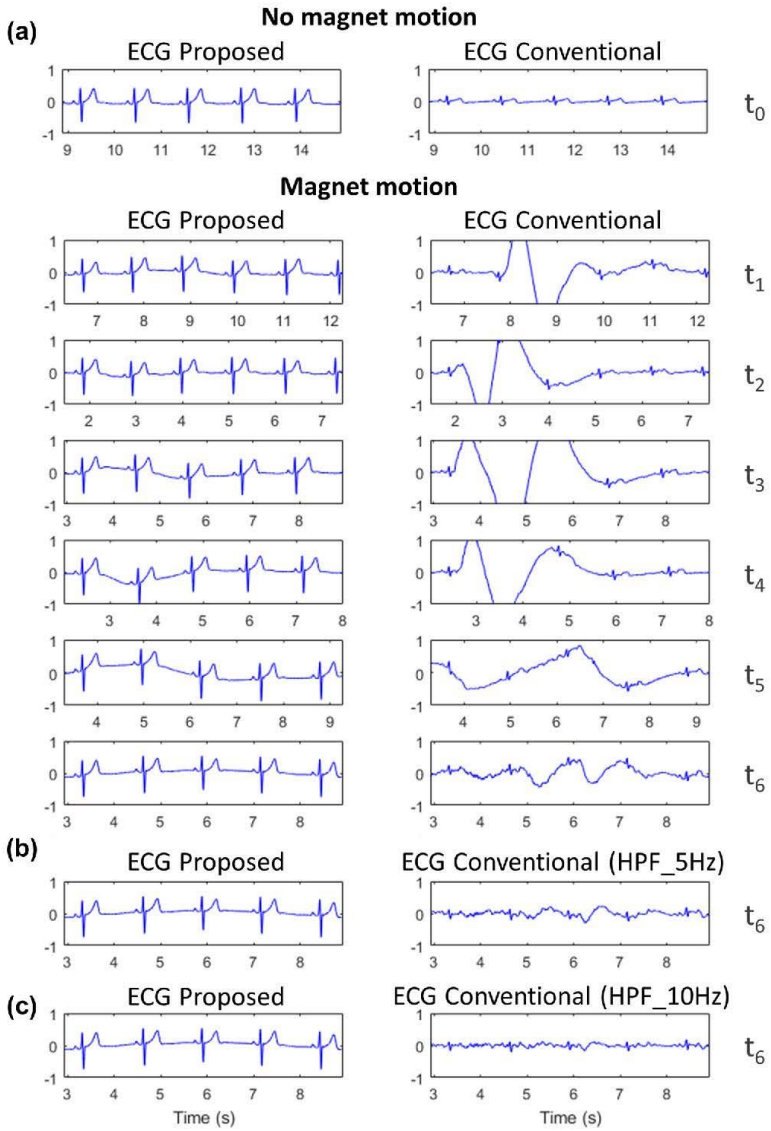

FIGURE 5. (a) Example the distortions and noise observed on the ECG signal (ECG3 lead) during various magnet motion sequences: (t_0) no magnet motion ($\alpha = 0°$); (t_1) $\alpha = 180°$; (t_2) $\alpha = 90°$; (t_3) $\alpha = 180°$; (t_4) $\alpha = 90°$; (t_5) $\alpha = 180°$; (t_6): $\alpha = 3 \times 360°$. Comparison with conventional ECG after simple baseline correction: (b) HPF_5 Hz, (t_6); c HPF_10 Hz (t_6).

acquisition system may occur in practice as shown in Fig. 1.

In the phantom experiments, when abrupt motion was applied, a saturation effect was observed on the monitor of the vendor's system but it was not present in the raw ECG recording. This means that this saturation is applied by the software of the console, during post-processing or display. Due to the presence of a high-pass filter in the acquisition device (typically with a cutoff set to 0.05 Hz), such artifacts would result in

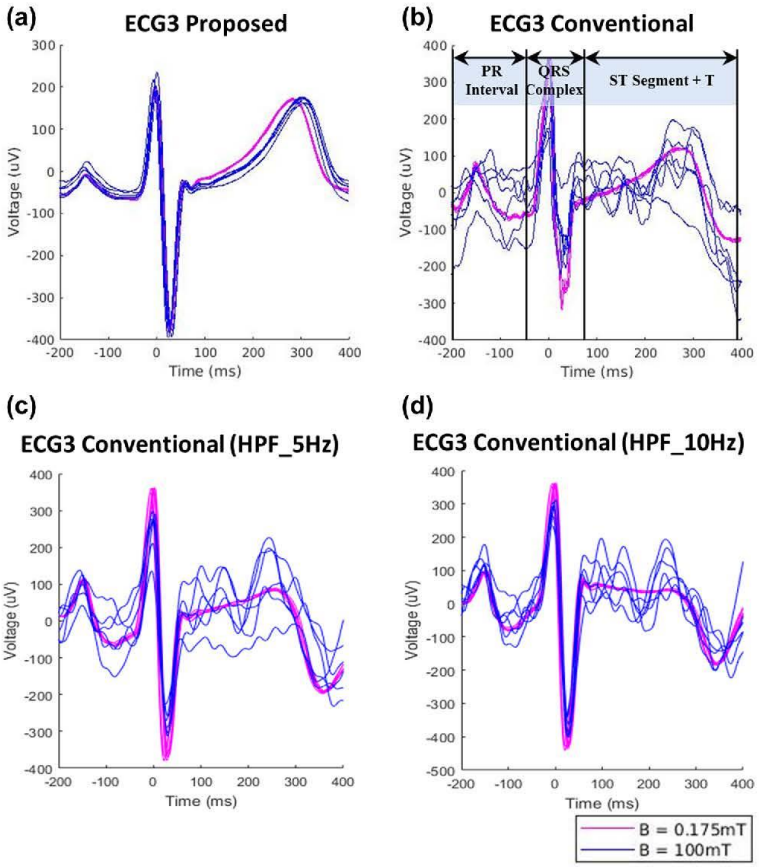

FIGURE 6. Example distortions and noise observed on the ECG signal (ECG3 lead) during magnet motion sequence t_6. Superimposed signals from 6 occurrences of the PQRST waves (signals were statistically centered and normalized). (a) Proposed ECG, (b) conventional ECG, (c) conventional ECG after HPF_5 Hz; (d) conventional ECG after HPF_10 Hz.

additional periods of 5 10 s during which the ECG is hardly interpretable, even after completion of the magnet motion. This delay adds up to the delay required for the catheter to reach its target position, which is on the order of 2 3 s in most cases. In practice the cardiologists has to wait for the ECG signal to be stabilized before acquiring electro-anatomical data with the catheter. Therefore the proposed device might help optimize the workflow of the procedure, as the data could be acquired as soon as the catheter has reached its target position. Currently a typical VT treatment procedure requires approximately 100 data points to be acquired, i.e. 100 changes of catheter position with the magnetic navigation system. The time saved with the new sensor might be used to either speed-up the procedure or acquire more data points. Higher density electro-anatomical maps might indeed improve the accuracy and robustness of the VT localization and ablation.

For most clinical procedures with RMS, the magnet motion periods only result in undesired delays and are not expected to impact the clinical outcome of the treatment significantly. However when quantitative ECG morphology is necessary, as for VT ablation by the pacemapping technique, special care should be given to the ECG signal quality. The quantitative analysis of ECG morphology shows the potential of the method for improving the robustness of VT localization. In previous studies,[4] performed without an RMN system, a critical threshold was defined for considering that a given pacing site does match the exit site of the VT circuit, namely when the correlation

TABLE 2. Global correlation coefficients from the ECG waves during various magnet operation modes (volunteers V1 and V2).

		Magnetic field 80 mT			Magnetic field 100 mT		
ECG sensor	t	PR interval	QRS complex	ST segment + T wave	PR interval	QRS complex	ST segment + T wave
Proposed	t_0	0.931 ± 0.05	0.949 ± 0.05	0.989 ± 0.00	0.931 ± 0.05	0.949 ± 0.05	0.989 ± 0.00
	t_1	0.831 ± 0.04	0.949 ± 0.04	0.960 ± 0.01	0.801 ± 0.06	0.934 ± 0.05	0.953 ± 0.01
	t_2	0.913 ± 0.04	0.953 ± 0.04	0.961 ± 0.01	0.900 ± 0.05	0.955 ± 0.04	0.964 ± 0.01
	t_3	0.896 ± 0.04	0.942 ± 0.05	0.967 ± 0.01	0.914 ± 0.04	0.945 ± 0.04	0.962 ± 0.00
	t_4	0.879 ± 0.04	0.964 ± 0.03	0.959 ± 0.01	0.911 ± 0.03	0.954 ± 0.04	0.950 ± 0.01
	t_5	0.897 ± 0.04	0.963 ± 0.03	0.955 ± 0.01	0.923 ± 0.03	0.946 ± 0.05	0.975 ± 0.00
	t_6	0.921 ± 0.03	0.956 ± 0.04	0.961 ± 0.01	0.909 ± 0.04	0.960 ± 0.03	0.959 ± 0.01
Conventional	t_0	0.895 ± 0.07	0.935 ± 0.06	0.992 ± 0.00	0.895 ± 0.07	0.935 ± 0.06	0.992 ± 0.00
	t_1	0.544 ± 0.08	0.880 ± 0.06	0.748 ± 0.01	0.542 ± 0.09	0.749 ± 0.11	0.677 ± 0.00
	t_2	0.697 ± 0.06	0.924 ± 0.06	0.801 ± 0.00	0.619 ± 0.08	0.773 ± 0.10	0.846 ± 0.00
	t_3	0.599 ± 0.07	0.924 ± 0.06	0.842 ± 0.01	0.590 ± 0.07	0.906 ± 0.05	0.666 ± 0.00
	t_4	0.498 ± 0.07	0.916 ± 0.05	0.815 ± 0.00	0.686 ± 0.07	0.923 ± 0.07	0.671 ± 0.01
	t_5	0.739 ± 0.06	0.947 ± 0.04	0.903 ± 0.00	0.751 ± 0.06	0.929 ± 0.05	0.888 ± 0.01
	t_6	0.688 ± 0.07	0.937 ± 0.02	0.921 ± 0.00	0.687 ± 0.07	0.947 ± 0.04	0.852 ± 0.01

TABLE 3. Global correlation coefficients from the whole PQRST waves during various magnet operation modes (volunteers V1 and V2).

		Magnetic field	
ECG sensor	t	80 mT	100 mT
Proposed	t_0	0.971 ± 0.02	0.971 ± 0.02
	t_1	0.953 ± 0.02	0.930 ± 0.02
	t_2	0.963 ± 0.02	0.964 ± 0.02
	t_3	0.956 ± 0.03	0.956 ± 0.02
	t_4	0.954 ± 0.01	0.952 ± 0.02
	t_5	0.958 ± 0.02	0.954 ± 0.02
	t_6	0.962 ± 0.02	0.962 ± 0.02
Conventional	t_0	0.961 ± 0.03	0.961 ± 0.03
	t_1	0.680 ± 0.02	0.551 ± 0.04
	t_2	0.747 ± 0.03	0.674 ± 0.04
	t_3	0.742 ± 0.03	0.642 ± 0.03
	t_4	0.715 ± 0.03	0.686 ± 0.03
	t_5	0.849 ± 0.02	0.849 ± 0.02
	t_6	0.836 ± 0.02	0.766 ± 0.02
Conventional (HPF_5 Hz)	t_0	0.963 ± 0.03	0.963 ± 0.03
	t_1	0.724 ± 0.13	0.732 ± 0.17
	t_2	0.838 ± 0.14	0.811 ± 0.15
	t_3	0.844 ± 0.16	0.801 ± 0.18
	t_4	0.841 ± 0.14	0.805 ± 0.18
	t_5	0.928 ± 0.05	0.877 ± 0.05
	t_6	0.900 ± 0.04	0.890 ± 0.05
Conventional (HPF_10 Hz)	t_0	0.958 ± 0.04	0.958 ± 0.04
	t_1	0.730 ± 0.12	0.829 ± 0.11
	t_2	0.908 ± 0.06	0.775 ± 0.09
	t_3	0.900 ± 0.10	0.881 ± 0.09
	t_4	0.897 ± 0.10	0.894 ± 0.10
	t_5	0.941 ± 0.03	0.938 ± 0.03
	t_6	0.932 ± 0.04	0.927 ± 0.03

coefficient between QRS complexes was above 93%. In addition, poor correlation scores (less than 74%) in regions located next to the VT exit site were shown to indicate pacing sites corresponding to the critical zone of the VT circuit, i.e. a zone of slow electrical conduction that should be the target for the ablation. Our results show that errors in QRS correlation coefficient measures can be reduced to 4 7% with the proposed sensor, even during magnet motion. This seems acceptable with regard to the above-mentioned thresholds, unlike the conventional sensor which showed errors in the range of 6 26%.

In the present study on healthy subjects, it was assumed that the morphology of ECG waves remains identical from one cardiac cycle to the other, thereby 100% correlation scores were expected. In practice, values below 100% were measured, and varied with the subject, the lead placement, and magnet motion type. Correlation scores measured at t_0 (no magnet motion) represent the intrinsic variability of the ECG morphology for a given subject and lead placement. Inter-subject variability comes from differences in the particular actual activation pathways in the atria and ventricles, which depends on many factors, including: heart geometry, architecture and conduction velocities of myocardial fibers, architecture and conduction velocities of the Purkinje network,[15] presence of conduction abnormalities, and orientation of the heart with respect to the measurement electrodes.[8,11] Intra-subject variability, i.e. the variability in consecutive non-ectopic beats, as quantified by various metrics, has been shown to increase with the risk of cardiovascular death in several studies.[10,16] Respiratory motion can also partly explain intra-subject variabilities in morphology.[9] Finally the variability due to the type of magnet motion (t_1 t_6) comes from differences in orientation of the magnetic field changes (dB/dt) that create different magnetic fluxes in the ECG cables.

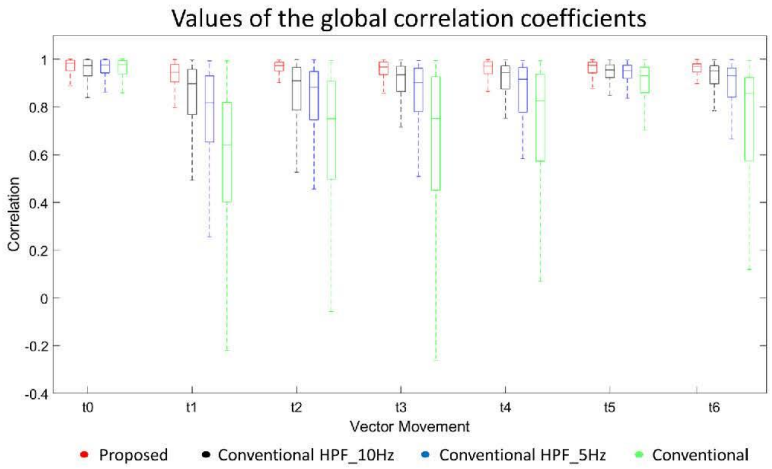

FIGURE 7. Global correlation coefficients computed from the proposed and conventional ECG sensors in volunteers. Results obtained with the three ECG leads are shown, for different magnet motion sequences (t_0–t_6) and a magnetic field of 100 mT. The coefficients corresponding to t_0 were acquired only once with each system.

A limitation of this study is that only a reduced number of ECG leads was tested with only one particular placement of the electrodes. This choice was made in order to ease the comparison through a simultaneous recording of the conventional and proposed sensors. In order to perform an actual EP procedure with the new sensor, a 12-lead ECG would be preferred by the cardiologist. Several solutions could be implemented for that purpose. On the one hand, the sensor might be modified by the addition of 6 supplementary electrodes that would provide all precordial leads (leads V1 to V6) with minimal cable length. Artifacts might be larger than in the present study due to longer cables. Such a setup should be tested in order to conclude whether artifacts would remain sufficiently small. On the other hand, multiple versions of the present sensor (without any modification) could be placed on the chest in order to obtain several independent electrical projections. The signals from such a sensor network could be combined using a simple matrix and a 12-lead ECG reconstruction technique as described by several authors.[17,18] In that case a calibration step might be necessary, at the beginning of the exam, for determining a patient-specific combination matrix. However the amount of distortions in the reconstructed ECG waves would need to be quantified. Indeed the reconstruction of the standard unipolar leads from such local bipolar measurements is not trivial. Alternatively, the cardiologist might also be able to work with non-standard ECG leads. Currently, a VT correlation map is used by the cardiologist to define the ablation targets. The correlation score is the average of the standard 12 leads (paced QRS signals against VT cycle). In principle, the morphological analysis technique used for VT localization does not depend on the particular electrode location, i.e. the correlation map could be calculated by averaging of non-standard leads; nevertheless, a sufficient number of independent electrical projections is required, so that any particular VT circuit location could be observed and its morphology could be discriminated efficiently. However, such a sensor network would certainly benefit from a standardization of the electrode placement.

An alternative to using the proposed device would be to use signal processing methods to denoise the conventional ECG. As shown in our results, simple high-pass filtering is not efficient. More advanced signal processing methods could be implement, provided the command signals of the magnet system can be accessed in real-time. Signal processing methods similar to those used in MRI might be implemented, e.g. to model and predict artifacts using a finite impulse response system and linear or Bayesian filtering.[1,12,13]

Finally, another limitation of the study is the small number of volunteers. This proof-of-concept technical work needs to be followed by an actual patient study in order to evaluate precisely the benefit for clinical EP procedures.

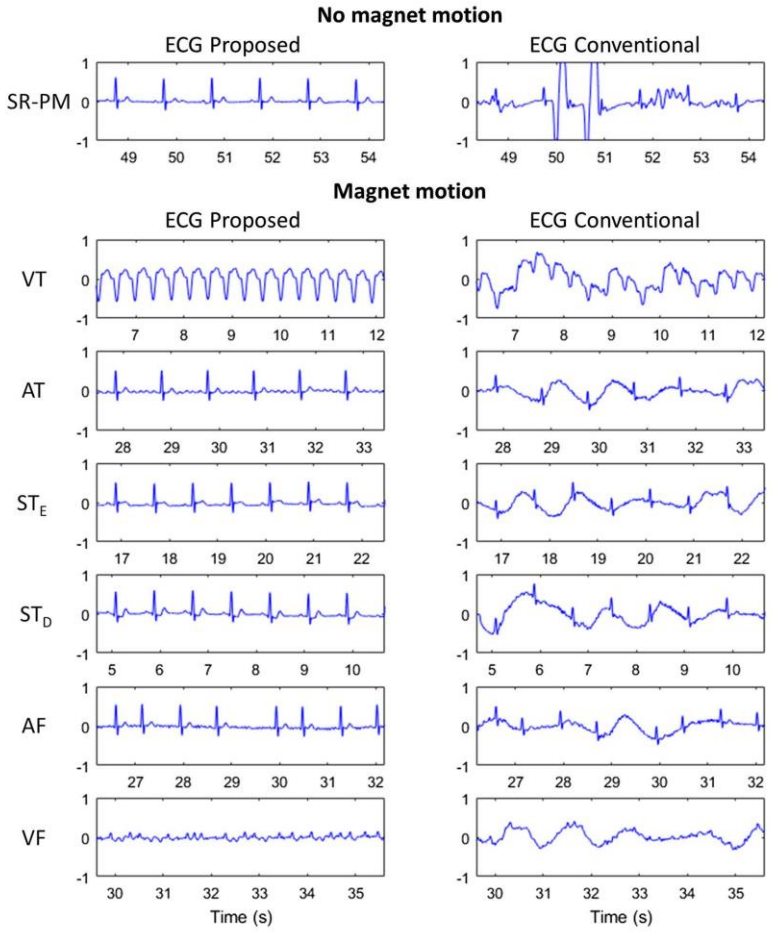

FIGURE 8. Example distortions and noise observed on the ECG signal (ECG1 lead) during t6 magnet motion with the ECG simulator in the conductive phantom: (SR-PM) sinus rhythm with simulated patient motion, no magnet motion; (VT) Ventricular Tachycardia; (AT) Atrial Fibrillation; (ST_E) ST Elevation; (ST_D) ST Depression; (AF) Atrial Fibrillation; (VF) Ventricular Fibrillation.

TABLE 4. Correlation coefficients from the whole PQRST wave during t6 magnet operation mode with phantom and ECG simulator.

Sinus rhythm	t	Proposed	Conventional
SR-PM	t_6	0.964 ± 0.01	0.385 ± 0.24
VT		0.993 ± 0.00	0.752 ± 0.11
AT		0.949 ± 0.03	0.507 ± 0.20
ST_E		0.964 ± 0.02	0.475 ± 0.18
ST_D		0.961 ± 0.02	0.524 ± 0.16
AF		–	–
VF		–	–

CONCLUSION

A novel ECG sensor has been designed and evaluated for use during remote magnetic catheter navigation. The sensor is based on an MRI-compatible technology with short wires and optical conversion. The sensor drastically reduces distortions on the ECG. It has the potential to allow uninterrupted monitoring of the patient during EP procedures with an RMN system. It might also be used to optimize the duration and the performance of the procedure, e.g. for pacemapping and VT localization based on QRS cor-

relation analysis. However, an evaluation of the proposed device with a larger number of human subjects would be necessary to accurately assess the benefit for EP clinical procedures.

ACKNOWLEDGMENT

This study was funded by the French "Investments for the Future" program under Grant Number ANR-15-RHU-0004. The authors also thank INSERM, CPER 2007 2013, Région Lorraine and FEDER for the funding of the Niobe Magnetic Navigation System, Stereotaxis Inc..

CONFLICT OF INTEREST

J.D.R. and G.M. are Schiller employees. P.H. is a Biosense employee. L.J. is a Stereotaxis employee.

REFERENCES

[1]Abächerli, R., C. Pasquier, F. Odille, M. Kraemer, J.-J. Schmid, and J. Felblinger. Suppression of MR gradient artefacts on electrophysiological signals based on an adaptive real-time filter with LMS coefficient updates. *Magma N. Y.* 18:41–50, 2005.

[2]Aryana, A., A. d'Avila, E. K. Heist, T. Mela, J. P. Singh, J. N. Ruskin, and V. Y. Reddy. Remote magnetic navigation to guide endocardial and epicardial catheter mapping of scar-related ventricular tachycardia. *Circulation* 115:1191–1200, 2007.

[3]Bauernfeind, T., F. Akca, B. Schwagten, N. de Groot, Y. Van Belle, S. Valk, B. Ujvari, L. Jordaens, and T. Szili-Torok. The magnetic navigation system allows safety and high efficacy for ablation of arrhythmias. *Europace* 13:1015–1021, 2011.

[4]de Chillou, C., L. Groben, I. Magnin-Poull, M. Andronache, M. MagdiAbbas, N. Zhang, A. Abdelaal, S. Ammar, J.-M. Sellal, J. Schwartz, B. Brembilla-Perrot, E. Aliot, and F. E. Marchlinski. Localizing the critical isthmus of postinfarct ventricular tachycardia: the value of pace-mapping during sinus rhythm. *Heart Rhythm* 11:175–181, 2014.

[5]Faddis, M. N., J. Chen, J. Osborn, M. Talcott, M. E. Cain, and B. D. Lindsay. Magnetic guidance system for cardiac electrophysiology: a prospective trial of safety and efficacy in humans. *J. Am. Coll. Cardiol.* 42:1952–1958, 2003.

[6]Felblinger, J., C. Lehmann, and C. Boesch. Electrocardiogram acquisition during MR examinations for patient monitoring and sequence triggering. *Magn. Reson. Med.* 32:523–529, 1994.

[7]Felblinger, J., J. Slotboom, R. Kreis, B. Jung, and C. Boesch. Restoration of electrophysiological signals distorted by inductive effects of magnetic field gradients during MR sequences. *Magn. Reson. Med.* 41:715–721, 1999.

[8]Huiskamp, G. J., and A. van Oosterom. Heart position and orientation in forward and inverse electrocardiography. *Med. Biol. Eng. Comput.* 30:613–620, 1992.

[9]Langley, P., E. J. Bowers, and A. Murray. Principal component analysis as a tool for analyzing beat-to-beat changes in ECG features: application to ECG-derived respiration. *IEEE Trans. Biomed. Eng.* 57:821–829, 2010.

[10]Liu, Y., Z. Syed, B. M. Scirica, D. A. Morrow, J. V. Guttag, and C. M. Stultz. ECG morphological variability in beat space for risk stratification after acute coronary syndrome. *J. Am. Heart Assoc.* 3:e000981, 2014.

[11]Odille, F., S. Liu, P. van Dam, and J. Felblinger. Statistical variations of heart orientation in healthy adults. *Computing* 44:1, 2017. https://doi.org/10.22489/cinc.2017.225-058.

[12]Odille, F., C. Pasquier, R. Abächerli, P.-A. Vuissoz, G. P. Zientara, and J. Felblinger. Noise cancellation signal processing method and computer system for improved real-time electrocardiogram artifact correction during MRI data acquisition. *IEEE Trans. Biomed. Eng.* 54:630–640, 2007.

[13]Oster, J., O. Pietquin, M. Kraemer, and J. Felblinger. Nonlinear bayesian filtering for denoising of electrocardiograms acquired in a magnetic resonance environment. *IEEE Trans. Biomed. Eng.* 57:1628–1638, 2010.

[14]Pappone, C., G. Vicedomini, F. Manguso, F. Gugliotta, P. Mazzone, S. Gulletta, N. Sora, S. Sala, A. Marzi, G. Augello, L. Livolsi, A. Santagostino, and V. Santinelli. Robotic magnetic navigation for atrial fibrillation ablation. *J. Am. Coll. Cardiol.* 47:1390–1400, 2006.

[15]Pollard, A. E., and R. C. Barr. Computer simulations of activation in an anatomically based model of the human ventricular conduction system. *IEEE Trans. Biomed. Eng.* 38:982–996, 1991.

[16]Syed, Z., C. M. Stultz, B. M. Scirica, and J. V. Guttag. Computationally generated cardiac biomarkers for risk stratification after acute coronary syndrome. *Sci. Transl. Med.* 3:102ra95, 2011.

[17]Tomašić, I., and R. Trobec. Electrocardiographic systems with reduced numbers of leads synthesis of the 12-lead ECG. *IEEE Rev. Biomed. Eng.* 7:126–142, 2014.

[18]Trobec, R., and I. Tomašić. Synthesis of the 12-lead electrocardiogram from differential leads. *IEEE Trans. Inf. Technol. Biomed.* 15:615–621, 2011.

3) Isthmus entrance calculator based on electrogram characteristics

Multiple electrogram characteristics have been found to be associated with re-entry circuits. However, the analysis of any parameter alone is insufficient to completely define the VT isthmus location. The following paper studies the value of 10 different electrogram characteristics in identifying a VT isthmus entrance[151]. The studied parameters were bipolar and unipolar voltage, time from QRS onset to electrogram onset, time from electrogram offset to QRS offset, electrogram duration, number of positive peaks, S-QRS interval as well as the presence of fragmentation, double potentials and late potentials. All the parameters can be collected in the absence of an induced VT.

My contribution to the paper was in acquiring all the different electrogram characteristics into the CARTO® system and precisely defining all the components of the isthmus. Once the left ventricular 3D map was entirely reconstructed, I helped defining the critical isthmus by drawing onto the map the lateral boundaries, entrance and exit channels as well as the mid-isthmus line. Isthmus dimensions were also measured. The isthmus definition played a critical role in the segmentation of the PM points as all the points were analyzed according to the VT isthmus entrance location.

Logistic regression analysis showed that bipolar voltage, number of electrogram positive peaks, and S-QRS interval were independently associated with VT isthmus entrance location. A multi-parameter electrogram evaluation is a promising approach to localize a VT isthmus entrance. Based upon these results, a web-based graphical user interface was developed and implemented in an automatic calculator to quickly determine the likelihood that a given site is located at a VT isthmus entrance. The calculator is accessible at the following link: VT Isthmus Entrance Calculator (figure 12).

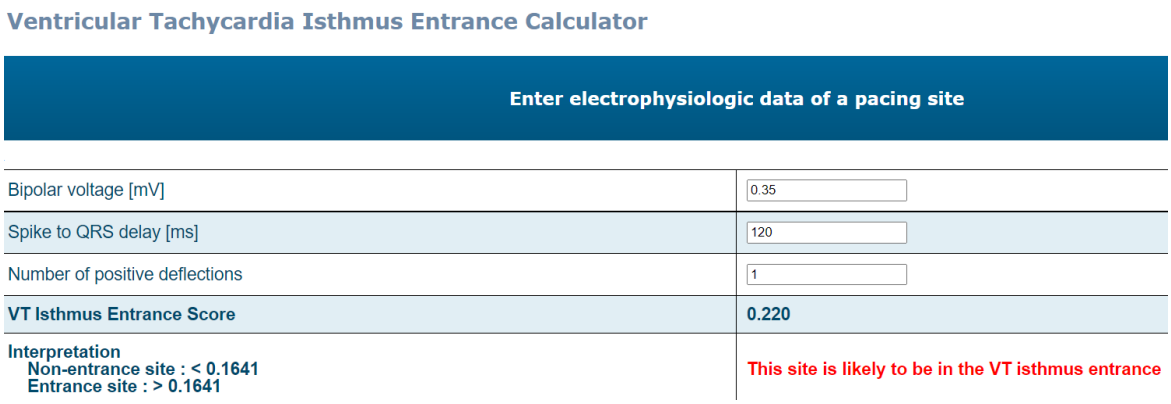

Figure 12. Screenshot of the ventricular tachycardia isthmus entrance calculator predicting whether a pacing site is likely to be in the VT isthmus entrance. A pacing site with a bipolar voltage of 0.35 mV, an S-QRS interval of 120 ms and 1 positive deflection is likely to be in the VT isthmus entrance VT Isthmus Entrance Calculator[151].

ESC European Society of Cardiology
Europace (2020) **22**, 109–116
doi:10.1093/europace/euz315

An efficient algorithm based on electrograms characteristics to identify ventricular tachycardia isthmus entrance in post-infarct patients

Alberto Battaglia[1,2†], Freddy Odille[2,3†], Isabelle Magnin-Poull[1], Jean-Marc Sellal[1,3], Philip Hoyland[2,3,4], Darren Hooks[5], Damien Voilliot[1,2], Jacques Felblinger[2,3†], and Christian de Chillou[1,3*†]

[1]Département de Cardiologie, CHRU de Nancy, Nancy F-54500, France; [2]CIC-IT, Université de Lorraine, INSERM, CHRU Nancy, Nancy F-54500, France; [3]IADI, Université de Lorraine, INSERM, Nancy F-54500, France; [4]Biosense Webster France, Johnson & Johnson, Issy les Moulineaux F-92787, France; and [5]Department of Cardiology, Wellington Hospital, Wellington, New Zealand

Received 9 August 2019; editorial decision 20 October 2019; accepted 24 October 2019; online publish-ahead-of-print 14 November 2019

Aims Our study assesses the value of electrograms (EGMs) characteristics to identify a ventricular tachycardia (VT) isthmus entrance in patients with post-infarct VT. Post-infarct VTs are mostly due to a re-entrant circuit. A pacemapping (PM) approach is able to localize the VT isthmus during sinus rhythm. Limited data are available about the role of local EGMs in defining VT isthmus location.

Methods and results Twenty consecutive patients (70% male) referred for post-infarct VT catheter ablation were included in the present study. The VT isthmus was defined according to the PM method. At each recording site, 10 characteristics of the local EGM were assessed to predict the location of the VT isthmus entrance. In total, 924 EGMs were acquired, of which 127 were located in the VT isthmus entrance. Logistic regression analysis showed that bipolar voltage, number of EGM positive peaks, and sQRS interval were independently associated with VT isthmus entrance location. The ROC curve best fitted the model at the cut-off 0.1641 (sensitivity 72%, specificity 75.2%, positive predictive value 31.3%, negative predictive value 94.4%, area under the curve 0.78, $P < 0.001$). Based upon these results, we developed an algorithm implemented in an automatic calculator to determine the likelihood that an EGM is located at a VT isthmus entrance.

Conclusion Our study suggests that three EGM characteristics: bipolar voltage, number of positive peaks, and sQRS interval can successfully identify a VT isthmus entrance in post-infarct patients.

Keywords Ventricular tachycardia • Ischaemic cardiomyopathy • Myocardial infarction • Re-entry circuit • Pacemapping • VT isthmus entrance • Ablation

Introduction

In most cases, a re-entrant mechanism is responsible for post-infarct ventricular tachycardias (VTs).[1] The relationship of these re-entrant circuits to the ventricular scar resulting from myocardial infarction was elegantly defined in early surgical studies.[2] Pathologically, the essential component of the ventricular scar that promotes re-entry is its histologic heterogeneity, with varying degrees of subendocardial myocardial fibre preservation within dense zones of fibrosis. These zones are detectable as low voltage areas during electroanatomic

* Corresponding author. Tel: +33 (0) 383157443; fax: +33 (0) 383154917. *E-mail address*: c.dechillou@chru-nancy.fr

† The first and last two authors contributed equally to this work.

What's new?

- Between 10 easy detectable local electrograms (EGMs) characteristics, bipolar voltage, number of EGM positive peaks, and sQRS interval were independently associated with ventricular tachycardia (VT) isthmus entrance location.
- The major advantage is related to the independency of this approach to any 12 leads electrocardiogram VT morphology.
- The automatic calculator will help rapid adoption of this method. The likelihood of a point to be located in a VT isthmus entrance can be quickly assessed by all.

mapping in sinus rhythm. The spatial extent of low voltage areas normally far exceeds that of the critical isthmus. The critical isthmus of the re-entrant circuit is a channel of viable myocardial cells delimitated by two lateral boundaries. These barriers are anatomical obstacles or simply areas of functional conduction block.[3] Identifying these areas of residual conduction deep inside a larger area of fibrosis is key to successful VT ablation. Different techniques, such as entrainment mapping or activation mapping during VT, have been proposed[4,5] to identify the VT isthmus. More recently, substrate-based approaches have been investigated,[6–8] especially in cases of poorly-tolerated VTs, in order to ablate the VT substrate during sinus rhythm. Recently, we demonstrated that pacemapping (PM) during sinus rhythm is a powerful technique to unmask the protected isthmus of post-infarct VT circuits.[9,10] This technique consists of comparing the paced electrocardiogram (ECG) to the clinical VT. Typically, VT exit pacing sites yield a highly matched QRS morphology. Conversely, the VT entrance channel is always located in a poor correlation zone. An abrupt transition between a paced-QRS that matches the clinical VT (exit site) and a non-matched paced-QRS (entrance site) identifies the core of a VT isthmus. The current PM technique is based on the availability of a 12-lead ECG during VT. Therefore the absence of an induced VT is a limitation which is inherent to the PM technique. In such cases analysis of electrogram (EGM) characteristics may be useful to identify a protected VT isthmus. In particular, it has been shown that the conduction velocity is reduced at VT isthmus entrance.[11] Therefore, we hypothesized that the characteristics of the EGM recorded during sinus rhythm at VT isthmus entrance may have some specific features. Our study aims to evaluate this hypothesis.

Methods

Patients

Twenty consecutive patients (14 men, mean age 65 ± 12 years) referred for post-infarct VT catheter ablation in our institution between January 2015 and January 2017 and fulfilling the following inclusion criteria were included in the present retrospective study: (i) presence of a spontaneous sustained monomorphic VT documented by a 12-lead ECG which was (ii) subsequently inducible during the electrophysiological study, (iii) identification of the index VT isthmus by the PM technique (with pacing cycle length at 600 ms), and (iv) confirmation that radiofrequency (RF) catheter ablation lesions applied across the VT isthmus prevented further VT induction. A consort diagram of the enrolled sample is available in the Supplementary material online, *Figure S1*.

Procedural details

Electrophysiological study and left ventricular anatomical mapping

Electrophysiological study, mapping, and catheter ablation were performed as previously described.[5,12] For each procedure, endocardial signal and surface ECG were recorded using the BARD LabSystem PRO (CR Bard Inc., Lowell, MA, USA) and CARTO® (Biosense Webster, Diamond Bar, CA, USA). In brief, a bipolar catheter was inserted via the femoral vein and positioned at the right ventricular apex and used primarily for VT induction with the application of up to three extrastimuli during spontaneous rhythm (600 ms and then 400 ms basic cycle length). Failure to induce a sustained VT promoted the same protocol from another site (alternatively right ventricle outflow tract or left ventricle). The 12-lead ECG of the induced VT was captured on the PASO software of the CARTO® system. Sinus rhythm was then restored by overdrive pacing or external cardioversion before mapping. Access to the left ventricle was achieved anterogradely through trans-septal puncture. Anticoagulation was maintained with unfractioned heparin, targeting an ACT 250–350 s. Sedation was obtained with 10 mg IV nalbuphine, with incremental doses at 5 mg as necessary. A 7 Fr, 3.5 mm-irrigated tip catheter (THERMOCOOL®, Biosense-Webster, Johnson & Johnson) was used for both left ventricular volume reconstruction and mapping/ablation of VT circuits, in a respiration-gated mode. All procedures were performed with the Niobe® robotic magnetic navigation system (Stereotaxis Inc., St. Louis, MO, USA). Radiofrequency delivery was performed with Stockert-Cordis RF generator (Stockert GmbH, Freiburg, Germany).

Pacemapping points acquisition

Bipolar pacing (600 ms cycle length) with an output at twice diastolic threshold was performed at each pacing site, tagged as 'Pacing Site'. At each pacing site, the corresponding paced 12-lead ECG was stored in the CARTO® system. In order to accurately define the critical isthmus, points were acquired with highest density within zones of (i) low voltage (bipolar voltage <1.5 mV), (ii) diastolic potentials, and (iii) double potentials or fractionated EGMs The mapping procedure was terminated when a sufficient density of points was obtained to understand the VT circuit. For each pacing site, the PASO™ software calculated the percentage of morphology match between the paced-QRS and the 12-lead ECG during VT (range −100% to +100%). These values were displayed as spectrum of colour on the anatomical model [the so-called 'pacemapping (PM) map'].

Ventricular tachycardia circuit and ventricular tachycardia isthmus definition

The interpretation of a PM map starts with the identification of the VT exit zone which corresponds to the endocardial region where paced-QRS ECG matches (correlation values above 90%) the VT morphology. Dense PM in areas just adjacent to the VT exit zone shows a gradual decrease in match, except at the entrance of the VT isthmus where, within a few millimetres of distance, an abrupt transition between a good and a poor correlation (correlation values usually lower than 30%) is observed. The VT critical isthmus was defined in between a zone of good correlation (exit site, red coloured) and the poorest correlation zone (entrance site, purple coloured) surrounded by a zone of intermediate correlation (lateral boundaries, green-yellow-blue coloured).[9,13] All portions of each VT isthmus (lateral boundaries, entrance and exit channel, mid-isthmus line) were manually drawn on the 3D map.

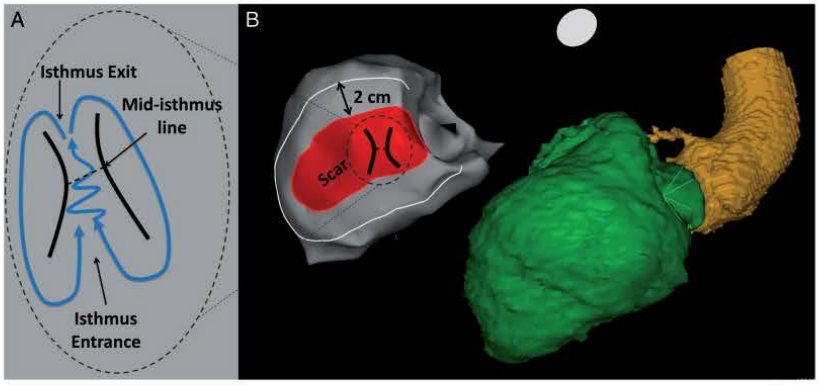

Figure 1 Example of area of interest analysed. (*A*) Isthmus channel classification according to published criteria. (*B*) Caudal postero-anterior view showing the 3D shell of the left ventricle (left panel) and the anatomical 3D reconstruction according to the CT scan performed the day before the procedure (right panel). The area of interest was all the myocardial scar (defined by bipolar cut-off value < 1.5 mv) and a surrounding area of 2 cm. CT, computed tomography.

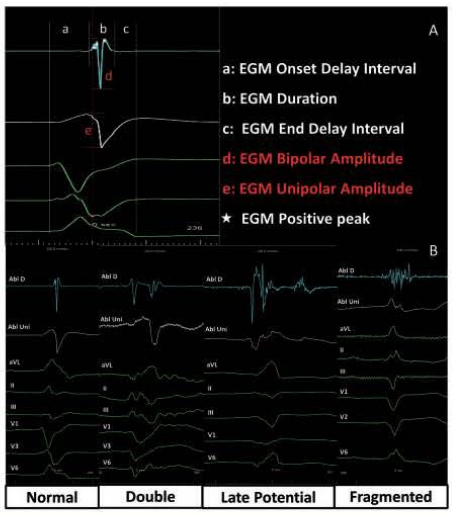

Figure 2 Local electrogram analysis. (*A*) Variables measured for each electrogram. (*B*) Examples of electrogram classification.

Radiofrequency ablation and endpoint

Identification of the ablation target was based on the analysis of the colour-coded PM map. Linear RF lesions were placed to transect the VT isthmus. Radiofrequency energy was delivered in a temperature-controlled mode for 60–120 s at each ablation site with a maximal temperature/power target of 45°C/40 W.

A programmed ventricular stimulation protocol was again performed. Non-inducibility of sustained monomorphic VT <270/min was considered as an acute procedural success. After ablation, patients were monitored for 72 h by telemetry. Transthoracic echocardiography was performed within 2 days after ablation, prior to discharge.

Post hoc analysis

All EGMs recorded during sinus rhythm at each pacing site in the scar area (defined by bipolar voltage <1.5 mV) and 2 cm around were analysed (*Figure 1*). Each EGM was classified (*Figure 2*) according to the following published criteria.[13] Electrograms with sharp, biphasic, or triphasic spikes, amplitude >1.5 mV and duration <70 ms were defined as normal. Fragmented EGMs were defined by the presence of more than 4 sharp spikes with amplitude of less than 1.5 mV. Double potentials EGMs were defined by two discrete deflections separated by an isoelectric interval. Electrograms with late potentials EGMs were defined by a sharp component occurring after the end of the QRS.

The 10 following EGM characteristics were assessed for statistical analysis: (1) bipolar voltage, (2) unipolar voltage, (3) time interval from QRS onset to EGM onset, (4) time interval from EGM offset to QRS offset, (5) EGM duration, (6) number of positive peaks, (7) presence of fragmentation, (8) presence of double potentials, (9) presence of late potentials, and (10) time interval between the pacing spike and the resulting QRS complex (sQRS interval).

Statistical analysis

Categorical variables are reported as counts and percentages, while continuous variables as median and interquartile range. Correlations between baseline characteristics stratified for isthmus entrance location points were tested in cross-tabulation tables by means of the Pearson χ^2 or Fisher's exact test and by one-way ANOVA, respectively for categorical and continuous variables. To test the independent correlation of these parameters with entrance isthmus location, all variables reporting a significant correlation at univariate analysis were included in a stepwise forward multivariate logistic regression model. Reliability of the obtained model was tested by ROC curve. A two-sided *P*-value <0.05 was

Table 1 Baseline population characteristics

Variables	Sample population (20 patients)
Age (years), mean ± SD	65 ± 12
Male, *n* (%)	14 (70)
Cardiovascular risk factors, *n* (%)	
Arterial hypertension	15 (75)
Diabetes	5 (25)
Dyslipidaemia	11 (80)
Active smoker	9 (45)
Body mass index (kg/m^2)	29.9 ± 7.0
History of dysthyroidism, *n* (%)	5 (32)
History of stroke/TIA (%), *n* (%)	4 (20)
Peripheral vasculopathy, *n* (%)	5 (20)
History of atrial fibrillation, *n* (%)	3 (15)
Ejection fraction, mean ± SD	31.1 ± 12.2
CAD history	
Years of CAD history, mean ± SD	17.1 ± 11.5
At least two vessels involved	7 (35)
Presence of totally occluded coronary artery, *n* (%)	9 (45)
Previously positioned ICD	14 (70)
Of which in secondary prevention	11 (55)
ICD shocks in the 30 days before the procedure (mean)	2.1
ATP delivered in the 30 days before the procedure (mean)	39.0
Antiarrhythmic drug treatment at admission, *n* (%)	
Amiodarone	12 (60)
Beta-blockers	19(95)
ACE-inhibitors/ARB	15 (75)
Oral anticoagulation	11(55)
Antiaggregant therapy	16 (80)

ACE-inhibitors, angiotensin-converting enzyme inhibitors; ARB, angiotensin II receptor blockers; CAD, coronary artery disease; ICD, implantable cardioverter-defibrillator; SD, standard deviation; TIA, transient ischaemic attack.

considered statistically significant. All analyses were performed with SPSS 21.0 (SPSS Inc., Chicago, IL, USA).

Calculator development

A web-based graphical user interface was developed in order to predict whether a pacing site was likely to be in the VT isthmus entrance based on the aforementioned multivariate logistic regression model (link: http://freddy.odille.free.fr/software/VTIsthmusEntranceCalculator/VTIsthmusEntranceCalculator.html).

Results

The clinical characteristics of the baseline population are shown in *Table 1*.

The clinical VT was inducible in all patients. Inducted VTs were assessed, according to the PM technique, in each and every patient. Mean VTs cycle length was 377 ± 64 ms. As a result, 20 VT isthmuses were identified. Mean isthmus dimensions were 39.5 ± 10.6 mm (length) and 28.2 ± 10.3 mm (width). Radiofrequency application (mean 1276 ± 797 s) across the mid-isthmus line prevented clinical VT induction in all patients. Sixteen out of 20 (80%) patients were non-inducible at the end of the procedure. In the remaining four cases, a non-clinical non-sustained polymorphic VT (mean cycle length 276 ± 19 ms) was inducible.

In total, 924 PM points were analysed, of which 127 (14%) were located at a VT isthmus entrance.

As shown in *Table 2*, eight of the 10 EGMs characteristics were significantly different between VT isthmus entrance and other zones. Hence, EGMs located in the VT isthmus entrance showed lower bipolar voltage (0.52 ± 0.54 vs. 1.44 ± 1.64 mV, $P < 0.001$), lower unipolar voltage (3.18 ± 1.93 vs. 5.33 ± 3.76 mV, $P < 0.001$), and had more positive peaks (6.4 ± 3.6 vs. 4.4 ± 2.6, $P < 0.001$). Fragmented EGM and EGM with late potential were more frequently located in the VT isthmus entrance (64% vs. 35%, $P < 0.001$ and 14% vs. 6%, $P = 0.002$, respectively). Finally, the sQRS interval was significantly longer when pacing at the VT isthmus entrance (89.1 ± 34.9 ms vs. 49.9 ± 31.3 ms, $P < 0.001$).

The multivariate model identified three EGM parameters as independent predictors of isthmus entrance: (i) EGM bipolar voltage, (ii) number of EGM positive peaks, and (iii) sQRS duration (*Table 2*). The reliability of this model was tested by a ROC curve analysis (*Figure 3*). The ROC curve best fitted the model at the cut-off 0.1641 (sensitivity 72%, specificity 75.2%, positive predictive value 31.3%, negative predictive value 94.4%, area under the curve 0.78, $P < 0.001$). Based upon the logistic regression analysis, we developed an automatic calculator (link: http://freddy.odille.free.fr/software/VTIsthmusEntranceCalculator/VTIsthmusEntranceCalculator.html). The user is asked to enter values of bipolar voltage, sQRS interval, and EGM number of positive deflections of a given EGM (Figure 4). Then the calculator returns the score given by the model along with the likelihood that this EGM is located in the VT isthmus entrance. *Figure 5* shows two examples of maps with EGM assigned as 'VT isthmus entrance points' or 'non-VT isthmus entrance points' by the calculator.

Discussion

We assessed the value of several EGM parameters to identify a VT isthmus entrance in patients with post-infarct VT.

Historically, EGM fragmentation was firstly targeted. Electrogram fractionation is generated by slowed and non-uniform conduction due to the transverse uncoupling of myocytes by fibrosis. Bogun *et al.*[14] showed 'late potentials' (defined as EGM ending after the end of the QRS without diastolic activity) in 57 out of 94 ablation sites where concealed entrainment was performed during VT. Only 31 'late potential' sites were observed out of 51 sites where RF application interrupted the VT (sensitivity 61%, positive predictive value 54%). Despite the selection bias that only concealed entrainment sites were assessed, the 'late potential' specificity and the negative predictive value were low (39% and 46%, respectively). Consequently, targeting fractionated signals alone is not an optimal strategy to correctly guide VT ablation.

Table 2 Local electrograms characteristics analysed according to VT isthmus entrance location

	Entrance isthmus site	Other site	*P*-value univariate	Entrance *P*-value multivariate	Odd ratio (95% CI)
Number (%)	127	797			
Bipolar voltage (mV), mean ± SD	0.52 ± 0.54	1.44 ± 1.64	<0.001	0.005	0.581 (0.397–0.851)
Unipolar voltage (mV), mean ± SD	3.18 ± 1.93	5.33 ± 3.76	<0.001	NS	
Stimulus to QRS interval (ms), mean ± SD	89.1 ± 34.9	49.9 ± 31.3	<0.001	<0.001	1.014 (1.009–1.020)
EGM duration (ms), mean ± SD	144.3 ± 68.9	117.7 ± 68.9	<0.001	NS	
Delay QRS onset—EGM onset (ms), mean ± SD	26.0 ± 38.4	21.9 ± 36.2	0.24		
Delay EGM offset—QRS offset (ms), mean ± SD	36.5 ± 63.9	12.8 ± 64.9	<0.001	NS	
Number of EGM positive deflections, mean ± SD	6.4 ± 3.6	4.4 ± 2.6	<0.001	0.021	1.089 (1.013–1.170)
Fragmented EGM	81 (64%)	277 (35%)	<0.001	NS	
Double potentials EGM	8 (6%)	30 (4%)	0.18		
EGM with late potentials	18 (14%)	51 (6%)	0.002	NS	

CI, confidence interval; EGM, electrogram; SD, standard deviation; NS, non significant.

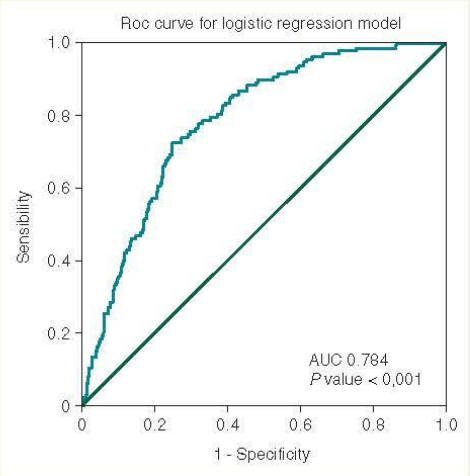

Figure 3 ROC curve testing the logistic regression model. The ROC curve best fitted the model at the cut-off 0.1641 (sensibility 72%, specificity 75.2, positive predictive value 31.3%, negative predictive value 94.4%, AUC 0.78, $P<0.001$). AUC, area under the curve; ROC, receiver operating characteristic.

The effectiveness of the local bipolar voltage scanning to predict a VT isthmus location has also been investigated. In patients without known cardiovascular disease, 95% of EGMs have a bipolar voltage >1.55 mV. Accordingly, 1.5 mV has become the established bipolar voltage cut-off for identifying myocardial scar.[15] Relative voltage preservation within denser regions of scar is a hallmark of central conducting channels that may form anatomically constrained diastolic isthmuses during VT. These zones can be seen by altering the voltage representation on colour isopotential maps. In the original study by

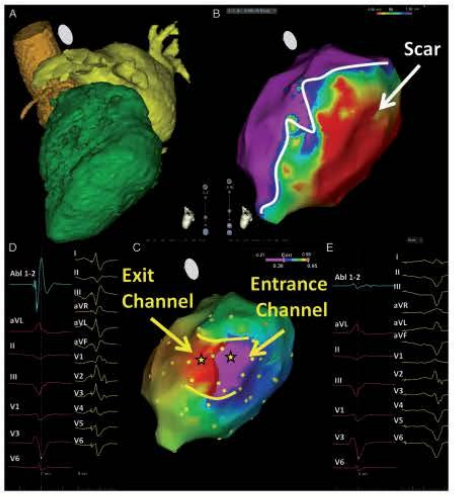

Figure 4 Different EGM characteristics and sQRS intervals according to PM site location. (*A*) CT scan heart three-dimensional reconstruction. (*B*) Bipolar left ventricular voltage map showing wide infero-lateral myocardial scar (white line). (*C*) PM map showing exit site (red coloured) based on PM points with a VT correlation greater than 95%, next to the entrance channel (violet coloured) based on PM points with less than 30% VT correlation. Lateral borders delimitated by areas of intermediate correlation. Yellow stars highlight pacing points. (*D*) Exit site located PM point. Local EGM characteristics: bipolar voltage 1.36 mV, number of positive peaks 2, sQRS interval 0 ms. (*E*) Entrance site located PM point. Local EGM characteristics: bipolar voltage 0.14 mV, number of positive peaks 6, sQRS interval 182 ms. CT, computed tomography; EGM, electrogram; PM, pacemapping; VT, ventricular tachycardia.

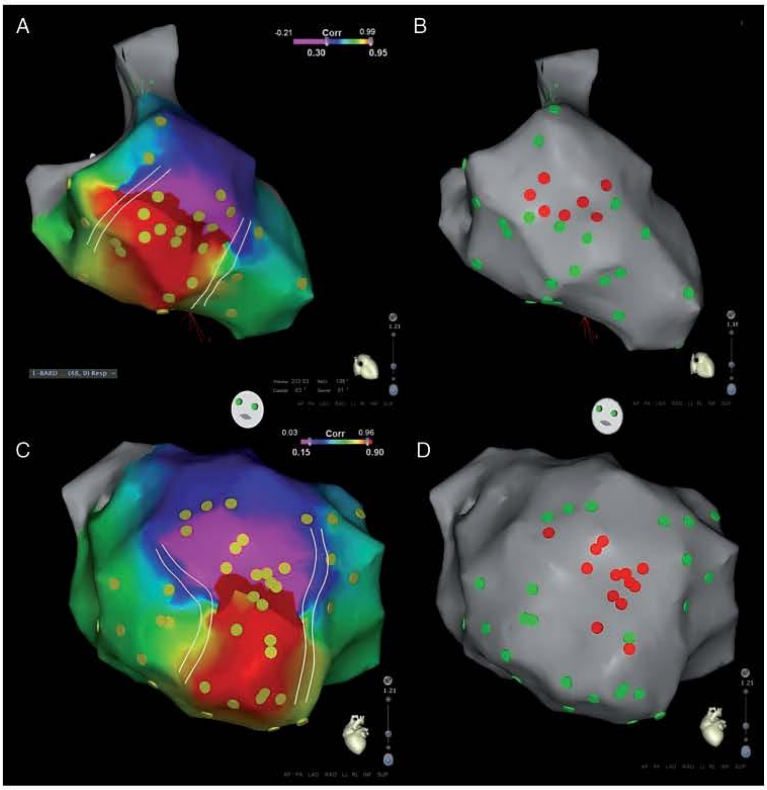

Figure 5 Examples of calculator guided map. (*A*) PM map showing infero-lateral VT isthmus with exit channel located inferiorly. Yellow points show pacing points. (*B*) Calculator guided map showing entrance located points (red coloured). Pacing points not located in VT isthmus entrance are green coloured. Note that the calculator identify three PM sites in the proximal exit channel. (*C*) PM map showing an anterior wall VT isthmus with exit channel located inferiorly. Yellow points show pacing points. (*D*) Calculator guided map showing entrance located points (red coloured). Pacing points not located in VT isthmus entrance are green coloured. Note the identification of some points in the VT exit channel. PM, pacemapping; VT, ventricular tachycardia.

Arenal *et al.*,[7] electroanatomic maps from 26 patients with post-infarction cardiomyopathy were analysed for presence of voltage channels and their relationship with clinical or induced VTs. The authors found that 20 out of 23 (87%) identified channels were associated with a VT isthmus. They used five pre-specified voltage cut-offs with only a 0.01 mV difference between the upper and lower voltage limits. It is unclear whether such a small difference is truly important. These encouraging results were not confirmed thereafter. Mountantonakis *et al.*,[16] in a larger sample size of patients, showed that voltage channels could be identified in 88% of patients with post-infarction VT. In his study, only 11 out of 25 induced VT were maintained by an identified channel (sensitivity 44%). Moreover, only 11 out of 37 channels contained a clinical VT isthmus (positive predicting value 29.7%). Nevertheless, the voltage channel ability to accurately guide ablation is poor.

The sQRS interval may provide additional information about VT isthmus location. By pacing in low voltage areas the time required for the electrical impulse to reach the healthy surrounding myocardial tissue may be long. Thus slow conducting zones are often unmasked by the presence of a long sQRS interval. Stevenson *et al.*,[17] in his sample of 13 post-infarct VT patients, considered 75 PM sites showing fragmented EGM during sinus rhythm. A sQRS >40 ms was observed in 41 out of 75 sites (55%). Participation of each site in a re-entry circuit was then evaluated by entrainment techniques during induced VT. Out of 28 points showing concealed entrainment during VT, 21 showed sQRS >40 ms in sinus rhythm (sensitivity 75%). Between 41 points with sQRS >40 ms only 21 were correctly located in a re-entry circuit (positive predictive value 51%). The resulting specificity and negative predictive values were 51% and 79%, respectively (considering the selection bias the only fragmented EGM sites were

assessed in this study). A subsequent study,[18] based on a larger sample of 829 PM points, confirmed the higher prevalence of a slow conducting zone in a re-entry circuit. By only considering the sQRS >40 ms the sensitivity/specificity of a point to be located in a VT isthmus were 68% and 53%, respectively. The positive/negative predictive value were 33% and 83%. Sites with prolonged sQRS intervals during sinus rhythm pacing were frequently associated with re-entry circuits. However, sQRS interval measurements are not sufficient to precisely identify the VT isthmus.

None of these three variables (EGM fragmentation, local bipolar voltage, and the sQRS interval), taken correctly guide VT isthmus localization.

Multiple EGM parameters evaluation is a promising approach to correctly localize slow conducting zones responsible for VT.

The first multi-parameters EGM evaluation showed promising results. Brunckhorst *et al.*[19] simultaneously analysed EGM duration, EGM bipolar voltage, and sQRS interval. This model, based on 931 PM points, showed a sensitivity of 80% and a specificity of 51% (positive and negative predictive values of this model were not disclosed). This proposed model showed good agreement with ours. Recently, Nayyar *et al.*,[20] analysed 1292 PM points and reported that EGM activation time and EGM entropy accurately identified VT channels during sinus rhythm. This model was of impressive performance (sensitivity 86%, specificity 100%, positive predictive value 93%, and negative predictive value 100%). Electrogram parameters considered in both experiences are quite similar to ours. Main differences arise from the uniform pacing cycle length used in our study. Differences in reported model performance may be linked to different definitions of the target zones. In our study, VT isthmus was clearly anatomically defined, including mid-isthmus lines and lateral boundaries. Using this clear anatomical definition we were able to consider only PM points performed in the isthmus entrance: the anatomical area above the mid-isthmus line. In the Nayyar *et al.*[20] experience a target area named 'channel' was used. Its relation with the VT isthmus was not clearly stated. A VT channel is usually located between the mid-isthmus line and the isthmus exit. It is not clearly demonstrated if a single VT channel ablation may effectively suppress all possible pathways inside a VT isthmus whose width may be wider. In fact, in their experience, several VT channels were identified in each patient leading to a wider ablation area. Patients enrolled in our experience showed only one VT isthmus enhancing our conclusion strength.

Our study first demonstrated that three EGM parameters (local bipolar voltage, number of EGM positive peaks, and sQRS interval) are strong independent predictors of VT isthmus entrance. All 924 pace-map points were acquired at the same pacing cycle length of 600 ms. Each point was blindly reviewed by two independent Electrophysiologists. Each isthmus found was precisely anatomically defined. Mid-isthmus lines and lateral boundaries were clearly defined. To our knowledge, our study constitutes the largest sample of PM maps performed with a uniform pacing cycle length reported in the literature. Using an in-house calculator, the likelihood of a point to be located in a VT isthmus entrance can be quickly assessed. Our methodology is more rigorous and our performance statistics are as high as other published studies (sensitivity 72%, specificity 75%). The observed low positive predictive value of 31.3% is comparable with published studies considering an un-biased series of PM points. The low positive predictive value derives from the calculator inability to differentiate points located on the mid-isthmus line from those in the proximal VT isthmus exit channel. These points, statistically considered as false positive points, are anyway located inside the VT isthmus, the target area of each VT ablation. The negative predictive value of 94.4% of our model further strengthens its clinical utility. The calculator can be used in cases where clinical VT is non-inducible. Our approach is particularly easy and quick to apply, thus facilitating rapid adoption. Integration of this calculator in mapping software could refine the definition of the critical isthmus entrance and enhance the efficacy of VT ablation. This approach leads to significant clinical amendments.

Limitations

This is a non-randomized study. Consecutive cases were analysed to limit the consequences of selection bias. A routine LP or LAVA ablation was not performed in this series of patients. Electrogram information were acquired only in sinus rhythm. Further prospective studies need to be performed to validate the utility of the model derived from the current study.

Conclusion

The local bipolar voltage, EGM characteristics, and sQRS interval are strongly related with VT isthmus entrance. We have identified a selection criteria determining whether a point is located in the isthmus entrance. This approach does not rely on the induction of any VT. The criteria has been integrated in a calculator, thus facilitating adoption.

Supplementary material

Supplementary material is available at *Europace* online.

Conflict of interest: none declared.

References

1. Klein H, Karp RB, Kouchoukos NT, Zorn GL Jr, James TN, Waldo AL. Intra-operative electrophysiologic mapping of the ventricle during sinus rhythm in patients with a previous myocardial infarction: identification of the electrophysiologic substrate of ventricular arrhythmias. *Circulation* 1982;**66**:847–53.
2. de Bakker JM, van Capelle FJ, Janse MJ, Wilde AA, Coronel R, Becker AE *et al.* Reentry as a cause of ventricular tachycardia in patients with chronic ischemic heart disease: electrophysiologic and anatomic correlation. *Circulation* 1988;**77**:589–606.
3. Stevenson WG, Khan H, Sager P, Saxon LA, Middlekauff HR, Natterson PD *et al.* Identification of reentry circuit sites during catheter mapping and radiofrequency ablation of ventricular tachycardia late after myocardial infarction. *Circulation* 1993;**88**:1647–70.
4. Stevenson WG, Friedman PL, Sager PT, Saxon LA, Kocovic D, Harada T *et al.* Exploring postinfarction reentrant ventricular tachycardia with entrainment mapping. *J Am Coll Cardiol* 1997;**29**:1180–9.
5. de Chillou C, Lacroix D, Klug D, Magnin-Poull I, Marquié C, Messier M *et al.* Isthmus characteristics of reentrant ventricular tachycardia after myocardial infarction. *Circulation* 2002;**105**:726–31.
6. Marchlinski FE, Callans DJ, Gottlieb CD, Zado E. Linear ablation lesions for control of unmappable ventricular tachycardia in patients with ischemic and nonischemic cardiomyopathy. *Circulation* 2000;**101**:1288–96.
7. Arenal A, del Castillo S, Gonzalez-Torrecilla E, Atienza F, Ortiz M, Jimenez J *et al.* Tachycardia-related channel in the scar tissue in patients with sustained monomorphic ventricular tachycardias influence of the voltage scar definition. *Circulation* 2004;**110**:2568–74.

8. Jaïs P, Maury P, Khairy P, Sacher F, Nault I, Komatsu Y et al. Elimination of local abnormal ventricular activities: a new end point for substrate modification in patients with scar-related ventricular tachycardia. *Circulation* 2012;**125**:2184–96.
9. de Chillou C, Groben L, Magnin-Poull I, Andronache M, MagdiAbbas M, Zhang N et al. Localizing the critical isthmus of post-infarct ventricular tachycardia: the value of pace-mapping during sinus rhythm. *Heart Rhythm* 2014;**11**:175–81.
10. de Chillou C, Sellal J-M, Magnin-Poull I. Pace mapping to localize the critical isthmus of ventricular tachycardia. *Card Electrophysiol Clin* 2017;**9**:71–80.
11. Anter E, Tschabrunn CM, Buxton AE, Josephson ME. High-resolution mapping of postinfarction reentrant ventricular tachycardia: electrophysiological characterization of the circuit. *Circulation* 2016;**134**:314–27.
12. Pauriah M, Cismaru G, Magnin-Poull I, Andronache M, Sellal J-M, Schwartz J et al. A stepwise approach to the management of postinfarct ventricular tachycardia using catheter ablation as the first-line treatment: a single-center experience. *Circ Arrhythm Electrophysiol* 2013;**6**:351–6.
13. de Chillou C, Magnin-Poull I, Andronache M, Sacher F, Groben L, Abdelaal A et al. Showing up channels for postinfarct ventricular tachycardia ablation. *Pacing Clin Electrophysiol* 2012;**35**:897–904.
14. Bogun F, Bender B, Li YG, Groenefeld G, Hohnloser SH, Pelosi F et al. Analysis during sinus rhythm of critical sites in reentry circuits of postinfarction ventricular tachycardia. *J Interv Card Electrophysiol* 2002;**7**:95–103. 7
15. Koa-Wing M, Ho SY, Kojodjojo P, Peters NS, Davies DW, Kanagaratnam P. Radiofrequency ablation of infarct scar-related ventricular tachycardia: correlation of electroanatomical data with post-mortem histology. *J Cardiovasc Electrophysiol* 2007;**18**:1330–3.
16. Mountantonakis SE, Park RE, Frankel DS, Hutchinson MD, Dixit S, Cooper J et al. Relationship between voltage map "channels" and the location of critical isthmus sites in patients with post-infarction cardiomyopathy and ventricular tachycardia. *J Am Coll Cardiol* 2013;**61**:2088–95.
17. Stevenson WG, Sager PT, Natterson PD, Saxon LA, Middlekauff HR, Wiener I. Relation of pace mapping QRS configuration and conduction delay to ventricular tachycardia reentry circuits in human infarct scars. *J Am Coll Cardiol* 1995;**26**:481–8.
18. Brunckhorst CB, Stevenson WG, Soejima K, Maisel WH, Delacretaz E, Friedman PL et al. Relationship of slow conduction detected by pace-mapping to ventricular tachycardia re-entry circuit sites after infarction. *J Am Coll Cardiol* 2003;**41**:802–9.
19. Brunckhorst CB, Delacretaz E, Soejima K, Jackman WM, Nakagawa H, Kuck KH et al. Ventricular mapping during atrial and right ventricular pacing: relation of electrogram parameters to ventricular tachycardia reentry circuits after myocardial infarction. *J Interv Card Electrophysiol* 2004;**11**:183–91.
20. Nayyar S, Kuklik P, Ganesan AN, Sullivan TR, Wilson L, Young GD et al. Development of time- and voltage-domain mapping (V-T-mapping) to localize ventricular tachycardia channels during sinus rhythm. *Circ Arrhythm Electrophysiol.* 2016 Dec;9(12). pii: e004050.

EP CASE EXPRESS

doi:10.1093/europace/euz164
Online publish-ahead-of-print 15 June 2019

Peritoneal pericardial fistula post epicardial ventricular tachycardia ablation

Sharon Shalom Natanzon*, Roy Beinart, and Eyal Nof

Davidai Arrhythmia Center, Leviev Heart Center, Sheba Medical Center, Tel Hashomer and The Sackler Faculty of Medicine, Tel Aviv University, Tel Aviv, Israel

* Corresponding author. Tel: 00972522586251; fax: 0097235302171. *E-mail address:* sharonnatanzon@gmail.com

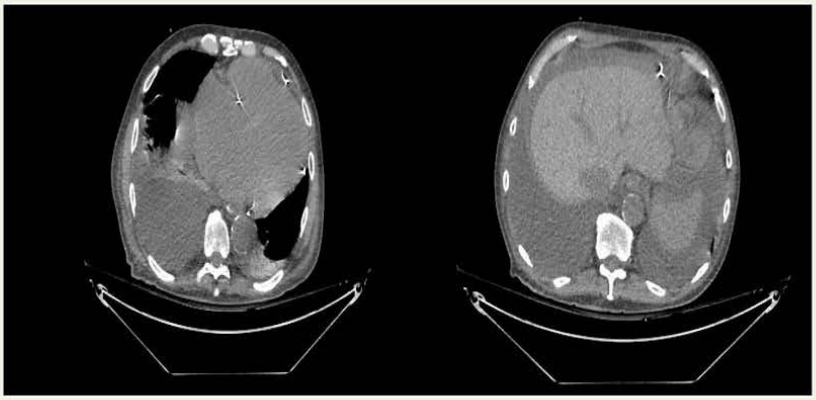

Ventricular tachycardia (VT) ablation is commonly used in order to allow the electrophysiologist a treatment option against a disabling and life-threatening arrhythmia.

Our case report demonstrates an uncommon and unexpected complication of the procedure: ascites drainage after pericardial puncture. The fact that the sheath could not pass following wire placement in the pericardium space was probably due to a sub-diaphragmatic puncture. As a result, the sheath was unable to go beyond the diaphragm. However, the wire and sheath combined did create a passage from the abdominal cavity to the pericardial space (as shown in the *Figure*). Interestingly, this fistula was active only when the vacuum was open.

A significant number of patients undergoing VT ablation also present with worsening heart failure symptoms with clinical volume overload. This clinical scenario unintentionally facilitated drainage of a large amount of fluid improving the patient's heart failure symptoms.

In summary, we report an uncommon complication of epicardial VT ablation. In this case, the complication resulted in draining a large amount of ascites leading to the patient's clinical improvement.

The full-length version of this report can be viewed at: https://www.escardio.org/Education/E-Learning/Clinical-cases/Electrophysiology.

4) Paced-ECG detector and delineator for automatic multi-parametric mapping

The analysis of data collected during sinus rhythm and pacemapping enables the detailed study of the electrical characteristics of a given ventricle. This analysis is currently limited because of the time-consuming steps that the interventional cardiologist needs to do to visualize the information of interest. The lack of already implemented detection techniques hinder the use of pace-mapping data. The following paper presents a novel method to automatically extract the key information. Wavelet, time and energy criteria are used to detect pacing spikes and paced beats as well as to delineate the onset and peak of a QRS. The overall goal is to provide the physician with a software tool to rapidly visualize the most relevant maps (voltage, correlation gradient and S-QRS interval) to identify potential VT circuits.

My contribution to the paper was the design, implementation and validation of the signal processing methods. I also developed the in-house software in order to validate the automated detection tool, and I extracted the relevant metrics to evaluate the detection performance. The detector and delineator performed well and the maps using the physician and the algorithm inputs looked very similar. The automatic processing reduced the need for manual annotations and facilitated the visualization of the relevant maps. The joint analysis of the multi-parametric maps helps identify the location of the entrance, core and exit of the VT circuit. Once the circuit is identified, ablation targets can be determined in order to eliminate the critical slow-conducting zones.

IEEE Access
Multidisciplinary | Rapid Review | Open Access Journal

Received November 27, 2020, accepted December 6, 2020, date of publication December 9, 2020,
date of current version December 29, 2020.

Digital Object Identifier 10.1109/ACCESS.2020.3043542

A Paced-ECG Detector and Delineator for Automatic Multi-Parametric Catheter Mapping of Ventricular Tachycardia

PHILIP HOYLAND[1,2], NÉFISSA HAMMACHE[3], ALBERTO BATTAGLIA[3], JULIEN OSTER[1], JACQUES FELBLINGER[1,4], (Member, IEEE), CHRISTIAN DE CHILLOU[1,3], AND FREDDY ODILLE[1,4]

[1]IADI U1254, Inserm and Université de Lorraine, 54000 Nancy, France
[2]Biosense Webster France, Johnson & Johnson, 92130 Issy-les-Moulineaux, France
[3]Pôle Cardiologie, CHRU Nancy, 54000 Nancy, France
[4]CIC-IT 1433, Inserm, Université de Lorraine and CHRU Nancy, 54000 Nancy, France

Corresponding author: Philip Hoyland (phoyland@its.jnj.com)

This work was supported by the French "Investments for the Future" Program under Grant ANR-15-RHU-0004.

ABSTRACT Ventricular tachycardia (VT) is a life-threatening arrhythmia, which can be treated by catheter intervention. Accurate identification of the underlying reentrant circuit is often challenging, yet it is key to successful ablation of the VT. In practice, the cardiologist often uses electrocardiography (ECG) data provided by various catheter mapping techniques, including parameters acquired during sinus rhythm (voltage maps, presence of fragmented/late potentials) and during controlled pacing from different sites of the ventricle, so-called pace-mapping. A novel method is presented here to automatically extract the key information from pace-mapping data with automated detection of paced heartbeats from the surface ECG signals, using wavelet detection of pacing spikes and combined time/energy criteria, and automated delineation of paced beats, QRS peak, and QRS onset. This allows the generation of correlation gradient maps (indicating QRS morphology changes as the catheter is moved) and stimulus-to-QRS maps (sQRS, indicating the delay between pacing and activation of the healthy myocardium). The delineator is shown to be in good agreement with manual annotations from experts in a retrospective study of 18 VT ablation procedures. Paced-QRS detection had 95.2% sensitivity and 98.4% positive predictive value. Resulting sQRS maps had a mean absolute error of 11.1 ms, which was in the same range as the inter-observer errors (9.7 ms). The automatic processing drastically reduces the need for manual annotations. Therefore it makes it feasible to process and visualize, during the procedure, all the relevant parametric maps, which can be analyzed jointly to identify VT circuits and corresponding ablation targets.

INDEX TERMS Arrhythmia, cardiac interventional electrophysiology, electrocardiography, radiofrequency catheter ablation.

I. INTRODUCTION

After myocardial infarction, the presence of damaged tissue can modify the electrical propagation within the myocardium. Some areas do not conduct anymore and are responsible for directional block, whereas intermediate areas with sparse surviving myocardial fibers are responsible for slow conducting zones. The coupling of these two elements form the basis for reentrant ventricular tachycardia (VT) [1]. A reentrant VT circuit may indeed exist if there is a slow conducting zone from which the electrical influx exits with a delay greater than the myocyte refractory period, thus exciting healthy tissue again. VT is a life-threatening arrhythmia, which can be treated by catheter intervention provided the core zone of the underlying reentrant circuit can be identified accurately and ablated.

The most direct technique to identify the circuit is activation mapping [2]. It consists of creating a 3D map of the activation pathway during VT by moving the electrodes of a catheter and measuring the activation times from the

The associate editor coordinating the review of this manuscript and approving it for publication was Filbert Juwono.

intra-cardiac signals. Automatic activation mapping has been aided by the development of algorithmic delineation tools to automatically assess the local activation time of intracardiac atrial [3] as well as ventricular signals [4]. Unfortunately, in practice, activation mapping can only be performed in the small proportion of patients who can tolerate VT long enough for the duration of the mapping.

Noninvasive methods have also been developed to reconstruct the electrical activation sequences of the ventricle. These techniques are based on analyzing the ECG morphology during tachycardia to help the physician determine the area of interest [5]. This information can therefore help reduce the searching area, thus leading to shorter procedure times. However, some technical challenges remain especially as some features seem to be inaccurately captured [6]. Further clinical benefit remains to be shown for the widespread adoption of this technique [7].

Alternative indirect methods consist of collecting data during sinus rhythm and during catheter-controlled pacing from different sites of the ventricle (so-called pace-mapping) to study the local electrical characteristics of the ventricle and attempt to identify the critical components of the VT circuit.

Sinus rhythm measurements include voltage mapping, which maps the amplitude of the intracardiac electrical signals (electrograms). High voltage measurements correspond to viable myocardial fibers and low voltage to tissues with impaired electrical conductivity. Intermediate voltage characterized by abnormal electrograms correspond to surviving myocardial fibers [8][9]. The recent development of high-density mapping catheters enables the detection of late or fragmented potentials. The elimination of such electrograms has been assessed as a procedural endpoint [10]. Unfortunately, a disadvantage of such a technique is that it induces larger tissue destruction than would be required if the actual VT circuits could be accurately identified.

Pace-mapping data include surface electrocardiography (ECG) signals collected during pacing from many sites of the ventricle. They can be used to determine the VT circuit. Indeed, the exit site of the VT circuit is identified when the paced QRS morphology best matches that of the clinical VT [11], as assessed by a VT correlation map. A drawback of VT correlation mapping is that it requires a reference ECG recording during VT (spontaneous or induced at the beginning of the procedure). However secondary VT circuits may also exist and are not mapped by this technique. Reference-less pace mapping has also been proposed to identify critical slow conducting zones, independently of any VT recording (i.e. potentially core zones of several VT circuits) [12]. It uses correlation gradient maps, indicating zones of abrupt changes on the surface ECG as the catheter is moved to neighboring ventricular sites. Additionally, the entrance of the circuit has been shown to be associated with long (or longer) intervals between pacing and the resulting QRS complex (sQRS intervals) [13]. A combined analysis of these multi-parametric pace-mapping data may therefore help better identify all likely VT circuits for one patient and determine the minimal surface where tissue destruction needs to be applied.

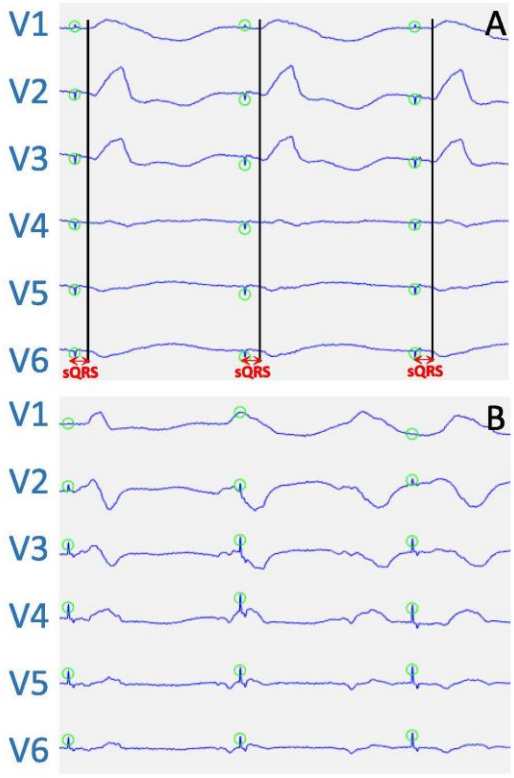

FIGURE 1. Illustration of the 6 precordial leads of two different pacing sites. The green circle represents the pacing spike. In A, the black line represents the beginning of the QRS and the red arrow is the sQRS interval, the time interval between both features. The three QRS present the same morphology as well as the same sQRS interval, therefore they can be identified as three correctly paced QRS. In B, this is not the case, the beats cannot be considered as paced and mustn't be analyzed.

Currently, the use of pace-mapping data is coupled with time-consuming manual steps. Firstly, it is important to quickly identify a correctly paced QRS. For example, bad catheter to tissue contact and poor local electrical activity can lead to defaults in tissue capture. The subsequent non-paced QRS complexes must not be analyzed. As illustrated in Fig. 1, a paced beat can be easily identified by a constant delay between the stimulation spike and the QRS onset, i.e. a constant sQRS interval, as well as a constant QRS morphology (same overall electrical depolarization induced by the stimulation). The spike as well as the start of the QRS need to be detected in order to determine the valuable sQRS intervals. The lack of already implemented detection techniques hinder the current use of pace-mapping data in clinical practice.

Pacing spike detection in patients with pacemakers has already been developed using slope based [14]–[16] and power envelopes with moving statistical windows [17] detection algorithms but to our knowledge these methods have not been used for catheter pacing. Convolution with a spike template has already been used in [12] for catheter induced pacing detection but the application of this method is complicated by the varying amplitude of the stimulus as well as the great diversity in localization of the pacing. The spike frequency range being higher than the frequency of the other features present on the ECG, we propose a new wavelet-based method for detecting pacing spikes in a catheter-induced pacing environment. Moreover, conventional ECG signal processing techniques are developed for natural recordings (sinus rhythm or spontaneous arrhythmia) and have not been applied to detect and delineate catheter-paced beats [18]–[20].

Therefore in this work we propose a specific and innovative method for catheter paced-ECG data, combining a wavelet-based detection of stimulation spikes and a delineation of the subsequent QRS complex (peak and onset).

The objective of the study is to evaluate the performance of the proposed paced-ECG detection and delineation and to demonstrate its potential for multi-parametric catheter mapping of VT in the clinical setting. The overall goal is to provide the interventional cardiologist with a software tool to rapidly visualize the relevant maps (voltage, correlation and sQRS) and identify the potential VT circuit(s) to be ablated.

II. METHODS

A. PATIENT DATA ACQUISITION

Thirteen patients (9 men, mean age = 59 ± 12 years) consecutively referred for post-infarct VT catheter ablation between March 2016 and October 2017 were included in this retrospective, non-interventional study. Inclusion criteria were: (i) spontaneous sustained monomorphic VT inducible during the electrophysiological study; (ii) identification of the VT isthmus by the pace-mapping technique and (iii) radiofrequency catheter ablation lesions along the isthmus prevented VT induction. The study complied with the declaration of Helsinki and all procedures complied with the CHRU-Nancy guidelines. All 18 procedures were performed with the CARTO3®(Biosense Webster, Inc., Irvine, USA) and the Niobe®system (Stereotaxis Inc., St. Louis, USA).

Anonymized data were exported from the CARTO3® workstation and were then processed using an in-house software written in MATLAB language (The Mathworks, Natick, USA), version R2020a. Electro-anatomic data were first loaded into the software, including: catheter positions and 2.5 s of 12-lead ECG data acquired for each pace-mapping site; high-resolution vendor-generated 3D meshes of the ventricular cavity, as well as bipolar and unipolar voltage maps acquired in sinus rhythm. All other maps used in this study were generated offline with the MATLAB software, as described henceforth.

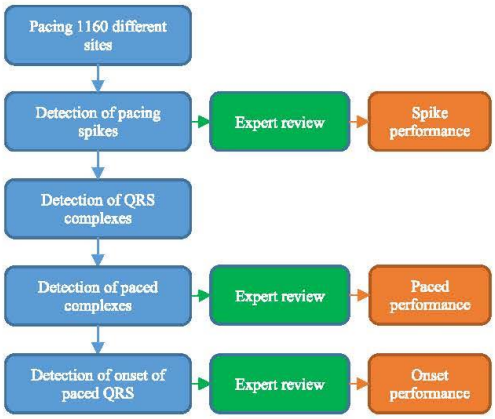

FIGURE 2. Flow diagram presenting the different steps of the detection algorithm.

B. AUTOMATED DETECTION AND DELINEATION OF PACE-ECG DATA

To analyze pace-mapping ECG data, an automatic detection and delineation of paced beats was proposed in order to only select one paced QRS for analysis at a given pacing site. This detection is necessary because some QRS complexes at a given site are not paced. The cardiac electric potentials can be expressed in vector quantities that varies over time in magnitude and direction. The overall projection of the human equivalent heart dipole in three orthogonal axes is the vectorcardiogram [21]. The maximum of its module correspond to the peak of depolarization of cardiac cells, thus useful to detect the QRS complex.

Moreover, the stimulation spike does not always induce a paced beat, especially in low-voltage hard to capture areas. Finally, mechanically induced premature beats must not be taken into account.

Figure 2 presents the different steps of the automated detection and delineation (i.e. determination of QRS peak and onset):

1. Detection of pacing spikes by using the continuous wavelet transform (CWT). The bump wavelet was selected as the mother wavelet for its frequency localization properties. The CWT was computed numerically using Matlab's *cwt* function, which uses L1 normalization of the coefficients, instead of L2 normalization in the integral definition of the CWT. This makes the time-frequency analysis easier as oscillatory components with the same amplitude in the signal always have the same magnitude in the CWT (independent of the scale). The wavelet coefficients $c_i(.)$ for each lead i corresponding to frequencies between $f_1 = 125$ Hz and $f_2 = 166$ Hz were summed in a signal S:

$$S = \sum_{i=1}^{12} \sum_{f \in \{f_1, \ldots, f_2\}} |c_i(f)| \quad (1)$$

The local maxima of S were extracted using Matlab's *findpeaks* function, with the following constrains: local maxima should reach at least 33% of the maximum of S, and two peaks should be separated by at least 350 ms. Overall 5138 spikes were analyzed.

2. Detection of QRS complexes present after each spike n using a maximum search of the vectorcardiogram. The synthetic vectorcardiogram $VCG\,(t)$, for a given time t, was reconstructed by inverse Dower transformation T from the available (independent) leads $L\,(t)$ [22] as already used in [12] (2), as shown at the bottom of the page. The time $t_{QRS,n}$ of the QRS complex after spike n was determined by the maximum of the module of the vectorcardiogram $\|VCG\,(t)\|$ between time t_{n} of spike n and time $t_{\mathrm{n}+1}$ of spike $n+1$:

$$t_{QRS,n} = \underset{\substack{t \\ for\ t\in[t_n,t_{n+1}[}}{\arg\max} \|VCG\,(t)\| \tag{3}$$

3. Determination of a paced-QRS flag by analysis of the previous QRS. A QRS was considered to be a paced QRS if similar to the previous one; similarity was defined by a distance-to-spike variation lower than 35 ms and a variation in the module of the vectorcardiogram below 33%. Overall 5176 QRS were present, of whom 2991 were paced.
4. Detection of the onset of a QRS by using the module of the vectorcardiogram. The QRS start was determined by backward search from the maximum of the VCG amplitude, until the module reached 5% of the maximum module.

The time interval between pacing and the start of the resulting QRS complex, the sQRS interval, was finally determined. The dataset was split between a training set consisting of the first 5 patients and a test set with the data from the remaining 13 patients. The optimization process was performed on the training set by tuning the 4 parameters (33% for pacing spike detection, the similarity criteria of 35 ms and 33% for paced beat detection and 5% for onset delineation) using a grid search. The parameters were chosen only based on the training set and then evaluated once on the test set.

Overall, bipolar pace-mapping was performed at 1160 different sites. It should be noted that several QRS complexes are present in each 2.5 s recording (i.e. at one given pacing site). For each site, the second QRS in the sequence of QRS identified as paced by the algorithm was studied.

C. VALIDATION AGAINST EXPERT ANOTATIONS

The software tool allowed visualization of all the automatically detected QRS signals. An experienced interventional cardiologist (N.H.) was asked to review the ECG signals (pacing spike, whether a QRS was paced or not). The efficiency of the automated processing was assessed by common statistics for binary classifiers (using the cardiologist input as the ground truth), including the positive predictive value (PPV) and the sensitivity (Se). The position of the QRS onset varies slightly between cardiologists. To quantify this inter-observer variation, two experts were asked to mark the QRS onset: a clinical support specialist (P.H) defined as expert 1 and an interventional cardiologist (N.H.) defined as expert 2. We also introduced a virtual delineation represented by the mean of both experts. Mean, standard deviation, median and mean absolute errors were calculated for the definition of the QRS onset time. The agreement between expert and automated S-QRS maps was also assessed by correlation analysis (using both Spearman's and Lin's definitions) and by Bland-Altman analysis.

D. RECONSTRUCTION OF MULTI-PARAMETRIC MAPS

Multiple 3D maps were generated to visualize the information. The bipolar voltage map was directly derived from the vendor's CARTO3®software. Additionally, a 3D surface mesh was generated from the pacemapping sites and used to create the following maps: (i) a sQRS interval map was generated by color-coding the sQRS interval induced by the pacing stimuli; (ii) a reference-less correlation gradient map was generated as described in [12] by calculating the local change in Pearson correlation coefficient $c\,(.,.)$ between each lead of QRS complexes from two neighboring pacing sites, x_1 and x_2, $S^{lead}_{PacedQRS}(x_1)$ and $S^{lead}_{PacedQRS}\,(x_2)$ normalized by the distance between the two sites $||x_1 - x_2||$:

$$\frac{\frac{1}{12}\sum_{lead=1}^{12} c\left(S^{lead}_{PacedQRS}\,(x_1) - S^{lead}_{PacedQRS}\,(x_2)\right)}{||x_1 - x_2||} \tag{4}$$

The target for the clinician was to collect points with a distance of 10 mm in areas of low voltage. The distance between two points was higher in healthy areas. Correlation gradient values were considered to be defined only when the site-to-site distance was less than 20 mm. The rationale for computing these three maps is that sQRS maps are expected to highlight VT circuit entrance sites [13] and correlation gradient maps are expected to highlight VT circuit core zones [12]. Finally, voltage maps are expected to help identify

$$\begin{aligned} VCG\,(t) &= T * L\,(t)^T, \\ L\,(t) &= [V_1\,(t)\,V_2\,(t)\,V_3\,(t)\,V_4\,(t)\,V_5\,(t)\,V_6\,(t)\,I\,(t)\,II\,(t)], \\ T &= \begin{bmatrix} -0.172 & -0.074 & 0.122 & 0.231 & 0.236 & 0.194 & 0.156 & -0.010 \\ 0.057 & -0.019 & -0.106 & -0.022 & 0.041 & 0.048 & -0.227 & 0.887 \\ -0.229 & -0.310 & -0.246 & -0.063 & 0.055 & 0.108 & 0.022 & 0.102 \end{bmatrix} \end{aligned} \tag{2}$$

TABLE 1. Performance of the Proposed Detection of Stimulation Spikes and Paced QRS Complexes.

	Training set		Test set		Training and Test set	
	Sensitivity	Positive Predictive value	Sensitivity	Positive Predictive value	Sensitivity	Positive Predictive value
Spike detector	97.64%	98.86%	97.48%	99.61%	97.51%	99.46%
Paced QRS detector	94.99%	97.69%	95.23%	98.63%	95.19%	98.44%

TABLE 2. Onset Performance Results.

	Training set				Test set				Training and Test set			
	Mean	Standard Deviation	Median	Mean Absolute Error	Mean	Standard Deviation	Median	Mean Absolute Error	Mean	Standard Deviation	Median	Mean Absolute Error
Between algorithm and expert 1	-2.36ms	21.99ms	-4ms	15.71ms	-1.19ms	16.14ms	-2ms	10.89ms	-1.42ms	17.43ms	-3ms	11.82ms
Between algorithm and expert 2	4.65ms	21.37ms	3ms	14.34ms	0.13ms	17.12ms	-2ms	11.30ms	1.01ms	18.11ms	-1ms	11.88ms
Between algorithm and mean delineation of both experts	1.15ms	20.65ms	-0.5ms	13.71ms	-0.53ms	15.37ms	-2ms	10.30ms	-0.21ms	16.54ms	-2ms	10.96ms
Between the two experts	7.01ms	13.21ms	7ms	11.77ms	1.32ms	12.74ms	1ms	9.25ms	2.42ms	13.03ms	+2ms	9.73ms

the exit of the VT circuit, which should be at the border between scar and healthy tissue.

For better visualization purpose, the maps were finally projected from the coarse mesh formed by pacing sites onto the high-resolution anatomical mesh (distance between the vertices was 0.8mm) provided by the vendor (using nearest-neighbor interpolation). For final visualization of the 3D maps, the rendering engine (still within MATLAB in this study) was set to use interpolation of values defined at each vertex of the high resolution mesh, similarly to the vendor's CARTO3®software.

III. RESULTS

A. PACED-QRS DETECTION AND DELINEATION

Quantitative results for the automatic detection of pacing spikes and paced QRS complexes are summarized in Table 1. The performance was very similar between the training set, the test set and the entire study population (training and test). The overall results for the entire population show excellent agreement between the algorithm and the cardiologist, with Se>95% and PPV>98%.

Regarding the detection of the QRS onset, quantitative results on the training, test and entire population set are summarized in Table 2. The onset algorithm performed better on the test set than on the training set. For 94% of QRS onset detections, a difference lower than 30 ms was found between expert 2 and the algorithm inputs. The difficulty of defining an objective location for the beginning of the QRS complex is highlighted by the relatively large mean absolute error between the two experts (9.73 ms). When compared to the delineation represented by the mean of both experts, the proposed algorithm performed well (mean of −0.21 ms, a SD of 16.54 ms, a MED of −2 ms and a MAE of 10.96 ms) and demonstrated only a slightly higher difference than between both experts.

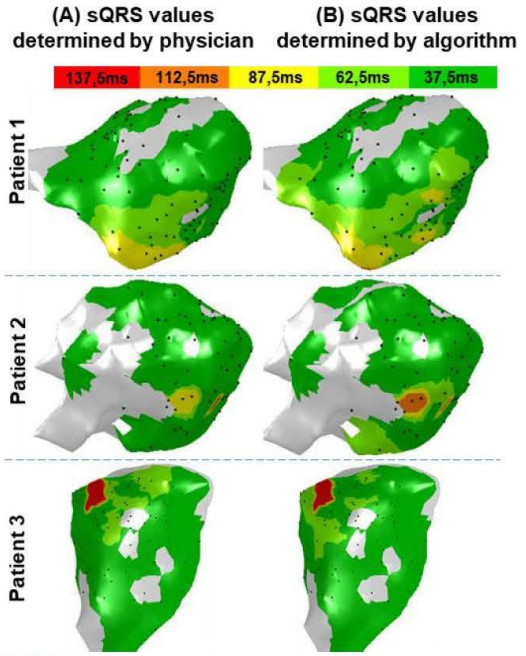

FIGURE 3. Comparison of left ventricle SQRS maps determined between (A) the physician (N.H) and (B) the algorithm. For each patient, both maps indicate the same interesting zones with longer SQRS intervals.

B. RECONSTRUCTION OF MULTIPARAMETRIC MAPS

The delay between the stimulation spike and the QRS onset, the sQRS interval, was calculated for each pacing site and projected onto the high-resolution anatomical mesh. Figure 3 shows examples of sQRS interval maps generated by values determined by the physician N.H. in comparison with values determined by the proposed algorithm.

TABLE 3. Final Visualization Vertex Results Between s-QRS Maps Generated by Algorithm and Physician Inputs of the Test Set.

	Mean	Standard deviation	Median	Mean Absolute Error	Spearman's correlation	Lin's correlation
Between algorithm and expert 1	-1.95ms	14.80ms	-2ms	10.06ms	0.71	0.86
Between algorithm and expert 2	0.15ms	15.46ms	-1ms	10.64ms	0.72	0.86
Between the two experts	2.10ms	13.92ms	1ms	9.26ms	0.75	0.88

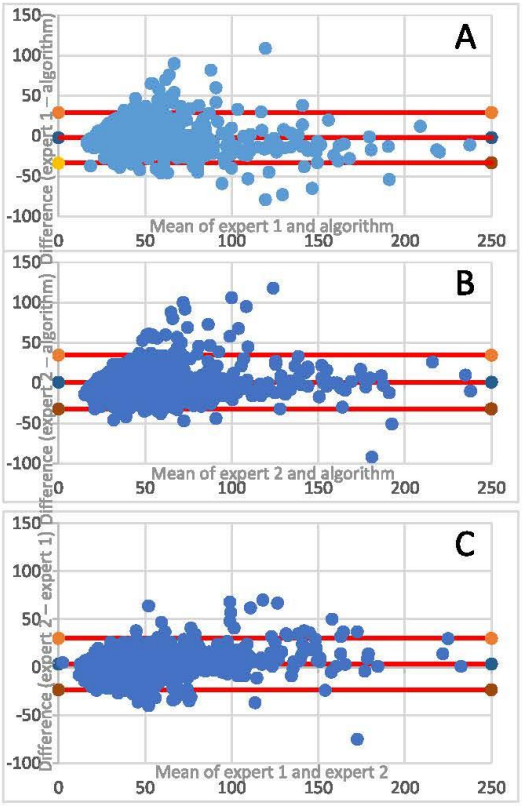

FIGURE 4. Bland Altman plot of agreement between methods. The lower red line represent the average difference −1,96 times the standard deviation of the difference, the middle red line the average difference and the upper red line the average difference +1,96 times the standard deviation of the difference. (A) between inputs from expert 1 and algorithm (B) between inputs from expert 2 and algorithm (C) between inputs from expert 2 and expert 1.

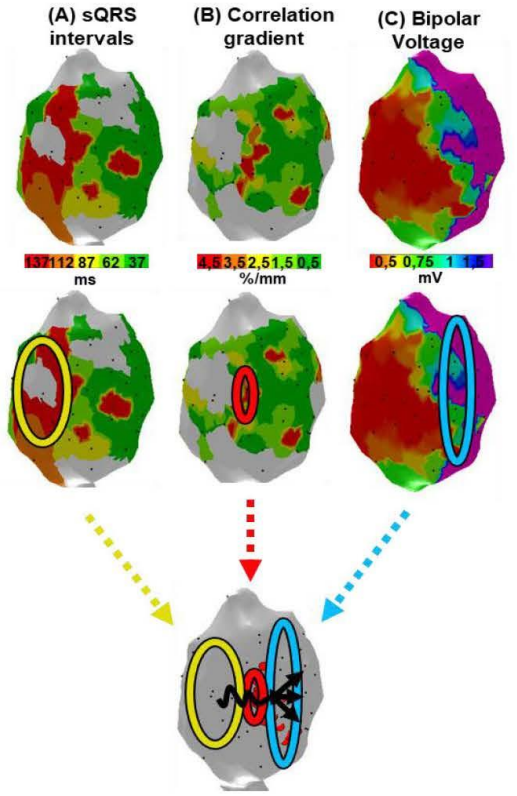

FIGURE 5. Illustration of the possible identification steps using maps calculated by the algorithm to determine the location of the critical section of the VT circuit or isthmus: (A) sQRS intervals, with longest values in red; the yellow circle includes the highest sQRS values and is likely located at the entrance of the isthmus (B) correlation gradient map indicating in red zones a high morphology mismatch; the red circle includes the highest values, likely located in the mid-isthmus section (C) bipolar voltage map, with low voltage in red representing the scar region and purple representing the healthy area; the blue circle includes the border between scar and healthy tissue, likely located at the exit of the isthmus.

The resulting QRS maps using the physician and the algorithm inputs looked very similar. Both versions of the maps enabled the quick identification of areas of interest marked by long sQRS intervals.

Quantitative differences between the detector-generated sQRS maps and the physician-generated sQRS maps, as assessed by vertex-wise differences and by correlation analysis between the final visualization meshes from the test set are summarized in Table 3. Bland-Altman plots (figure 4) show a good agreement between experts and the algorithm. The linear interpolation, which was used to reconstruct the final high resolution meshes, further decreased the impact of the difference between the algorithm and the experts' annotations.

Figure 5 shows an example of multi-parametric mapping (3 maps) of the same patient. The sQRS interval map (A)

and the correlation gradient map (B) were generated using the algorithm generated values. The bipolar voltage map (C) was derived from the CARTO3®software. The visualization of this multi-parametric mapping may help to determine the localization of the entrance, core and exit of the VT circuit.

IV. DISCUSSION

The objective of a VT ablation procedure is to identify the main components of all the fast reentrant circuits the patient is capable of sustaining. Activation mapping during tachycardia is the most direct technique but can only be performed in the small proportion of patients who can tolerate VT long enough for the duration of the mapping. Furthermore it only identifies the principal VT circuit, i.e. it does not identify secondary VT circuits that may occur after ablation of the principal one. The analysis of data collected during sinus rhythm and pace-mapping enables the detailed study of the local electrical characteristics of the ventricle. Currently, this type of analysis is limited because of the high number and time-consuming steps that the physician needs to do. Once the physician is stable in a position and starts pacing, a point is taken. The necessary manual steps are the following: selecting a correctly paced beat, determining the position of the pacing spike and onset of the QRS, calculating the difference to establish the sQRS interval, aligning the QRS morphology of the point regarding the QRS morphology of its closest neighbors. In order to integrate this full workflow and take full advantage of pace map data, we have estimated that the physician currently needs 30 seconds per point, adding up to 50 minutes for 100 pace map points. The added value of an automated algorithm is to facilitate the use of the data. Out of 100 pace map points, the proposed method correctly identifies 99 paced QRS. If we consider a tolerance threshold of 30 ms for the start of the QRS, only 6% of points will be incorrectly marked. All in all, for a 100 pace map points, 7 points will need to be corrected and 93 would be rapidly visualized for validation leading to a total time of less than 5 minutes. This time is short compared to the total procedure time of several hours and will help by making the time allocated to analyzing the data more predictable, leading to an increased standardization of the physician's approach to ischemic VT. Reviewing data is standard in clinical practice as it helps the physician determine the most effective ablation strategy. It is also important that the physician reviews all points because, in certain cases, although the algorithm performed well, the result will need to be modified. For example, after reviewing the surrounding paced beat morphologies, the physician might consider a beat as being correctly paced even if the recording does not have two consecutive beats with the same morphology.

The pace-mapping based method described here has the main advantage of being feasible in all patients, regardless of being able to induce a VT episode. Once the likely circuits are identified, ablation targets can be determined in order to eliminate the critical slow-conducting zones. Once ablated, these areas will not conduct anymore, thus preventing the reentrant circuit from forming and curing the patient.

The proposed software tool automatically creates voltage, correlation and sQRS maps. The creation of these multiparametric maps help determine the different characteristics of the VT isthmus. Previous articles have shown the importance of these parameters in identifying the isthmus. The isthmus is a complex structure and the visualization of a single parameter is not enough to be able to reconstruct the VT circuit. For each map, the global patterns with the highest and the lowest group of values are useful. Indeed it is important to know whether a sQRS is long (over 100 ms) or short (under 50 ms), thus the mean absolute error of 11.1 ms is low enough for the automatic sQRS maps to be analyzed. It is important to have a global approach and take into account all the relevant information before establishing a diagnosis. In this study only a qualitative analysis of the maps is presented, which is meant to show the added value of visualizing the maps together, rather than to provide a full clinical validation of the method.

The combination of the multi-parametric maps can bring to light multiple slow-conducting zones in the ventricle. These zones can then result in the creation of multiple tachycardia circuits. Highlighting the multiple isthmuses is of interest when elaborating a VT ablation strategy.

An increased understanding of VT circuits will lead to increased VT ablation results. The proposed study enables to automatically extract the relevant data. This data is acquired during sinus rhythm or pacing from the catheter and thus has the advantage of not requiring any tachycardia during acquisition. The data can therefore be easily obtained, not requiring any stimulating maneuvers with unpredictable results. If the VT can be induced and is well tolerated, activation data can also be automatically extracted and could further increase our understanding of the VT circuits.

Large datasets can now more easily be used as inputs for the development of future algorithms. These algorithms need to automatically determine all likely VT circuits, further facilitating the diagnosis and improving long-term ablation outcomes.

V. CONCLUSION

We developed a paced-ECG detector and delineator that is useful for multi-parametric catheter mapping. This automated method facilitates the creation and visualization of the relevant maps, which can be analyzed jointly to identify VT circuits and the corresponding ablation targets.

ACKNOWLEDGMENT

The authors would like to thank INSERM, CPER 2007–2013, Region Lorraine, and FEDER for the funding of the Niobe Magnetic Navigation System, Stereotaxis, Inc.

REFERENCES

[1] N. El-Sherif, B. J. Scherlag, R. Lazzara, and R. R. Hope, "Re-entrant ventricular arrhythmias in the late myocardial infarction period. 1. conduction characteristics in the infarction zone.," *Circulation*, vol. 55, no. 5, pp. 686–702, May 1977.

[2] W. G. Stevenson, H. Khan, P. Sager, L. A. Saxon, H. R. Middlekauff, P. D. Natterson, and I. Wiener, "Identification of reentry circuit sites during catheter mapping and radiofrequency ablation of ventricular tachycardia late after myocardial infarction," *Circulation*, vol. 88, no. 4, pp. 1647–1670, Oct. 1993.

[3] M. El Haddad, R. Houben, R. Stroobandt, F. Van Heuverswyn, R. Tavernier, and M. Duytschaever, "Algorithmic detection of the beginning and end of bipolar electrograms: Implications for novel methods to assess local activation time during atrial tachycardia," *Biomed. Signal Process. Control*, vol. 8, no. 6, pp. 981–991, Nov. 2013.

[4] A. Alcaine, D. Soto-Iglesias, M. Calvo, E. Guiu, D. Andreu, J. Fernandez-Armenta, A. Berruezo, P. Laguna, O. Camara, and J. P. Martinez, "A wavelet-based electrogram onset delineator for automatic ventricular activation mapping," *IEEE Trans. Biomed. Eng.*, vol. 61, no. 12, pp. 2830–2839, Dec. 2014.

[5] T. Yang, S. M. Pogwizd, G. P. Walcott, L. Yu, and B. He, "Noninvasive activation imaging of ventricular arrhythmias by spatial gradient sparse in frequency domain—Application to mapping reentrant ventricular tachycardia," *IEEE Trans. Med. Imag.*, vol. 38, no. 2, pp. 525–539, Feb. 2019.

[6] L. R. Bear, O. Bouhamama, M. Cluitmans, J. Duchateau, R. D. Walton, E. Abell, C. Belterman, M. Haissaguerre, O. Bernus, R. Coronel, and R. Dubois, "Advantages and pitfalls of noninvasive electrocardiographic imaging," *J. Electrocardiol.*, vol. 57, pp. S15–S20, Nov. 2019.

[7] M. Cluitmans, D. H. Brooks, R. MacLeod, O. Dössel, M. S. Guillem, P. M. van Dam, J. Svehlikova, B. He, J. Sapp, L. Wang, and L. Bear, "Validation and opportunities of electrocardiographic imaging: From technical achievements to clinical applications," *Frontiers Physiol.*, vol. 9, p. 1305, Sep. 2018.

[8] J. M. de Bakker, F. J. van Capelle, M. J. Janse, A. A. Wilde, R. Coronel, A. E. Becker, K. P. Dingemans, N. M. van Hemel, and R. N. Hauer, "Reentry as a cause of ventricular tachycardia in patients with chronic ischemic heart disease: Electrophysiologic and anatomic correlation.," *Circulation*, vol. 77, no. 3, pp. 589–606, Mar. 1988.

[9] A. Arenal, "Tachycardia-related channel in the scar tissue in patients with sustained monomorphic ventricular tachycardias: Influence of the voltage scar definition," *Circulation*, vol. 110, no. 17, pp. 2568–2574, 2004.

[10] P. Jais, P. Maury, and P. Khairy, "Elimination of local abnormal ventricular activities clinical perspective: A new end point for substrate modification in patients with scar-related ventricular tachycardia," *Circulation*, vol. 125, no. 18, pp. 2184–2196, 2012.

[11] C. de Chillou, L. Groben, I. Magnin-Poull, M. Andronache, M. M. Abbas, N. Zhang, A. Abdelaal, S. Ammar, J.-M. Sellal, J. Schwartz, B. Brembilla-Perrot, E. Aliot, and F. E. Marchlinski, "Localizing the critical isthmus of postinfarct ventricular tachycardia: The value of pace-mapping during sinus rhythm," *Heart Rhythm*, vol. 11, no. 2, pp. 175–181, Feb. 2014.

[12] F. Odille, A. Battaglia, P. Hoyland, J.-M. Sellal, D. Voilliot, C. de Chillou, and J. Felblinger, "Catheter treatment of ventricular tachycardia: A reference-less pace-mapping method to identify ablation targets," *IEEE Trans. Biomed. Eng.*, vol. 66, no. 11, pp. 3278–3287, Nov. 2019.

[13] A. Battaglia, F. Odille, I. Magnin-Poull, J.-M. Sellal, P. Hoyland, D. Hooks, D. Voilliot, J. Felblinger, and C. de Chillou, "An efficient algorithm based on electrograms characteristics to identify ventricular tachycardia isthmus entrance in post-infarct patients," *EP Europace*, vol. 22, no. 1, pp. 109–116, Nov. 2019.

[14] E. D. Helfenbein, J. M. Lindauer, S. H. Zhou, R. E. Gregg, and E. C. Herleikson, "A software-based pacemaker pulse detection and paced rhythm classification algorithm," *J. Electrocardiol.*, vol. 35, p. 95, Mar. 2002.

[15] I. I. Jekova, I. T. Iliev, V. V. Tsibulko, and S. D. Tabakov, "Algorithm for pace pulses detection in a single lead ECG: Performance in case of EMG artifacts," in *Proc. IEEE XXVII Int. Sci. Conf. Electron. (ET)*, Sep. 2018, pp. 1–4.

[16] I. Jekova, S. Tabakov, I. Iliev, V. Tsibulko, and K. Kostikova, "Real-time detection of pace pulses in a single lead ECG," in *Proc. Comput. Cardiology Conf. (CinC)*, Dec. 2018, pp. 1–4.

[17] J. Jurco, F. Plesinger, J. Halamek, P. Jurak, M. Matejkova, P. Leinveber, and J. Lipoldova, "Precise pacing artefact detection," in *Proc. Comput. Cardiol. Conf. (CinC)*, Sep. 2016, pp. 761–764.

[18] B.-U. Kohler, C. Hennig, and R. Orglmeister, "The principles of software QRS detection," *IEEE Eng. Med. Biol. Mag.*, vol. 21, no. 1, pp. 42–57, Jan./Feb. 2002.

[19] J. P. Martinez, R. Almeida, S. Olmos, A. P. Rocha, and P. Laguna, "A wavelet-based ECG delineator: Evaluation on standard databases," *IEEE Trans. Biomed. Eng.*, vol. 51, no. 4, pp. 570–581, Apr. 2004.

[20] I. Silva, "Robust detection of heart beats in multimodal data," *Physiol. Meas.*, vol. 36, no. 8, p. 1629, 2015.

[21] E. Frank, "An accurate, clinically practical system for spatial vectorcardiography," *Circulation*, vol. 13, no. 5, pp. 737–749, May 1956.

[22] G. E. Dower, H. B. Machado, and J. A. Osborne, "On deriving the electrocardiogram from vectorcardiographic leads," *Clin. Cardiol.*, vol. 3, no. 2, pp. 87–95, 1980.

PHILIP HOYLAND received the master's degree in electrical engineering from the Ecole Supérieure d'Electricité (Supélec), France, in 2014, and the M.Sc. degree (Hons.) in biomedical engineering from the University of Oxford, in 2014. He is currently pursuing the Ph.D. degree in signal processing with the Diagnosis and Interventional Adaptive Imaging (IADI) Unit, Inserm (U1254), Université de Lorraine. He is also a Clinical Specialist of cardiac electrophysiology for Biosense Webster. His research interests include electrophysiology, and imaging and signal processing.

NÉFISSA HAMMACHE was born in Paris in June 1990. She received the M.D. degree in cardiology from the Université de Lorraine, in 2018. She is currently pursuing the degree in interventional rhythmology, thanks to a chief residency, with the Cardiology Unit, CHRU Nancy, France.

ALBERTO BATTAGLIA was born in Turin in January 1986. He received the degree *(cum laude)* in medicine from the University of Turin, in 2011. In 2017, he received the Fellowship *(cum laude)* in cardiology from the University of Turin. In 2017, he moved to France for an Electrophysiology Fellowship from the Pôle Cardiologie, CHRU Nancy, Nancy, France, under the direction of Prof. Christian de Chillou. His research interests include the mechanisms of ventricular and supraventricular arrhythmias, and interventional electrophysiology.

JULIEN OSTER received the master's degree in electrical engineering, the master's degree in fundamental and applied mathematics from the Ecole Supérieure d'Electricité (Supélec), France, in 2006 and 2007, respectively, and the Ph.D. degree from the Université de Lorraine, Nancy, France, in 2009. In 2010, he was with the Centre Suisse d'Electronique and also with the Microtechnique (CSEM), Neuchâtel, Switzerland, where he was involved in the development of wearable technology. He received the Newton International Fellowship from the Royal Society, in 2010. He joined the University of Oxford, U.K. Since 2016, he has been a senior Research Fellow of Inserm (French Institute of Biomedical Research and Human Health), IADI Lab (U1254), Nancy, France. His research interests include the use of modeling and signal processing methods to extract novel clinical parameters and the use of machine learning techniques to provide predictive actionable information to clinicians.

JACQUES FELBLINGER (Member, IEEE) received the master's degree in biological and medical engineering in Nancy, France, the Ph.D. degree in instrumentation and signal processing in 1990, and the M.B.A. degree. His algorithm on the automatic detection of ventricular fibrillation, developed during his thesis, equips the automatic defibrillators of the Schiller Company (150 000 devices sold). From 1991 to 2001, he was with the University of Bern, where he developed several MRI-compatible devices and also developed cerebral and cardiac H1 spectroscopy. Following a second postdoctorate in neurosciences, he obtained a position as a Professor of medical imaging with the University of Nancy, in 2001. In 2005, he created the Diagnostic and Interventional Adaptive Imaging (IADI) Laboratory, which became a joint University-INSERM Unit. The laboratory specializes in the development of innovative instrumentation and methods for MRI. In 2008, it created the Clinical Investigation and Technological Innovation Centre (CIC-IT) for the validation and enhancement of medical devices in an MRI environment. In 2012, he founded the company Healtis, which offers solutions for validating the MRI compatibility of medical devices. Since his beginnings in MRI, he has been very involved in the safety aspects of MRI.

CHRISTIAN DE CHILLOU received the M.D. and Ph.D. degrees from Nancy University and the degree in cardiology in 1990. In the early 90's, he was a Fellow of electrophysiology with the Department of Cardiology, University Hospital of Maastricht, The Netherlands, headed by Prof. Hein Wellens. He is currently the Head of the Clinical Electrophysiology Unit, CHRU Nancy, France. He has authored more than 250 original articles, abstracts, and book chapters mainly focusing on clinical arrhythmia, electrophysiology, and radiofrequency catheter ablation. In 1998, he was honored with the Prix Medtronic for research on clinical arrhythmia. He is a member of the French Society of Cardiology, of the European Society of Cardiology, and of the European Heart Rhythm Association. He actively participates in the EHRA educational program for several years.

FREDDY ODILLE received the Ph.D. degree from Nancy University, Nancy, France, in 2007. In 2011, he was appointed as a Research Fellow of Inserm (French Institute of Healthcare Research), IADI Team, Nancy. Since 2015, he has also been with Nancy University Hospital, Nancy. He is currently the Deputy Head of IADI. His research interests include magnetic resonance imaging, image reconstruction, biomedical signal and image processing, and cardiac electrophysiology modeling and intervention.

5) Graph-based Reconstruction of Arrhythmic Activations by Pacing the Heart (GRAAPH)

a. Introduction

Automatic processing during pace-mapping reduces the need for manual annotations and has the potential of quickly extracting all the relevant information. These parameters are interconnected and influence the formation of VT circuits. For example, the analysis of correlation gradient maps enables the identification of the core zones of potential VT circuits. We wish to further take advantage of all the available information and will describe in this section a graph-based method to combine multiple parameters in order to visualize the detailed pathway of the underlying reentrant circuit. The connections between each pacing site during pace-mapping are analyzed to generate a suggested activation pattern of the VT circuit. This new method led to the filing of a U.S. provisional patent, Computer assisted electrophysiological intervention for reentrant circuit identification, application number 63179054.

b. Technical background

Graphs are widely used to mathematically model interconnected objects[152]. We will briefly present the main mathematical definitions used in graph theory. A graph G is composed of elements called vertices $V(G) = \{v_1, v_{2,} v_3 \dots\}$ (or nodes) and a set of pairs of elements called edges $E(G) = \{e_1 = \{v_1, v_{2,}\}, e_2 = \{v_2, v_{3,}\}, \dots\}$. In our study, the pacing sites are the nodes of the graph and the links between adjacent pairs of pacing sites are the edges. Simple directed graphs are graphs with no loops and with edges that are ordered pairs of distinct vertices. If we have n pacing sites, the corresponding graph can be represented by an $n \times n$ adjacency matrix $A = (a_{ij})$, with $a_{ij} = 0$ if pacing sites i and j are not connected and $a_{ij} = 1$ if pacing sites i and j are adjacent pairs. Each edge e can be assigned a number, or weight $w(e)$. Solving the shortest path problem consists in finding the path with a minimum total weight between two connected vertices. Dijkstra algorithm is a commonly used algorithm to solve shortest path problems[153]. It relies on the fact that if node v_y is on the shortest path between v_x and v_z, knowing the shortest path between v_x and v_z, implies knowing the shortest between v_x and v_y. The minimal path from v_x to all the other nodes is constructed by starting with adjacent nodes and then investigating edges that are further away and determining whether they give rise to a shorter path.

c. Graph-based modeling of VT circuits

Pacing sites can be studied as vertices of a simple directed graph. A distance threshold between vertices can be used to define whether any two vertices are connected. Information found in the data collected

from pace-mapping is then extracted. The model is based on defining for each pair of adjacent vertices the ease for an electrical influx to go from one point to another. During tachycardia, the electrical influx will preferentially propagate along the path that provides the least resistance. Solving the shortest path could indicate the most likely pathway from one pacing site to all the other pacing sites. Once the most likely pathway is determined, an estimation of the delay along the calculated shortest path is used to generate a pseudo-activation map.

d. Implementation

Two patients referred for post-infarct VT catheter ablation were retrospectively analyzed with GRAAPH. During the procedure, both activation and pace mapping had been performed to identify the VT isthmus. Anonymized data was exported from the CARTO® workstation and then processed using the in-house GRAAPH software written in MATLAB language (The Mathworks, Natick, USA), version R2020a.

The GRAAPH method begins by analyzing the locations and ECG morphologies of the pace-mapping sites. Reference-less correlation gradient values of neighboring pacing sites were calculated by semiautomatic analysis as previously described in [148], [154]. A graph is generated using the pacing sites as vertices. Pairs of pacing sites with a high correlation gradient were then identified as a being part of a core zone of a reentrant circuit. Two adjacent pacing sites were considered to be connected, forming an edge of the graph, if they were separated by a distance below 40 mm and the reference-less correlation gradient between them was below 2%/mm. An example of such a graph is shown figure 13.

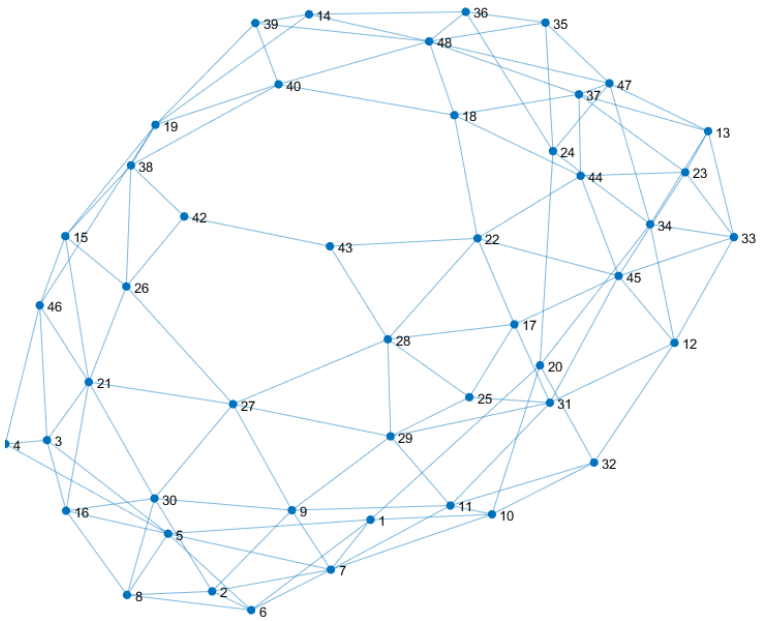

Figure 13. Graph using the pacing sites as vertices.

A weight was calculated and applied to each edge to represent the ease for electricity to go from one point to another. The weight of the edge between pacing sites i and j was determined as a combination of $\Delta sQRS_{(i,j)}$ (absolute difference in S-QRS delay between site i and site j) and $CG_{(i,j)}$ (correlation gradient between site i and site j) by the following equation:

$$W_{(i,j)} = \alpha * \Delta sQRS_{(i,j)} + \beta * CG_{(i,j)} + \gamma * \Delta sQRS_{(i,j)} * CG_{(i,j)} \quad (5)$$

α, β, γ can be modified to change the weight applied to the edges. Then, for a given α, β, γ, a shortest path based on Dijkstra's algorithm was calculated from each of the pacing sites of the core zone PM_{core} to all of the other pacing sites.

Each pacing site i was then given a pseudo-activation delay, $Delay_{PM_{core}}(i)$, estimated by the sum of $\Delta sQRS$ absolute differences along the shortest path $SP_{(PM_{core},i)} = \{j_1, \dots, j_N\}$ (an ordered set of vertices), according to the following:

$$Delay_{PM_{core}}(i) = \sum_{n=1}^{n=N-1} \Delta sQRS_{(j_n, j_{n+1})} \quad (6)$$

These values were called the pseudo-activation values and were projected on the ventricle. The resulting map was called the pseudo-activation map. An example of a pseudo-activation map from the first procedure with $PM_{core} = 40$ and weight $W = \Delta sQRS$ ($\alpha = 1, \beta = 0, \gamma = 0$) can be seen figure 14.

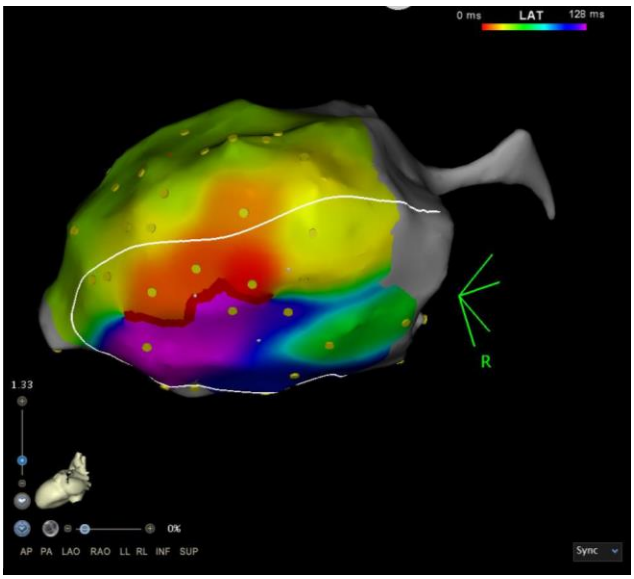

Figure 14. Pseudo activation map for patient 1 and pacing site 40 (Biosense Webster Inc., Diamond Bar).

The pseudo-activation map was finally compared to the activation pattern of the tachycardia. When the starting point was located in the exit zone of the reentrant circuit, the pseudo activation map was compared to the activation map. When the starting point was located in the entrance zone of the reentrant circuit, the pseudo activation map had an opposite activation pattern and was compared to the opposite activation map. The tachycardia being a circuit, the local activation time $LAT_{PM_{core}}(i)$ of each pacing site i of the tachycardia can be defined modulo the cycle length. For a given pacing site of an identified core zone, PM_{core} site, an activation time, $LAT_{PM_{core}}(PM_{core})$ of 0 was used. Additionally, only positive values for $LAT_{PM_{core}}(i)$ were used. The local activation values were thus between 0 and the value of the cycle length. The opposite activation time $LAT_{OppositePM_{core}}(i)$ was determined by giving the opposite activation time$LAT_{OppositePM_{core}}(PM_{core})$ the value of 0 and to affect to all the other points the value of $Cycle\ Length - LAT_{PM_{core}}(i)$. The local opposite activation values thus varied between 0 and the value of the cycle length and represented the opposite activation pattern of the tachycardia.

The pseudo-activation maps, activation maps, and opposite activation maps were integrated into the CARTO® system for visualization. The agreement between pseudo-activation maps, activation maps, and opposite activation maps was assessed by correlation analysis (mean, standard deviation, median, mean absolute error and both Spearman's and Lin's definitions).

e. Results

The GRAAPH method can enable quick identification of areas of interest and the pseudo activation map is similar to the activation pattern. Figure 15 represents the calculated pseudo-activation values and activation values from the first procedure with pacing site 42 using the weight $W = \Delta sQRS$. When comparing both methods, the mean was 5.92 ms; the standard deviation 30.43 ms; the median 8.4 ms; the mean absolute error 23.27 ms, Lin's coefficient 0.67 and Spearman's 0.40. Figure 16 shows the visual representation of the corresponding pseudo-activation map (A) and an opposite activation map (B) for patient 1, pacing site 42 as well as the pseudo-activation map (C) and activation map (D) for patient 2, pacing site 74. Regarding patient 1, the pacing site 42 is located at the entrance of the reentrant circuit and was correctly identified as being part of a core zone of the circuit. The pacing site 42 is located at the entrance of the reentrant circuit and the resulting pseudo-activation map has an opposite activation pattern to the activation map. Patient 2 only had a limited activation map but the tachycardia circuit could still be clearly identified. Pacing site 74 is located at the exit site of the reentrant circuit and was correctly identified as being part of a core zone of the circuit. In both patients, the pseudo-activation map and the activation map are similar and both maps enable quick identification of areas of interest and show the overall activation pattern of a reentrant circuit.

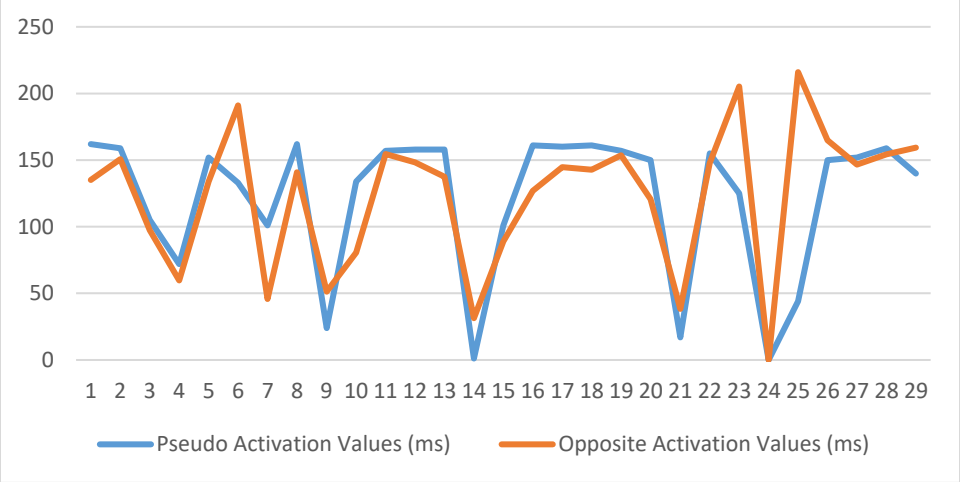

Figure 15. The calculated pseudo activation values and opposite activation values for pacing site 42.

The Lin's coefficient was optimized by tuning the parameters α, β, γ using a grid search. The best combination resulting in the highest similitude between the pseudo activation and the activation map was not only patient dependent but also changed depending on which initial pacing site of the core zone was selected. The Lin's coefficient varied between 0.5 and 0.76.

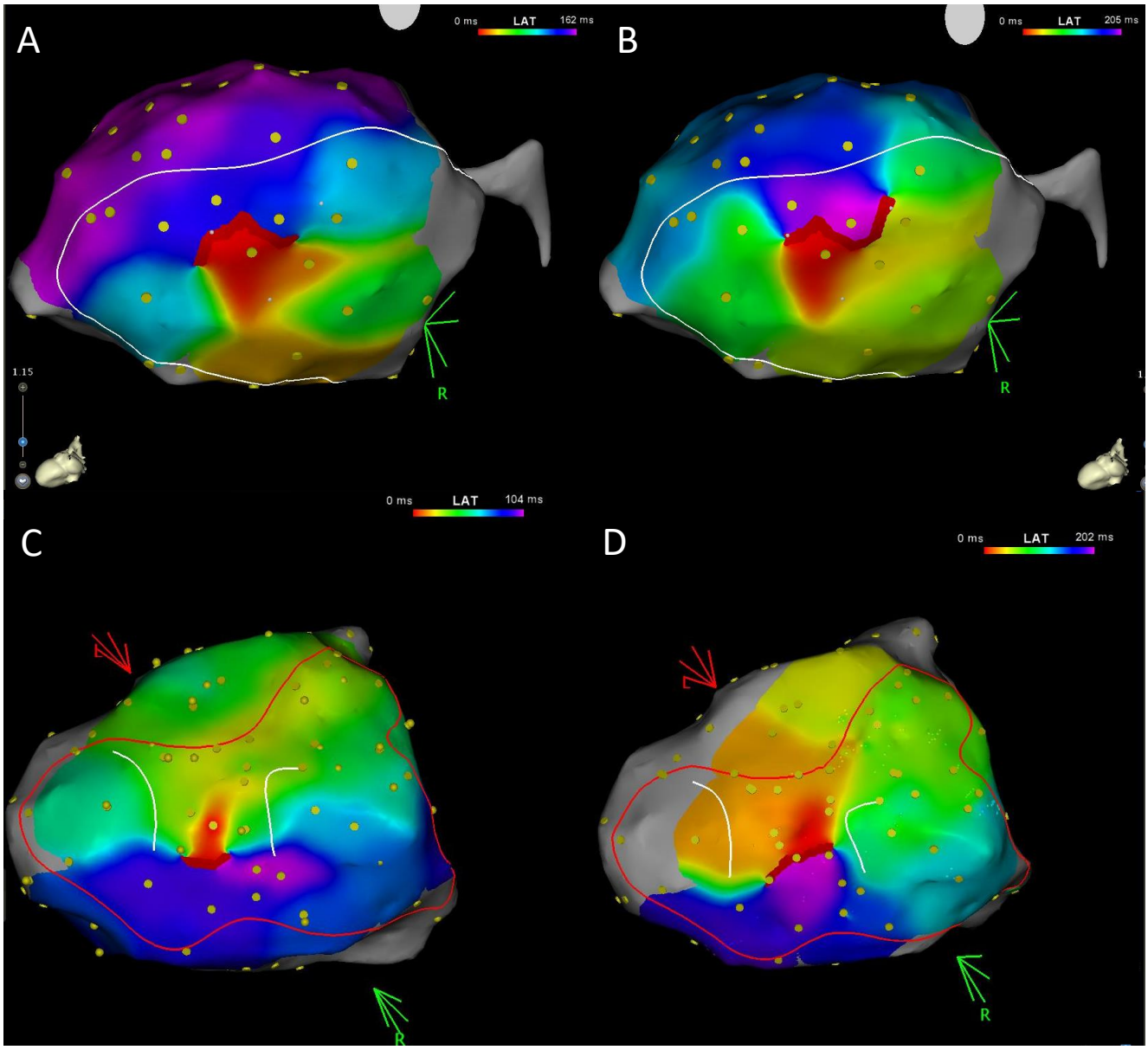

Figure 16. Pseudo-activation map (A) and the opposite activation map (B) for patient 1 and pacing site 42. Pseudo-activation map (C) and the activation map (D) for patient 2 and pacing site 74 (Biosense Webster Inc., Diamond Bar).

f. Discussion and conclusion

A novel method has been proposed that highlights possible activation patterns without the need of the reference VT. GRAAPH generates a map, the pseudo-activation map, which provides an indication of the direction of the underlying reentrant circuit. The pseudo-delay given to each point, determined by the sum of $\Delta sQRS$ absolute differences gives an indication of the activation sequence.

Additional work could be done to improve the current method by looking into better estimating the activation delay during tachycardia. This could be achieved by taking into account sinus rhythm activation delays and studying its implications on tachycardia activation values.

Further research on a larger number of patients is needed to try to determine the best weight formula that needs to be applied to the edges. Applying machine learning techniques might further improve the method. The objective would be to determine a weight formula independent of the initial pacing site of the patient that generates a pseudo activation map the most similar to the activation pattern of the circuit as possible.

The GRAAPH method could be particularly interesting in patients with multiple high correlation gradient zones. The method would therefore generate multiple pseudo activation maps providing the physician with an overview of the suggested activation patterns of the different VT circuits. The analysis of the pseudo-activation maps highlighting the electrical propagation pattern of the ventricle could provide further insights to help the physician determine the most effective ablation strategy.

Conclusion

The future of electrophysiology will likely be marked by the use of catheters with an increased number of electrodes and a decrease in electrode size. More information will be detected by this ever-growing array of sensors enabling maps of higher density to be created. This new information collected will need to be coupled with new automatic algorithms to quickly pinpoint the electrophysiologist towards the information of interest. To further increase their performance, these algorithms will not only take into account electroanatomic data but also incorporate information from different modalities. For example, magnetic resonance imaging could provide valuable insights about transmural scar depth as well as fiber orientation. In particular, the analysis of scar geometry could help determine the direction of a reentrant circuit.

Moreover, with the ageing population, the number of patients will increase, and techniques that treat patients faster and cheaper will be favored to limit the cost of healthcare. For example, robotic systems are not currently widely used as their development is limited by financial and speed considerations. The demand for faster and cheaper systems has already started and will likely gain momentum in the near future.

This thesis presented several novel approaches for identifying VT circuits. The studied methods are particularly useful in the event that the tachycardia is not inducible during the electrophysiology study. Special attention was given to automatically extract the key information and facilitate its visualization. The easier it is to visualize the data, the easier it is to then identify the links between the key parameters.

A long term goal of a post-infarct VT electrophysiology study is to be able to determine whether a given ventricle that has never sustained a tachycardia has the substrate to sustain one. If it is the case, targeted catheter ablation could be delivered to prevent the patient from sustaining any tachycardia. This approach focused on treating before the first life threatening event would significantly change how patients are treated today. This solution could also reduce the burden of healthcare by for example limiting the number of costly defibrillator implementations.

The use of more complex mathematical tools such as artificial intelligence might be needed to identify new patterns. Machine learning could be interesting to use because of the complexity of the data that needs to be taken into account. The development of such techniques needs to be done in a language that physicians can understand. This is the key for widespread adoption.

Résumé

Après une lésion du myocarde, la perturbation de l'apport sanguin peut modifier les voies électriques et conduire à la formation de circuits réentrants. Ces circuits possèdent une entrée, une partie centrale et une sortie et peuvent entraîner des rythmes cardiaques réguliers et rapides, épisodes qui sont nommés tachycardie ventriculaire (TV). L'électrophysiologie est l'étude du fonctionnement électrique et des propriétés électriques du cœur. Des cathéters munis d'électrodes permettent l'enregistrement des données électriques du cœur. Les cathéters peuvent être utilisés en conjonction avec des systèmes de cartographie pour créer des cartes 3D électro-anatomiques précises.

Le domaine de l'ablation par cathéter a progressé grâce au développement de nouveaux outils permettant d'analyser en détail les données électrophysiologiques disponibles. La carte d'activation repose sur l'analyse des temps d'activation locale pendant la tachycardie des différents sites du ventricule. Cette technique est la plus directe pour identifier le schéma d'activation de la tachycardie. Malheureusement, l'échec de l'induction de la tachycardie est fréquent et d'autres méthodes indirectes sont nécessaires, comme la technique de pace-mapping. Le pace-mapping consiste à stimuler le myocarde et à analyser le signal induit. Ce signal reflète l'emplacement du site de stimulation et ses propriétés électriques. Les faisceaux de myocytes survivants au sein d'une cicatrice hétérogène et les zones de bloc sont des éléments clés du substrat de la tachycardie et l'analyse des zones électriques anormaux a permis d'améliorer notre compréhension des arythmies ventriculaires. Une fois que le circuit de réentrée est clairement identifié, l'ablation par cathéter est utilisée pour traiter la tachycardie.

L'ischémie modifie la conduction des impulsions électriques dans le ventricule et peut créer les conditions nécessaires à la formation d'une tachycardie par réentrée. Le déclenchement et la stabilité d'un circuit réentrant donné sont déterminés par les propriétés conductrices globales du circuit. L'analyse du signal en rythme sinusal, l'activation, l'entraînement et le pace-mapping ont été développés pour identifier le circuit de tachycardie mais ces techniques sont considérablement limitées lorsque la tachycardie ne peut être induite. Ce travail s'intéresse aux nouvelles méthodes permettant de tirer le meilleur parti des informations disponibles pour identifier les composants critiques des mécanismes du circuit de la TV en explorant 5 axes : le pace-mapping sans référence, l'amélioration de la qualité du signal, l'analyse des caractéristiques de l'entrée de l'isthme, l'automatisation des calculs et la reconstruction graphique des schémas d'activation.

Le pace-mapping sans référence est une nouvelle méthode basée uniquement sur l'analyse des données de l'électrocardiogramme (ECG) obtenues pendant le pace-mapping. Cette approche ne nécessite pas d'enregistrement de la TV de référence et est particulièrement utile lorsque la tachycardie ne peut être induite. Le pace-mapping sans référence identifie avec précision les mêmes zones cibles que la cartographie de rythme conventionnelle ainsi que des zones supplémentaires qui peuvent être à l'origine d'autres circuits de TV.

Dans la pratique clinique actuelle, la technique conventionnelle du pace-mapping consiste à stimuler le myocarde et à comparer la morphologie des 12 dérivations du signal ECG induit avec un enregistrement de la TV de référence. La principale difficulté de la technique conventionnelle réside dans le fait qu'un enregistrement de la TV de référence est nécessaire. De plus, cette technique met en évidence le circuit de l'enregistrement de TV. D'autres circuits secondaires peuvent apparaître et méritent également d'être étudiés. Nous avons étudié une nouvelle méthode du pace-mapping sans référence, basée uniquement sur l'analyse des données ECG obtenues pendant la technique de pace-mapping. Une carte de corrélation locale est définie en analysant les corrélations par paires entre les signaux QRS stimulés provenant de sites de stimulation voisins. Cette méthode sans référence est proposée afin de quantifier les changements locaux dans les voies d'activation. Les propriétés électriques de l'influx électrique entre deux points ne dépendent pas de l'enregistrement de TV de référence sélectionné. Les points anormaux sont identifiés par des valeurs de gradient de corrélation élevées.

La méthode conventionnelle et la méthode sans référence ont été évaluées rétrospectivement sur 24 procédures d'ablation de TV. La technique de pace-mapping sans référence peut identifier avec précision les mêmes zones cibles que la technique de pace-mapping conventionnelle, ainsi que des zones supplémentaires pouvant être à l'origine d'autres circuits de TV. Le passage abrupt de bonnes à mauvaises valeurs aide également à déterminer l'orientation de l'isthme en définissant la transition entre la zone de sortie et la zone d'entrée. La méthode sans référence peut être utilisée en plus de la méthode conventionnelle, et est particulièrement utile pour traiter les patients chez qui une TV ne peut pas être induit pendant l'intervention.

Un nombre croissant de procédures sont réalisées avec la navigation magnétique à distance et la qualité du signal ECG recueilli dans le cadre du champ magnétique modificateur a été étudiée avec un nouveau dispositif d'acquisition.

Dans la navigation magnétique à distance, l'orientation de l'extrémité du cathéter est contrôlée en déplaçant deux aimants qui modifient à leur tour le champ magnétique. Selon la loi d'induction de Faraday, Φ(B) le flux du champ magnétique va également induire une force électromotrice Ɛ dans les différents câbles autour du patient.

$$\mathcal{E} = -\frac{d\Phi(B)}{dt}$$

Cette force Ɛ peut induire du bruit dans les câbles de l'ECG 12 dérivations. Le bruit induit couplé à la présence du filtre d'acquisition passe-haut peut rendre le suivi de l'ECG difficile jusqu'à 10 secondes après chaque mouvement de l'aimant. La technique de pace-mapping repose sur des comparaisons précises des signaux ECG et de tels artefacts peuvent limiter la capacité du médecin à analyser les données de pace-mapping. De plus, tout bruit induit par un mouvement dans le circuit d'acquisition sera amplifié à cause du champ magnétique, ce qui entrave encore davantage les comparaisons précises des ECG. Les causes possibles de ces mouvements peuvent être les tremblements du patient ou des appareils voisins tels que la pompe. Nous avons étudié et testé un nouveau dispositif d'acquisition basé sur la transmission optique pour limiter les distorsions corrélées au champ magnétique sur l'ECG.

Le concept original a d'abord été développé pour l'IRM (imagerie par résonance magnétique) et cette étude est le résultat de son adaptation au contexte de l'électrophysiologie. Le nouveau dispositif d'acquisition étudié améliore la qualité du signal ECG recueilli dans le cadre de la navigation magnétique. Cela pourrait contribuer à optimiser le flux de travail, à produire des cartes de plus grande densité et à réduire la durée des procédures.

Un calculateur automatique d'électrogrammes multiparamétriques a été mis au point pour déterminer la probabilité qu'un site donné soit situé à l'entrée d'un isthme de TV, une localisation clé du circuit.

On a constaté que de multiples caractéristiques de l'électrogramme sont associées aux circuits de réentrée. Cependant, l'analyse d'un seul paramètre est insuffisante pour définir complètement la localisation de l'isthme de TV. Nous avons étudié 10 caractéristiques d'électrogramme différentes pour identifier une entrée d'isthme de TV. Les paramètres étudiés sont l'amplitude bipolaire et unipolaire, le temps entre le début du QRS et le début de l'électrogramme, le temps entre le début de l'électrogramme et le début du QRS, la durée de l'électrogramme, le nombre de pics positifs, l'intervalle S-QRS ainsi que la présence de fragmentation, de potentiels doubles et de potentiels tardifs. Tous ces paramètres peuvent être recueillis en l'absence de TV induite.

L'analyse de régression logistique a montré que l'amplitude bipolaire, le nombre de pics positifs de l'électrogramme et l'intervalle S-QRS étaient indépendamment associés à la localisation de l'entrée de l'isthme TV. Une évaluation multiparamétrique de l'électrogramme est une approche prometteuse pour localiser l'entrée d'un isthme TV. Sur la base de ces résultats, une interface utilisateur graphique a été développée et mise en œuvre dans un calculateur automatique pour déterminer rapidement la probabilité qu'un site donné soit situé à l'entrée d'un isthme de TV.

La détection automatique a été développée car l'analyse des points de pace-map est actuellement limitée en raison des étapes fastidieuses que le cardiologue interventionnel doit effectuer pour visualiser les informations importantes. Le traitement automatique a réduit le besoin d'annotations manuelles et a facilité la visualisation des cartes multiparamétriques identifiant l'emplacement de l'entrée, du cœur et de la sortie du circuit TV.

L'analyse des données recueillies pendant le rythme sinusal et le pace-mapping permet l'étude détaillée des caractéristiques électriques d'un ventricule donné. Cette analyse est actuellement limitée en raison des étapes fastidieuses que le cardiologue interventionnel doit effectuer pour visualiser les informations d'intérêt. L'absence de techniques de détection déjà implémentées entrave l'utilisation des données de pace-mapping. Nous présentons une nouvelle méthode pour extraire automatiquement les informations clés. Des critères d'ondelettes, de temps et d'énergie sont utilisés pour détecter les pics de stimulation et les battements rythmés, ainsi que pour délimiter le début et le sommet d'un QRS. L'objectif global est de fournir au médecin un outil logiciel permettant de visualiser rapidement les cartes les plus pertinentes (amplitude, gradient de corrélation et intervalle S-QRS) pour identifier les circuits potentiels de TV.

Le traitement automatique a réduit le besoin d'annotations manuelles et a facilité la visualisation des cartes pertinentes. L'analyse conjointe des cartes multiparamétriques permet d'identifier l'emplacement de l'entrée, du cœur et de la sortie du circuit de TV. Une fois le circuit identifié, les cibles d'ablation peuvent être déterminées afin d'éliminer les zones critiques à conduction lente.

Une nouvelle méthode graphique GRAAPH (Graph-based Reconstruction of Arrhythmic Activations by Pacing the Heart) a été mise en œuvre pour tirer pleinement parti de toutes les informations disponibles obtenues par la technique de pace-mapping. Cette méthode permet d'extraire automatiquement les informations clés et de faciliter l'utilisation des données de pace-mapping. Les connexions entre chaque site de stimulation pendant la technique de pace-mapping ont été analysées pour générer un modèle d'activation suggéré du circuit de TV. La méthode GRAAPH met en évidence avec succès les schémas d'activation possibles sans avoir besoin d'une TV de référence. Cette nouvelle méthode a conduit au dépôt d'un brevet provisoire américain, Computer assisted electrophysiological intervention for reentrant circuit identification, numéro de demande 63179054.

GRAAPH génère une carte, la carte de pseudo-activation, qui fournit une indication de la direction du circuit réentrant sous-jacent. Le pseudo-délai donné à chaque point, déterminé par la somme des différences absolues des intervalle S-QRS ($\Delta sQRS$) donne une indication de la séquence d'activation.

Des travaux supplémentaires pourraient être effectués pour améliorer la méthode actuelle en cherchant à mieux estimer le délai d'activation pendant la tachycardie. Ceci pourrait être réalisé en prenant en compte les retards d'activation en rythme sinusal et en étudiant ses implications sur les valeurs d'activation en tachycardie.

Des recherches supplémentaires sur un plus grand nombre de patients sont nécessaires pour essayer de déterminer la meilleure formule de pondération qui doit être appliquée aux bords. L'application de techniques d'apprentissage automatique pourrait encore améliorer la méthode. L'objectif serait de déterminer une formule de pondération indépendante du site de stimulation initial du patient qui génère une carte de pseudo-activation la plus similaire possible au schéma d'activation du circuit.

La méthode GRAAPH pourrait être particulièrement intéressante chez les patients présentant de multiples zones à gradient de corrélation élevé. La méthode génèrerait donc plusieurs cartes de pseudo-activation fournissant au médecin un aperçu des schémas d'activation suggérés des différents circuits de TV. L'analyse des cartes de pseudo-activation mettant en évidence le schéma de propagation électrique du ventricule pourrait fournir des informations supplémentaires pour aider le médecin à déterminer la stratégie d'ablation la plus efficace.

L'avenir de l'électrophysiologie sera probablement marqué par l'utilisation de cathéters comportant un nombre accru d'électrodes plus petites. Davantage d'informations seront détectées par un réseau toujours plus grand de capteurs, ce qui permettra de créer des cartes de plus grande densité. Ces nouvelles informations collectées devront être couplées à de nouveaux algorithmes automatiques pour orienter rapidement l'électrophysiologiste vers l'information qui l'intéresse. Pour accroître encore leurs performances, ces algorithmes ne prendront pas seulement en compte les données électroanatomiques mais intégreront également des informations provenant de différentes modalités. Par exemple, l'imagerie par résonance magnétique pourrait fournir des informations précieuses sur la profondeur de la cicatrice transmurale ainsi que sur l'orientation des fibres. En particulier, l'analyse de la géométrie de la cicatrice pourrait aider à déterminer la direction d'un circuit réentrant.

Par ailleurs, avec le vieillissement de la population, le nombre de patients va augmenter, et les techniques permettant de traiter les patients plus rapidement et à moindre coût seront privilégiées pour limiter le coût des soins de santé. Par exemple, les systèmes robotiques ne sont actuellement pas très utilisés car leur développement est limité par des considérations financières et de rapidité. La demande de systèmes plus rapides et moins chers a déjà commencé et va probablement s'amplifier dans un avenir proche.

Cette thèse a présenté plusieurs nouvelles approches pour identifier les circuits de TV. Les méthodes étudiées sont particulièrement utiles dans le cas où la tachycardie n'est pas inductible pendant l'étude électrophysiologique. Une attention particulière a été accordée à l'extraction automatique des informations clés et à la facilitation de leur visualisation. Plus il est facile de visualiser les données, plus il est facile d'identifier ensuite les liens entre les paramètres clés.

Un objectif à long terme d'une étude électrophysiologique de la TV post-infarctus est de pouvoir déterminer si un ventricule donné qui n'a jamais soutenu une tachycardie a le substrat pour en soutenir une. Si c'est le cas, une ablation ciblée par cathéter pourrait être pratiquée pour empêcher le patient de subir une tachycardie. Cette approche axée sur le traitement avant le premier événement mettant en danger la vie du patient modifierait considérablement la façon dont les patients sont traités aujourd'hui. Cette solution pourrait également réduire la charge des soins de santé en limitant par exemple le grand nombre d'implémentations coûteuses de défibrillateurs.

L'utilisation d'outils mathématiques plus complexes tels que l'intelligence artificielle pourrait être nécessaire pour identifier de nouveaux modèles. L'apprentissage automatique pourrait être intéressant à utiliser en raison de la complexité des données à prendre en compte. Le développement de ces techniques

doit se faire dans un langage que les médecins peuvent comprendre. C'est la clé d'une adoption généralisée.

Bibliography

[1] D. D. Streeter Jr, H. M. Spotnitz, D. P. Patel, J. Ross Jr, and E. H. Sonnenblick, "Fiber orientation in the canine left ventricle during diastole and systole," *Circ. Res.*, vol. 24, no. 3, pp. 339–347, 1969.

[2] A. D. Desai, T. S. Yaw, T. Yamazaki, A. Kaykha, S. Chun, and V. F. Froelicher, "Prognostic significance of quantitative QRS duration," *Am. J. Med.*, vol. 119, no. 7, pp. 600–606, 2006.

[3] R. Dhar *et al.*, "Association of prolonged QRS duration with ventricular tachyarrhythmias and sudden cardiac death in the Multicenter Automatic Defibrillator Implantation Trial II (MADIT-II)," *Heart Rhythm*, vol. 5, no. 6, pp. 807–813, 2008.

[4] E. Anter, C. M. Tschabrunn, A. E. Buxton, and M. E. Josephson, "High-resolution mapping of postinfarction reentrant ventricular tachycardia: electrophysiological characterization of the circuit," *Circulation*, vol. 134, no. 4, pp. 314–327, 2016.

[5] M. E. Josephson and E. Anter, "Substrate mapping for ventricular tachycardia: assumptions and misconceptions," *JACC Clin. Electrophysiol.*, vol. 1, no. 5, pp. 341–352, 2015.

[6] A. G. Kléber and Y. Rudy, "Basic mechanisms of cardiac impulse propagation and associated arrhythmias," *Physiol. Rev.*, 2004.

[7] T. Sano, N. Takayama, and T. Shimamoto, "Directional difference of conduction velocity in the cardiac ventricular syncytium studied by microelectrodes," *Circ. Res.*, vol. 7, no. 2, pp. 262–267, 1959.

[8] E. Carmeliet, "Cardiac ionic currents and acute ischemia: from channels to arrhythmias," *Physiol. Rev.*, vol. 79, no. 3, pp. 917–1017, 1999.

[9] J. J. Fenoglio Jr, T. D. Pham, A. H. Harken, L. N. Horowitz, M. E. Josephson, and A. L. Wit, "Recurrent sustained ventricular tachycardia: structure and ultrastructure of subendocardial regions in which tachycardia originates.," *Circulation*, vol. 68, no. 3, pp. 518–533, 1983.

[10] A. P. Wijnmaalen, M. J. Schalij, J. H. von der Thüsen, R. J. Klautz, and K. Zeppenfeld, "Early Reperfusion During Acute Myocardial Infarction Affects Ventricular Tachycardia Characteristics and the Chronic Electroanatomic and Histological Substrate," *Circulation*, vol. 121, no. 17, pp. 1887–1895, 2010.

[11] J. M. de Bakker *et al.*, "Slow conduction in the infarcted human heart. 'Zigzag' course of activation.," *Circulation*, vol. 88, no. 3, p. 915, Sep. 1993, doi: 10.1161/01.CIR.88.3.915.

[12] S. Baba, W. Dun, C. Cabo, and P. A. Boyden, "Remodeling in cells from different regions of the reentrant circuit during ventricular tachycardia," *Circulation*, vol. 112, no. 16, p. 2386, 2005.

[13] A. G. Kleber, M. J. Janse, F. J. Wilms-Schopmann, A. A. Wilde, and R. Coronel, "Changes in conduction velocity during acute ischemia in ventricular myocardium of the isolated porcine heart.," *Circulation*, vol. 73, no. 1, pp. 189–198, 1986.

[14] M. Potse, R. Coronel, A.-R. LeBlanc, and A. Vinet, "The role of extracellular potassium transport in computer models of the ischemic zone," *Med. Biol. Eng. Comput.*, vol. 45, no. 12, pp. 1187–1199, 2007.

[15] R. A. Luke and J. E. Saffitz, "Remodeling of ventricular conduction pathways in healed canine infarct border zones.," *J. Clin. Invest.*, vol. 87, no. 5, pp. 1594–1602, 1991.

[16] J.-M. Cao *et al.*, "Relationship between regional cardiac hyperinnervation and ventricular arrhythmia," *Circulation*, vol. 101, no. 16, pp. 1960–1969, 2000.

[17] O. A. Ajijola *et al.*, "Focal myocardial infarction induces global remodeling of cardiac sympathetic innervation: neural remodeling in a spatial context," *Am. J. Physiol.-Heart Circ. Physiol.*, vol. 305, no. 7, pp. H1031–H1040, 2013.

[18] J. B. Martins and D. P. Zipes, “Effects of sympathetic and vagal nerves on recovery properties of the endocardium and epicardium of the canine left ventricle.,” *Circ. Res.*, vol. 46, no. 1, pp. 100–110, 1980.
[19] T. Opthof *et al.*, “Dispersion of refractoriness in canine ventricular myocardium. Effects of sympathetic stimulation.,” *Circ. Res.*, vol. 68, no. 5, pp. 1204–1215, 1991.
[20] T. Opthof, L. R. Dekker, R. Coronel, J. T. Vermeulen, F. J. van Capelle, and M. J. Janse, “Interaction of sympathetic and parasympathetic nervous system on ventricular refractoriness assessed by local fibrillation intervals in the canine heart,” *Cardiovasc. Res.*, vol. 27, no. 5, pp. 753–759, 1993.
[21] S. R. Piers *et al.*, “Early reperfusion therapy affects inducibility, cycle length, and occurrence of ventricular tachycardia late after myocardial infarction,” *Circ. Arrhythm. Electrophysiol.*, vol. 4, no. 2, pp. 195–201, 2011.
[22] S. Miyazaki *et al.*, “Quantitative analysis of contraction band and coagulation necrosis after ischemia and reperfusion in the porcine heart.,” *Circulation*, vol. 75, no. 5, pp. 1074–1082, 1987.
[23] M. Matsuda *et al.*, “Quantitative analysis of infarct size, contraction band necrosis, and coagulation necrosis in human autopsied hearts with acute myocardial infarction after treatment with selective intracoronary thrombolysis.,” *Circulation*, vol. 76, no. 5, pp. 981–989, 1987.
[24] N. S. Peters and A. L. Wit, “Myocardial architecture and ventricular arrhythmogenesis,” *Circulation*, vol. 97, no. 17, pp. 1746–1754, 1998.
[25] J.-M. Cao *et al.*, “Nerve sprouting and sudden cardiac death,” *Circ. Res.*, vol. 86, no. 7, pp. 816–821, 2000.
[26] S. M. Pogwizd, R. H. Hoyt, J. E. Saffitz, P. B. Corr, J. L. Cox, and M. E. Cain, “Reentrant and focal mechanisms underlying ventricular tachycardia in the human heart.,” *Circulation*, vol. 86, no. 6, pp. 1872–1887, 1992.
[27] S. M. Dillon, M. A. Allessie, P. C. Ursell, and A. L. Wit, “Influences of anisotropic tissue structure on reentrant circuits in the epicardial border zone of subacute canine infarcts.,” *Circ. Res.*, vol. 63, no. 1, pp. 182–206, 1988.
[28] E. J. Ciaccio, J. Coromilas, A. L. Wit, N. S. Peters, and H. Garan, “Formation of reentrant circuits in the mid-myocardial infarct border zone,” *Comput. Biol. Med.*, vol. 71, pp. 205–213, 2016.
[29] E. J. Ciaccio *et al.*, “Model of reentrant ventricular tachycardia based on infarct border zone geometry predicts reentrant circuit features as determined by activation mapping,” *Heart Rhythm*, vol. 4, no. 8, pp. 1034–1045, 2007.
[30] E. Downar, L. Harris, L. L. Mickleborough, N. Shaikh, and I. D. Parson, “Endocardial mapping of ventricular tachycardia in the intact human ventricle: evidence for reentrant mechanisms,” *J. Am. Coll. Cardiol.*, vol. 11, no. 4, pp. 783–791, 1988.
[31] C. de Chillou *et al.*, “Isthmus characteristics of reentrant ventricular tachycardia after myocardial infarction,” *Circulation*, vol. 105, no. 6, pp. 726–731, 2002.
[32] D. J. Wilber, D. E. Kopp, D. N. Glascock DO, C. A. Kinder, and J. G. Kall, “Catheter ablation of the mitral isthmus for ventricular tachycardia associated with inferior infarction,” *Circulation*, vol. 92, no. 12, pp. 3481–3489, 1995.
[33] W. Kaltenbrunner *et al.*, “Epicardial and endocardial mapping of ventricular tachycardia in patients with myocardial infarction. Is the origin of the tachycardia always subendocardially localized?,” *Circulation*, vol. 84, no. 3, pp. 1058–1071, 1991.
[34] J. M. de Baker *et al.*, “Ventricular tachycardia in the infarcted, Langendorff-perfused human heart: Role of the arrangement of surviving cardiac fibers,” *J. Am. Coll. Cardiol.*, vol. 15, no. 7, pp. 1594–1607, 1990.
[35] J. Krafchek, G. M. Lawrie, and C. R. Wyndham, “Cryoablation of arrhythmias from the interventricular septum: initial experience with a new biventricular approach,” *J. Thorac. Cardiovasc. Surg.*, vol. 91, no. 3, pp. 419–427, 1986.

[36] E. Downar *et al.*, “Endocardial mapping of ventricular tachycardia in the intact human heart. II. Evidence for multiuse reentry in a functional sheet of surviving myocardium,” *J. Am. Coll. Cardiol.*, vol. 20, no. 4, pp. 869–878, 1992.
[37] J. M. De Bakker *et al.*, “Reentry as a cause of ventricular tachycardia in patients with chronic ischemic heart disease: electrophysiologic and anatomic correlation.,” *Circulation*, vol. 77, no. 3, pp. 589–606, 1988.
[38] W. G. Stevenson *et al.*, “Identification of reentry circuit sites during catheter mapping and radiofrequency ablation of ventricular tachycardia late after myocardial infarction.,” *Circulation*, vol. 88, no. 4, pp. 1647–1670, 1993.
[39] M. J. Janse and A. L. Wit, “Electrophysiological mechanisms of ventricular arrhythmias resulting from myocardial ischemia and infarction,” *Physiol. Rev.*, vol. 69, no. 4, pp. 1049–1169, 1989.
[40] F. Sacher *et al.*, “Ventricular tachycardia ablation: evolution of patients and procedures over 8 years,” *Circ. Arrhythm. Electrophysiol.*, vol. 1, no. 3, pp. 153–161, 2008.
[41] A. J. Moss *et al.*, “Long-term clinical course of patients after termination of ventricular tachyarrhythmia by an implanted defibrillator,” *Circulation*, vol. 110, no. 25, pp. 3760–3765, 2004.
[42] N. S. Peters, J. Coromilas, N. J. Severs, and A. L. Wit, “Disturbed connexin43 gap junction distribution correlates with the location of reentrant circuits in the epicardial border zone of healing canine infarcts that cause ventricular tachycardia,” *Circulation*, vol. 95, no. 4, pp. 988–996, 1997.
[43] J. M. Miller, M. G. Kienzle, A. H. Harken, and M. E. Josephson, “Subendocardial resection for ventricular tachycardia: predictors of surgical success.,” *Circulation*, vol. 70, no. 4, pp. 624–631, 1984.
[44] W. G. Stevenson, P. L. Friedman, D. Kocovic, P. T. Sager, L. A. Saxon, and B. Pavri, “Radiofrequency catheter ablation of ventricular tachycardia after myocardial infarction,” *Circulation*, vol. 98, no. 4, pp. 308–314, 1998.
[45] E. M. Cronin *et al.*, “2019 HRS/EHRA/APHRS/LAHRS expert consensus statement on catheter ablation of ventricular arrhythmias,” *EP Eur.*, vol. 21, no. 8, pp. 1143–1144, 2019.
[46] L. Gepstein, G. Hayam, and S. A. Ben-Haim, “A novel method for nonfluoroscopic catheter-based electroanatomical mapping of the heart: in vitro and in vivo accuracy results,” *Circulation*, vol. 95, no. 6, pp. 1611–1622, 1997.
[47] N. Ariyarathna, S. Kumar, S. P. Thomas, W. G. Stevenson, and G. F. Michaud, “Role of contact force sensing in catheter ablation of cardiac arrhythmias: evolution or history repeating itself?,” *JACC Clin. Electrophysiol.*, vol. 4, no. 6, pp. 707–723, 2018.
[48] H. Nakagawa *et al.*, “Comparison of in vivo tissue temperature profile and lesion geometry for radiofrequency ablation with a saline-irrigated electrode versus temperature control in a canine thigh muscle preparation,” *Circulation*, vol. 91, no. 8, pp. 2264–2273, 1995.
[49] A. González-Suárez, E. Berjano, J. M. Guerra, and L. Gerardo-Giorda, “Computational modeling of open-irrigated electrodes for radiofrequency cardiac ablation including blood motion-saline flow interaction,” *PloS One*, vol. 11, no. 3, p. e0150356, 2016.
[50] H. Nakagawa *et al.*, “Inverse relationship between electrode size and lesion size during radiofrequency ablation with active electrode cooling,” *Circulation*, vol. 98, no. 5, pp. 458–465, 1998.
[51] D. T. Nguyen *et al.*, “Radiofrequency ablation using an open irrigated electrode cooled with half-normal saline,” *JACC Clin. Electrophysiol.*, vol. 3, no. 10, pp. 1103–1110, 2017.
[52] D. T. Nguyen *et al.*, “Prospective multicenter experience with cooled radiofrequency ablation using high impedance irrigant to target deep myocardial substrate refractory to standard ablation,” *JACC Clin. Electrophysiol.*, vol. 4, no. 9, pp. 1176–1185, 2018.
[53] R. Fazel *et al.*, “Approaches to enhancing radiation safety in cardiovascular imaging: a scientific statement from the American Heart Association,” *Circulation*, vol. 130, no. 19, pp. 1730–1748, 2014.

[54] E. Picano *et al.*, “The appropriate and justified use of medical radiation in cardiovascular imaging: a position document of the ESC Associations of Cardiovascular Imaging, Percutaneous Cardiovascular Interventions and Electrophysiology,” *Eur. Heart J.*, vol. 35, no. 10, pp. 665–672, 2014.
[55] N. H. Von Bergen, S. Bansal, J. Gingerich, and I. H. Law, “Nonfluoroscopic and radiation-limited ablation of ventricular arrhythmias in children and young adults: a case series,” *Pediatr. Cardiol.*, vol. 32, no. 6, pp. 743–747, 2011.
[56] L. Venneri *et al.*, “Cancer risk from professional exposure in staff working in cardiac catheterization laboratory: insights from the National Research Council’s Biological Effects of Ionizing Radiation VII Report,” *Am. Heart J.*, vol. 157, no. 1, pp. 118–124, 2009.
[57] T. Reents *et al.*, “Catheter ablation of ventricular arrhythmias using a fluoroscopy image integration module,” *Pacing Clin. Electrophysiol.*, vol. 38, no. 6, pp. 700–705, 2015.
[58] Ó. Cano *et al.*, “Safety and feasibility of a minimally fluoroscopic approach for ventricular tachycardia ablation in patients with structural heart disease: influence of the ventricular tachycardia substrate,” *Circ. Arrhythm. Electrophysiol.*, vol. 9, no. 2, p. e003706, 2016.
[59] J. Skoda *et al.*, “Catheter ablation of ischemic ventricular tachycardia with remote magnetic navigation: STOP-VT multicenter trial,” *J. Cardiovasc. Electrophysiol.*, vol. 27, no. S1, pp. S29–S37, 2016.
[60] M. N. Faddis *et al.*, “Novel, magnetically guided catheter for endocardial mapping and radiofrequency catheter ablation,” *Circulation*, vol. 106, no. 23, pp. 2980–2985, 2002.
[61] P. Qian *et al.*, “Early and long-term outcomes after manual and remote magnetic navigation-guided catheter ablation for ventricular tachycardia,” *Ep Eur.*, vol. 20, no. suppl_2, pp. ii11–ii21, 2018.
[62] F. Akca, D. A. Theuns, L. D. Abkenari, N. M. de Groot, L. Jordaens, and T. Szili-Torok, “Outcomes of repeat catheter ablation using magnetic navigation or conventional ablation,” *Europace*, vol. 15, no. 10, pp. 1426–1431, 2013.
[63] R. Proietti *et al.*, “Remote magnetic with open-irrigated catheter vs. manual navigation for ablation of atrial fibrillation: a systematic review and meta-analysis,” *Europace*, vol. 15, no. 9, pp. 1241–1248, 2013.
[64] L. Di Biase *et al.*, “MAGNETIC VT study: a prospective, multicenter, post-market randomized controlled trial comparing VT ablation outcomes using remote magnetic navigation-guided substrate mapping and ablation versus manual approach in a low LVEF population,” *J. Interv. Card. Electrophysiol.*, vol. 48, no. 3, pp. 237–245, 2017.
[65] Q. Jin, P. K. Jacobsen, S. Pehrson, and X. Chen, “Acute and long term outcomes of catheter ablation using remote magnetic navigation for the treatment of electrical storm in patients with severe ischemic heart failure,” *Int. J. Cardiol.*, vol. 183, pp. 11–16, 2015.
[66] A. Ikeda *et al.*, “Relationship between catheter contact force and radiofrequency lesion size and incidence of steam pop in the beating canine heart: electrogram amplitude, impedance, and electrode temperature are poor predictors of electrode-tissue contact force and lesion size,” *Circ. Arrhythm. Electrophysiol.*, vol. 7, no. 6, pp. 1174–1180, 2014.
[67] F. Perna, E. K. Heist, S. B. Danik, C. D. Barrett, J. N. Ruskin, and M. Mansour, “Assessment of catheter tip contact force resulting in cardiac perforation in swine atria using force sensing technology,” *Circ. Arrhythm. Electrophysiol.*, vol. 4, no. 2, pp. 218–224, 2011.
[68] M. Martinek *et al.*, “Clinical impact of an open-irrigated radiofrequency catheter with direct force measurement on atrial fibrillation ablation,” *Pacing Clin. Electrophysiol.*, vol. 35, no. 11, pp. 1312–1318, 2012.
[69] H. Mizuno *et al.*, “Contact force monitoring for cardiac mapping in patients with ventricular tachycardia,” *J. Cardiovasc. Electrophysiol.*, vol. 24, no. 5, pp. 519–524, 2013.
[70] F. Sacher *et al.*, “Endocardial versus epicardial ventricular radiofrequency ablation: utility of in vivo contact force assessment,” *Circ. Arrhythm. Electrophysiol.*, vol. 6, no. 1, pp. 144–150, 2013.

[71] L. Jesel *et al.*, “Characterization of contact force during endocardial and epicardial ventricular mapping,” *Circ. Arrhythm. Electrophysiol.*, vol. 7, no. 6, pp. 1168–1173, 2014.
[72] J. M. Stinnett-Donnelly *et al.*, “Effects of electrode size and spacing on the resolution of intracardiac electrograms,” *Coron. Artery Dis.*, vol. 23, no. 2, pp. 126–132, 2012.
[73] J. Acosta *et al.*, “Multielectrode vs. point-by-point mapping for ventricular tachycardia substrate ablation: a randomized study,” *Ep Eur.*, vol. 20, no. 3, pp. 512–519, 2018.
[74] C. M. Tschabrunn, S. Roujol, N. C. Dorman, R. Nezafat, M. E. Josephson, and E. Anter, “High-resolution mapping of ventricular scar: comparison between single and multielectrode catheters,” *Circ. Arrhythm. Electrophysiol.*, vol. 9, no. 6, p. e003841, 2016.
[75] E. Leshem *et al.*, “High-resolution mapping of ventricular scar: evaluation of a novel integrated multielectrode mapping and ablation catheter,” *JACC Clin. Electrophysiol.*, vol. 3, no. 3, pp. 220–231, 2017.
[76] P. Della Bella, C. Bisceglia, and R. Tung, “Multielectrode contact mapping to assess scar modification in post-myocardial infarction ventricular tachycardia patients,” *Europace*, vol. 14, no. suppl_2, pp. ii7–ii12, 2012.
[77] B. Berte *et al.*, “Impact of electrode type on mapping of scar-related VT,” *J. Cardiovasc. Electrophysiol.*, vol. 26, no. 11, pp. 1213–1223, 2015.
[78] S. Yamashita *et al.*, “Impact of new technologies and approaches for post–myocardial infarction ventricular tachycardia ablation during long-term follow-up,” *Circ. Arrhythm. Electrophysiol.*, vol. 9, no. 7, p. e003901, 2016.
[79] M. El Haddad, R. Houben, R. Stroobandt, F. Van Heuverswyn, R. Tavernier, and M. Duytschaever, “Novel algorithmic methods in mapping of atrial and ventricular tachycardia,” *Circ. Arrhythm. Electrophysiol.*, vol. 7, no. 3, pp. 463–472, 2014.
[80] M. Nair, “New Mapping Technologies”.
[81] V. Luther, N. Qureshi, P. Kanagaratnam, and P. BOON LIM, “Automated activation and pace-mapping to guide ablation within the outflow tract,” *J. Cardiovasc. Electrophysiol.*, vol. 27, no. 1, pp. 127–128, 2016.
[82] H. Nakagawa, A. Ikeda, T. Sharma, R. Lazzara, and W. M. Jackman, “Rapid high resolution electroanatomical mapping: evaluation of a new system in a canine atrial linear lesion model,” *Circ. Arrhythm. Electrophysiol.*, vol. 5, no. 2, pp. 417–424, 2012.
[83] S.-S. Bun, D. G. Latcu, T. Delassi, M. El Jamili, A. Al Amoura, and N. Saoudi, “Ultra-high-definition mapping of atrial arrhythmias,” *Circ. J.*, vol. 80, no. 3, pp. 579–586, 2016.
[84] E. Anter *et al.*, “Infarct-related ventricular tachycardia: redefining the electrophysiological substrate of the isthmus during sinus rhythm,” *JACC Clin. Electrophysiol.*, vol. 4, no. 8, pp. 1033–1048, 2018.
[85] E. J. Ciaccio, A. W. Chow, R. A. Kaba, D. W. Davies, O. R. Segal, and N. S. Peters, “Detection of the diastolic pathway, circuit morphology, and inducibility of human postinfarction ventricular tachycardia from mapping in sinus rhythm,” *Heart Rhythm*, vol. 5, no. 7, pp. 981–991, 2008.
[86] F. E. Marchlinski, D. J. Callans, C. D. Gottlieb, and E. Zado, “Linear ablation lesions for control of unmappable ventricular tachycardia in patients with ischemic and nonischemic cardiomyopathy,” *Circulation*, vol. 101, no. 11, pp. 1288–1296, 2000.
[87] D. J. Callans, J.-F. Ren, J. Michele, F. E. Marchlinski, and S. M. Dillon, “Electroanatomic left ventricular mapping in the porcine model of healed anterior myocardial infarction: correlation with intracardiac echocardiography and pathological analysis,” *Circulation*, vol. 100, no. 16, pp. 1744–1750, 1999.
[88] R. Tung, M. E. Josephson, J. S. Bradfield, and K. Shivkumar, “Directional influences of ventricular activation on myocardial scar characterization: voltage mapping with multiple wavefronts during ventricular tachycardia ablation,” *Circ. Arrhythm. Electrophysiol.*, vol. 9, no. 8, p. e004155, 2016.

[89] D. M. Cassidy, J. A. Vassallo, F. E. Marchlinski, A. E. Buxton, W. J. Untereker, and M. E. Josephson, "Endocardial mapping in humans in sinus rhythm with normal left ventricles: activation patterns and characteristics of electrograms.," *Circulation*, vol. 70, no. 1, pp. 37–42, 1984.
[90] K. Soejima, W. G. Stevenson, W. H. Maisel, J. L. Sapp, and L. M. Epstein, "Electrically unexcitable scar mapping based on pacing threshold for identification of the reentry circuit isthmus: feasibility for guiding ventricular tachycardia ablation," *Circulation*, vol. 106, no. 13, pp. 1678–1683, 2002.
[91] J. Acosta *et al.*, "Elucidation of hidden slow conduction by double ventricular extrastimuli: a method for further arrhythmic substrate identification in ventricular tachycardia ablation procedures," *Ep Eur.*, vol. 20, no. 2, pp. 337–346, 2018.
[92] T. Dickfeld *et al.*, "MRI-Guided ventricular tachycardia ablation: integration of late gadolinium-enhanced 3D scar in patients with implantable cardioverter-defibrillators," *Circ. Arrhythm. Electrophysiol.*, vol. 4, no. 2, pp. 172–184, 2011.
[93] M. de Riva *et al.*, "Targeting the hidden substrate unmasked by right ventricular extrastimulation improves ventricular tachycardia ablation outcome after myocardial infarction," *JACC Clin. Electrophysiol.*, vol. 4, no. 3, pp. 316–327, 2018.
[94] A. Verma *et al.*, "Relationship between successful ablation sites and the scar border zone defined by substrate mapping for ventricular tachycardia post-myocardial infarction," *J. Cardiovasc. Electrophysiol.*, vol. 16, no. 5, pp. 465–471, 2005.
[95] A. Arenal *et al.*, "Tachycardia-related channel in the scar tissue in patients with sustained monomorphic ventricular tachycardias: influence of the voltage scar definition," *Circulation*, vol. 110, no. 17, pp. 2568–2574, 2004.
[96] S. E. Mountantonakis *et al.*, "Relationship between voltage map 'channels' and the location of critical isthmus sites in patients with post-infarction cardiomyopathy and ventricular tachycardia," *J. Am. Coll. Cardiol.*, vol. 61, no. 20, pp. 2088–2095, 2013.
[97] M. G. Kienzle, J. Miller, R. A. Falcone, A. Harken, and M. E. Josephson, "Intraoperative endocardial mapping during sinus rhythm: relationship to site of origin of ventricular tachycardia.," *Circulation*, vol. 70, no. 6, pp. 957–965, 1984.
[98] M. E. Josephson and A. L. Wit, "Fractionated electrical activity and continuous electrical activity: fact or artifact?," *Circulation*, vol. 70, no. 4, pp. 529–532, 1984.
[99] D. M. Cassidy, J. A. Vassallo, A. E. Buxton, J. U. Doherty, F. E. Marchlinski, and M. E. Josephson, "The value of catheter mapping during sinus rhythm to localize site of origin of ventricular tachycardia.," *Circulation*, vol. 69, no. 6, pp. 1103–1110, 1984.
[100] P. I. Gardner, P. C. Ursell, J. J. Fenoglio Jr, and A. L. Wit, "Electrophysiologic and anatomic basis for fractionated electrograms recorded from healed myocardial infarcts.," *Circulation*, vol. 72, no. 3, pp. 596–611, 1985.
[101] F. Bogun *et al.*, "Analysis during sinus rhythm of critical sites in reentry circuits of postinfarction ventricular tachycardia," *J. Interv. Card. Electrophysiol.*, vol. 7, no. 1, pp. 95–103, 2002.
[102] V. Jacquemet and C. S. Henriquez, "Genesis of complex fractionated atrial electrograms in zones of slow conduction: a computer model of microfibrosis," *Heart Rhythm*, vol. 6, no. 6, pp. 803–810, 2009.
[103] C. B. Brunckhorst *et al.*, "Ventricular mapping during atrial and ventricular pacing. Relationship of multipotential electrograms to ventricular tachycardia reentry circuits after myocardial infarction," *Eur. Heart J.*, vol. 23, no. 14, pp. 1131–1138, 2002.
[104] A. Arenal *et al.*, "Ablation of electrograms with an isolated, delayed component as treatment of unmappable monomorphic ventricular tachycardias in patients with structural heart disease," *J. Am. Coll. Cardiol.*, vol. 41, no. 1, pp. 81–92, 2003.

[105] S. Nakahara *et al.*, “Characterization of the arrhythmogenic substrate in ischemic and nonischemic cardiomyopathy: implications for catheter ablation of hemodynamically unstable ventricular tachycardia,” *J. Am. Coll. Cardiol.*, vol. 55, no. 21, pp. 2355–2365, 2010.
[106] F. Bogun *et al.*, “Isolated potentials during sinus rhythm and pace-mapping within scars as guides for ablation of post-infarction ventricular tachycardia,” *J. Am. Coll. Cardiol.*, vol. 47, no. 10, pp. 2013–2019, 2006.
[107] H. M. Haqqani *et al.*, “Fundamental differences in electrophysiologic and electroanatomic substrate between ischemic cardiomyopathy patients with and without clinical ventricular tachycardia,” *J. Am. Coll. Cardiol.*, vol. 54, no. 2, pp. 166–173, 2009.
[108] P. Vergara *et al.*, “Late potentials abolition as an additional technique for reduction of arrhythmia recurrence in scar related ventricular tachycardia ablation,” *J. Cardiovasc. Electrophysiol.*, vol. 23, no. 6, pp. 621–627, 2012.
[109] J. Silberbauer *et al.*, “Noninducibility and late potential abolition: a novel combined prognostic procedural end point for catheter ablation of postinfarction ventricular tachycardia,” *Circ. Arrhythm. Electrophysiol.*, vol. 7, no. 3, pp. 424–435, 2014.
[110] D. Tsiachris *et al.*, “Electroanatomical voltage and morphology characteristics in postinfarction patients undergoing ventricular tachycardia ablation: pragmatic approach favoring late potentials abolition,” *Circ. Arrhythm. Electrophysiol.*, vol. 8, no. 4, pp. 863–873, 2015.
[111] P. Jais, P. Maury, and P. Khairy, “Elimination of local abnormal ventricular activities clinical perspective: a new end point for substrate modification in patients with scar-related ventricular tachycardia,” *Circulation*, vol. 125, no. 18, pp. 2184–2196, 2012.
[112] N. Jackson *et al.*, “Decrement evoked potential mapping: basis of a mechanistic strategy for ventricular tachycardia ablation,” *Circ. Arrhythm. Electrophysiol.*, vol. 8, no. 6, pp. 1433–1442, 2015.
[113] A. Porta-Sánchez *et al.*, “Multicenter study of ischemic ventricular tachycardia ablation with decrement-evoked potential (DEEP) mapping with extra stimulus,” *JACC Clin. Electrophysiol.*, vol. 4, no. 3, pp. 307–315, 2018.
[114] V. Y. Reddy, D. Wrobleski, C. Houghtaling, M. E. Josephson, and J. N. Ruskin, “Combined epicardial and endocardial electroanatomic mapping in a porcine model of healed myocardial infarction,” *Circulation*, vol. 107, no. 25, pp. 3236–3242, 2003.
[115] A. Berruezo *et al.*, “Scar dechanneling: new method for scar-related left ventricular tachycardia substrate ablation,” *Circ. Arrhythm. Electrophysiol.*, vol. 8, no. 2, pp. 326–336, 2015.
[116] J. M. Miller, G. S. Tyson, W. C. Hargrove III, J. A. Vassallo, M. E. Rosenthal, and M. E. Josephson, “Effect of subendocardial resection on sinus rhythm endocardial electrogram abnormalities,” *Circulation*, vol. 91, no. 9, pp. 2385–2391, 1995.
[117] E. J. Ciaccio, A. C. Tosti, and M. M. Scheinman, “Relationship between sinus rhythm activation and the reentrant ventricular tachycardia isthmus,” *Circulation*, vol. 104, no. 5, pp. 613–619, 2001.
[118] H. L. Waxman and R. J. Sung, “Significance of fragmented ventricular electrograms observed using intracardiac recording techniques in man.,” *Circulation*, vol. 62, no. 6, pp. 1349–1356, 1980.
[119] D. M. Cassidy, J. A. Vassallo, A. E. Buxton, J. U. Doherty, F. E. Marchlinski, and M. E. Josephson, “Catheter mapping during sinus rhythm: relation of local electrogram duration to ventricular tachycardia cycle length,” *Am. J. Cardiol.*, vol. 55, no. 6, pp. 713–716, 1985.
[120] J. M. Miller, A. H. Harken, W. C. Hargrove, and M. E. Josephson, “Pattern of endocardial activation during sustained ventricular tachycardia,” *J. Am. Coll. Cardiol.*, vol. 6, no. 6, pp. 1280–1287, 1985.
[121] P. Brugada, H. Abdollah, B. Heddle, and H. J. Wellens, “Results of a ventricular stimulation protocol using a maximum of 4 premature stimuli in patients without documented or suspected ventricular arrhythmias,” *Am. J. Cardiol.*, vol. 52, no. 10, pp. 1214–1218, 1983.

[122] F. E. Marchlinski *et al.*, “Long-term success of irrigated radiofrequency catheter ablation of sustained ventricular tachycardia: post-approval THERMOCOOL VT trial,” *J. Am. Coll. Cardiol.*, vol. 67, no. 6, pp. 674–683, 2016.
[123] M. S. Rosenbaum, D. J. Wilber, D. Finkelstein, J. N. Ruskin, and H. Garan, “Immediate reproducibility of electrically induced sustained monomorphic ventricular tachycardia before and during antiarrhythmic therapy,” *J. Am. Coll. Cardiol.*, vol. 17, no. 1, pp. 133–138, 1991.
[124] H. Tanner *et al.*, “Catheter ablation of recurrent scar-related ventricular tachycardia using electroanatomical mapping and irrigated ablation technology: results of the prospective multicenter Euro-VT-study,” *J. Cardiovasc. Electrophysiol.*, vol. 21, no. 1, pp. 47–53, 2010.
[125] W. G. Stevenson *et al.*, “Irrigated radiofrequency catheter ablation guided by electroanatomic mapping for recurrent ventricular tachycardia after myocardial infarction: the multicenter thermocool ventricular tachycardia ablation trial,” *Circulation*, vol. 118, no. 25, p. 2773, 2008.
[126] W. G. Stevenson *et al.*, “Exploring postinfarction reentrant ventricular tachycardia with entrainment mapping,” *J. Am. Coll. Cardiol.*, vol. 29, no. 6, pp. 1180–1189, 1997.
[127] M. E. Josephson, L. N. Horowitz, A. Farshidi, and J. A. Kastor, “Recurrent sustained ventricular tachycardia. 1. Mechanisms.,” *Circulation*, vol. 57, no. 3, p. 431, Mar. 1978, doi: 10.1161/01.CIR.57.3.431.
[128] M. Yokokawa, B. Desjardins, T. Crawford, E. Good, F. Morady, and F. Bogun, “Reasons for recurrent ventricular tachycardia after catheter ablation of post-infarction ventricular tachycardia,” *J. Am. Coll. Cardiol.*, vol. 61, no. 1, pp. 66–73, 2013.
[129] K. Soejima *et al.*, “Catheter ablation in patients with multiple and unstable ventricular tachycardias after myocardial infarction: short ablation lines guided by reentry circuit isthmuses and sinus rhythm mapping,” *Circulation*, vol. 104, no. 6, pp. 664–669, 2001.
[130] R. Tung *et al.*, “Freedom from recurrent ventricular tachycardia after catheter ablation is associated with improved survival in patients with structural heart disease: an International VT Ablation Center Collaborative Group study,” *Heart Rhythm*, vol. 12, no. 9, pp. 1997–2007, 2015.
[131] O. R. Segal, A. W. Chow, V. Markides, R. J. Schilling, N. S. Peters, and D. W. Davies, “Long-term results after ablation of infarct-related ventricular tachycardia,” *Heart Rhythm*, vol. 2, no. 5, pp. 474–482, 2005.
[132] F. Bogun *et al.*, “Response to pacing at sites of isolated diastolic potentials during ventricular tachycardia in patients with previous myocardial infarction,” *J. Am. Coll. Cardiol.*, vol. 30, no. 2, pp. 505–513, 1997.
[133] S. Dixit and D. J. Callans, “Mapping for ventricular tachycardia,” *Card. Electrophysiol. Rev.*, vol. 6, no. 4, pp. 436–441, 2002.
[134] S. Tung, K. Soejima, W. H. Maisel, M. Suzuki, L. Epstein, and W. G. Stevenson, “Recognition of far-field electrograms during entrainment mapping of ventricular tachycardia,” *J. Am. Coll. Cardiol.*, vol. 42, no. 1, pp. 110–115, 2003.
[135] W. G. Stevenson, P. T. Sager, P. D. Natterson, L. A. Saxon, H. R. Middlekauff, and I. Wiener, “Relation of pace mapping QRS configuration and conduction delay to ventricular tachycardia reentry circuits in human infarct scars,” *J. Am. Coll. Cardiol.*, vol. 26, no. 2, pp. 481–488, 1995.
[136] E. P. Gerstenfeld, S. Dixit, D. J. Callans, Y. Rajawat, R. Rho, and F. E. Marchlinski, “Quantitative comparison of spontaneous and paced 12-lead electrocardiogram during right ventricular outflow tract ventricular tachycardia,” *J. Am. Coll. Cardiol.*, vol. 41, no. 11, pp. 2046–2053, 2003.
[137] C. De Chillou *et al.*, “Localizing the critical isthmus of postinfarct ventricular tachycardia: the value of pace-mapping during sinus rhythm,” *Heart Rhythm*, vol. 11, no. 2, pp. 175–181, 2014.
[138] J. P. Moak, K. Sumihara, J. Swink, S. Hanumanthaiah, and C. I. Berul, “Ablation of the vanishing PVC, facilitated by quantitative morphology-matching software,” *Pacing Clin. Electrophysiol.*, vol. 40, no. 11, pp. 1227–1233, 2017.

[139] C. B. Brunckhorst *et al.*, “Relationship of slow conduction detected by pace-mapping to ventricular tachycardia re-entry circuit sites after infarction,” *J. Am. Coll. Cardiol.*, vol. 41, no. 5, pp. 802–809, 2003.
[140] L. S. Green, R. L. Lux, P. R. Ershler, R. A. Freedman, F. I. Marcus, and K. Gear, “Resolution of pace mapping stimulus site separation using body surface potentials.,” *Circulation*, vol. 90, no. 1, pp. 462–468, 1994.
[141] A. H. Kadish, S. Schmaltz, and F. Morady, “A comparison of QRS complexes resulting from unipolar and bipolar pacing: Implications for pace-mapping,” *Pacing Clin. Electrophysiol.*, vol. 14, no. 5, pp. 823–832, 1991.
[142] A. H. Kadish, K. Childs, S. Schmaltz, and F. Morady, “Differences in QRS configuration during unipolar pacing from adjacent sites: implications for the spatial resolution of pace-mapping,” *J. Am. Coll. Cardiol.*, vol. 17, no. 1, pp. 143–151, 1991.
[143] R. Tung *et al.*, “Functional pace-mapping responses for identification of targets for catheter ablation of scar-mediated ventricular tachycardia,” *Circ. Arrhythm. Electrophysiol.*, vol. 5, no. 2, pp. 264–272, 2012.
[144] R. Goyal *et al.*, “Effect of coupling interval and pacing cycle length on morphology of paced ventricular complexes: implications for pace mapping,” *Circulation*, vol. 94, no. 11, pp. 2843–2849, 1996.
[145] M. E. Josephson, H. L. Waxman, M. E. Cain, M. J. Gardner, and A. E. Buxton, “Ventricular activation during ventricular endocardial pacing. II. Role of pace-mapping to localize origin of ventricular tachycardia,” *Am. J. Cardiol.*, vol. 50, no. 1, pp. 11–22, 1982.
[146] C. B. Brunckhorst, E. Delacretaz, K. Soejima, W. H. Maisel, P. L. Friedman, and W. G. Stevenson, “Identification of the ventricular tachycardia isthmus after infarction by pace mapping,” *Circulation*, vol. 110, no. 6, pp. 652–659, 2004.
[147] R. R. Tilz *et al.*, “Electrical isolation of a substrate after myocardial infarction: a novel ablation strategy for unmappable ventricular tachycardias—feasibility and clinical outcome,” *Europace*, vol. 16, no. 7, pp. 1040–1052, 2014.
[148] F. Odille *et al.*, “Catheter treatment of ventricular tachycardia: a reference-less pace-mapping method to identify ablation targets,” *IEEE Trans. Biomed. Eng.*, 2019.
[149] J. E. Dos Reis *et al.*, “Electrocardiogram Acquisition During Remote Magnetic Catheter Navigation,” *Ann. Biomed. Eng.*, vol. 47, no. 4, pp. 1141–1152, 2019.
[150] J. E. Dos Reis *et al.*, “Reconstruction of the 12-lead ECG using a novel MR-compatible ECG sensor network,” *Magn. Reson. Med.*, vol. 82, no. 5, pp. 1929–1945, 2019.
[151] A. Battaglia *et al.*, “An efficient algorithm based on electrograms characteristics to identify ventricular tachycardia isthmus entrance in post-infarct patients,” *EP Eur.*, vol. 22, no. 1, pp. 109–116, 2019.
[152] R. J. Wilson, *Introduction to graph theory*. Pearson Education India, 1979.
[153] E. Dijkstra, “A note on two problems in connexion with graphs,” *Numer. Math.*, vol. 1, pp. 269–271, 1959.
[154] P. Hoyland *et al.*, “A paced-ECG detector and delineator for automatic multi-parametric catheter mapping of ventricular tachycardia,” *IEEE Access*, 2020.
[155] A. Prakosa *et al.*, “Personalized virtual-heart technology for guiding the ablation of infarct-related ventricular tachycardia,” *Nat. Biomed. Eng.*, vol. 2, no. 10, pp. 732–740, 2018.

Title:

Computer assisted electrophysiological intervention treating complex ventricular arrhythmias

Summary:

Since the beginning of the 1990s and the use of radiofrequency to ablate cardiac arrhythmias, electrophysiologists treat increasing complex rhythm disorders. 3D mapping systems enable catheter locations to be known with high precision and therefore are very important tools for electrophysiology. Identifying zones of interest remains long and involves many steps based on indirect analyses of the heart's properties.

The main objective of the thesis is to develop new tools to locate the critical isthmus in post infarct ventricular tachycardia. The clear identification of the circuit components of the ventricular tachycardia enables the development of an ablation strategy to treat the patient. The studied methods do not require a 12-lead electrocardiogram of the ventricular tachycardia and therefore have the advantage of being able to be used even if the tachycardia cannot be initiated during the procedure.

A major area of research is the development of an algorithm that automatically extracts the relevant data obtained during pace mapping. This facilitates the display of multi-parametric maps highlighting potential reentry circuits.

Another area of research is the development of a graph-based method to study the variations of the electrical properties of the ventricle. The paced points are considered as vertices of a graph. Each edge is given a weight and finding the path between two vertices of minimum weight allows the analysis of potential reentry circuits.

Keywords:

Cardiac electrophysiology; Electrocardiography; Radiofrequency catheter ablation